LAYERED DOUBLE HYDROXIDES AS ANION- AND CATION-EXCHANGING MATERIALS

Mickey Charles Richardson, B.S.

Dissertation Prepared for the Degree of

DOCTOR OF PHILOSOPHY

UNIVERSITY OF NORTH TEXAS

May 2007

APPROVED:

Paul S. Braterman, Major Professor
Mohammad A. Omary, Committee Member
Teresa D. Golden, Committee Member
Trent Selby, Committee Member
Ruthanne D. Thomas, Chair of the Department of Chemistry
Sandra L. Terrell, Dean of the Robert B. Toulouse School of Graduate Studies

Richardson, Mickey Charles, Layered Double Hydroxides as Anion- and Cation-Exchanging Materials. Doctor of Philosophy (Inorganic Chemistry), May 2007, 182 pp., 64 figures, 22 tables, references, 213 titles.

Layered double hydroxides (LDH) have been principally known as anion-exchanging, clay-like materials for several decades, and continues to be the main driving force for current and future research.

The chemical interactions of LDH, with transition metallocyanides, have been a popular topic of investigation for many years, partly due to the use of powder x-ray diffraction and infrared spectroscopy as the main characterization tools. Each transition metallocyanide has a characteristic infrared stretching frequency that can be easily observed, and their respective sizes can be observed while intercalated within the interlayer of the LDH.

The ability of LDH to incorporate metal cations or any ions/molecules/complexes, that have a postive charge, have not been previously investigated, mainly due to the chemical and physical nature of LDH. The possibility of cationic incorporation with LDH would most likely occur by surface adsorption, lattice metal replacement, or by intercalation into the LDH interlayers.

Although infrared spectroscopy finds it main use through the identification of the anions incorporated with LDH, it can also be used to study and identify the various active and inactive bending and stretching modes that the metal hydroxide layers have.

ACKNOWLEDGEMENTS

I would like to thank my research advisor, Prof. Paul S. Braterman, for his guidance, patience and direction during my experience as a graduate student. I especially want to thank Prof. Braterman for giving me an extraordinary amount of experimental and intellectual freedom during my years here.

I would also like to thank all of the Braterman group members, past and present, for their support. I have learned much from you and I hope to have taught you a little in return: Dr Faith Yarberry, Dr Zhi Ping Xu, Dr Susanta Saha, Dr Sergei Rudenja, Brian Brister, Fang Wei-Brister and Sriram Ambadapadi.

I would also like to thank members from our collaborative group, over at the Materials Science and Engineering department, for some very interesting research projects over the years: Laxmi Sahu, Siddhi Pendse, Mithun Kamath and especially Prof. Nandika D'Souza.

I would like to thank Pankaj Sinha for running the DFT calculations on the tetracyanonickelate(II) complex (Chapter 3), the members from Prof. Golden's and Prof. Omary's research groups, and everyone on my committee.

Last but not least, I would like to thank my family and friends for their continued encouragement, which without I would have never made it through.

The agencies responsible for the funding of this research include NASA, NIST, the Robert A. Welch Foundation, and the UNT Faculty Research Fund.

Semper Fidelis

TABLE OF CONTENTS

Page

LIST OF TABLES

LIST OF FIGURES

CHAPTER 1

LAYERED DOUBLE HYDROXIDES (LDH)

1.1 General Description

Layered double hydroxides (LDH) are a class of natural and synthetic mixed-metal hydroxides, historically described as anion-exchanging, clay-like materials.[1-4] LDH are structurally similar to brucite, $Mg(OH)_2$, with one notable difference: LDH are mixed-metal hydroxides and brucite is a magnesium hydroxide. The most commonly studied LDH consists of divalent and trivalent metals (M), with the general formula:

$$[M^{(II)}_{1-x}M^{(III)}_{x}(OH)_2]^{+}[A^{n-}]_{x/n}\bullet yH_2O$$

The values of x vary,[5,6] but typically fall within the range: $0.25 \leq x \leq 0.33$, such that the above formula corresponds to a range from $[M^{(II)}_{0.75}M^{(III)}_{0.25}(OH)_2][A^{n-}]_{x/n}\bullet yH_2O$ to $[M^{(II)}_{0.67}M^{(III)}_{0.33}(OH)_2][A^{n-}]_{x/n}\bullet yH_2O$.

In whole number proportions, these two formulas transform into $[M^{(II)}_2M^{(III)}(OH)_6][A^{n-}]_{x/n}\bullet yH_2O$ and $[M^{(II)}_3M^{(III)}(OH)_8][A^{n-}]_{x/n}\bullet yH_2O$, which are simplified as either a 2:1 LDH or a 3:1 LDH, respectively. The values for y are dependent on the anion and conditions, with two being the most common.

The values for the counter-anion (A) depend on the charge of the anion, with respect to the amount of trivalent metal, such that the x/n term achieves charge neutrality throughout the LDH structure.

The above general formula in no way exhausts the possible chemical makeup of LDH as a whole. LDH have been synthesized using monovalent-trivalent metals, commonly in the form of a $LiAl_2$ hydroxide,[7-9] and with more than two types of metals within the metal hydroxide framework.[10-12]

1.2 Comparison with Brucite

LDH and brucite are similar, in that both exist by having sheet-like morphologies, in which the sheets grow in two dimensions (x,y plane). In both cases, each metal cation is directly bonded to six hydroxide groups and each hydroxide group is directly bonded to three metals (Figure 1.1). From a bonding perspective, each metal cation has a coordination number of six and each oxygen atom has a coordination number of four, except at the edges of the lattice sheets.

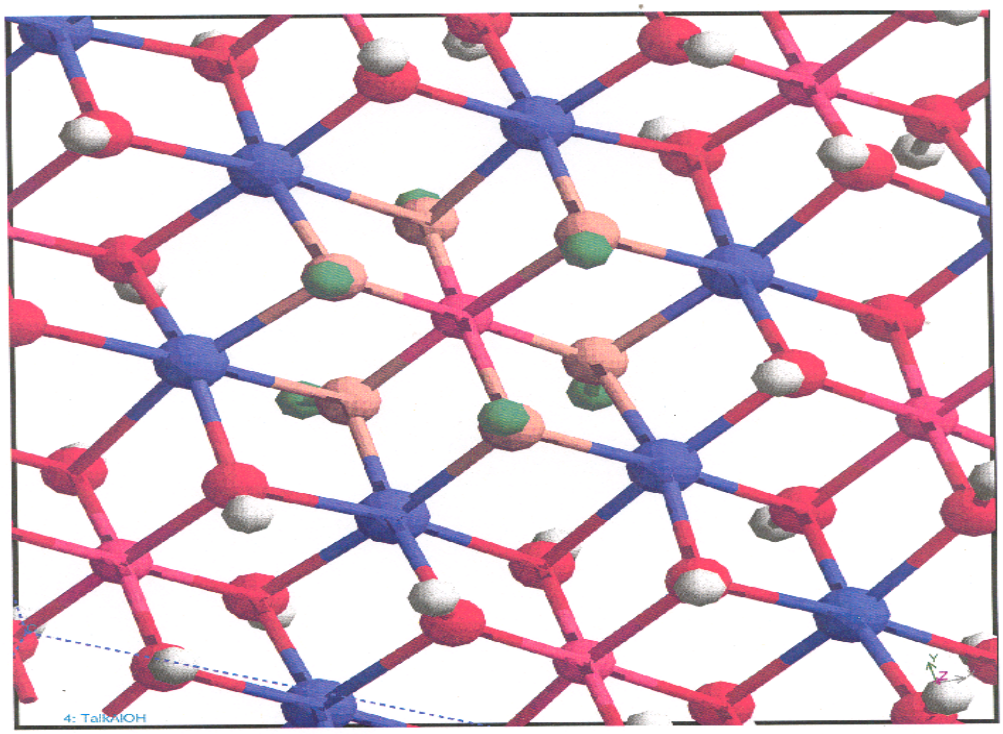

Figure 1.1: Molecular model of a divalent metal (blue) and trivalent metal (pink) LDH. Both metal types are surrounded by six hydroxide ligands (brown/green).

One difference between brucite and LDH is that the metal hydroxide framework is nearly planar, in brucite, but not so with LDH. The types of metals used for LDH will have different metal-oxygen bond distances. These bond distance differences result in a slightly corrugated lattice framework.[13] The essential difference between LDH and brucite is the development of a net positive charge on the lattice sheets due to the substitution of some of the magnesium cations with trivalent cations. It is this net positive charge that makes LDH extremely efficient with anionic uptake, such that the basic descriptive definition has been as anion-exchanging clays for several decades.

It is important to note that LDH exists both naturally and synthetically, where the most common naturally occurring LDH is a mineral, known as hydrotalcite. Hydrotalcite is a Mg_3Al-hydroxycarbonate with the formula: $Mg_6Al_2(OH)_{16}CO_3 \bullet 2H_2O$.[14,15] This is the type of LDH that was first compared against brucite. All other types of LDH, having a similar formula, are sometimes referred to as hydrotalcite-like compounds.

1.3 LDH Environment

The positively charged LDH layers are stacked on top of one another, in a vertical fashion, typically giving rise to what crystallographers describe as rhombohedral stacking.[16-18] The counter-anions and water molecules are located between each adjacent layer and on the outer layer's surface and edges. Anions that are between adjacent LDH layers, are termed intercalated, and anions on the edges and surfaces of the LDH layers are termed adsorbed.

The actual LDH layers stack on top of one another by a three-layer sequence, although two-layer sequences are also found. Each layer has the $M(OH)_6$ structures positioned in a D_{3d} point group, such that the top three hydroxides will be out-of-phase with the bottom three hydroxides (Figure 1.6).

There are numerous possibilities of such two or three-layer sequencing, depending on whether the top layer forms a prismatic structure with the nearest bottom layer (denoted as P-type) or whether the top layer forms an antiprismatic structure with the nearest bottom layer (denoted as O-type).

Some examples of two and three-layer sequencing possibilities include the 3R (three-layer, rhombohedral), 2H and 3H (two-layer and three-layer, hexagonal) polytypes. The many different polytypes arise from the relationships between the stacking of the layers and the intra-layer patterns, with the added possibility of disordered layer stacking.

There is no direct electrostatic attraction between the trivalent metal (where the net positive charge would be located) and the counter-anion, but rather through hydrogen bonding by the pendant lattice hydroxide and the counter-anion (hereafter described as just the anion). Water molecules also exist between the lattice sheets, and are also not only hydrogen-bonded to the pendant lattice hydroxides, but to each other and the anions.[19] In this regard, once charge neutrality is satisfied**,** hydrogen-bonding is the most important kind of bonding interaction in LDH (Figure 1.2).

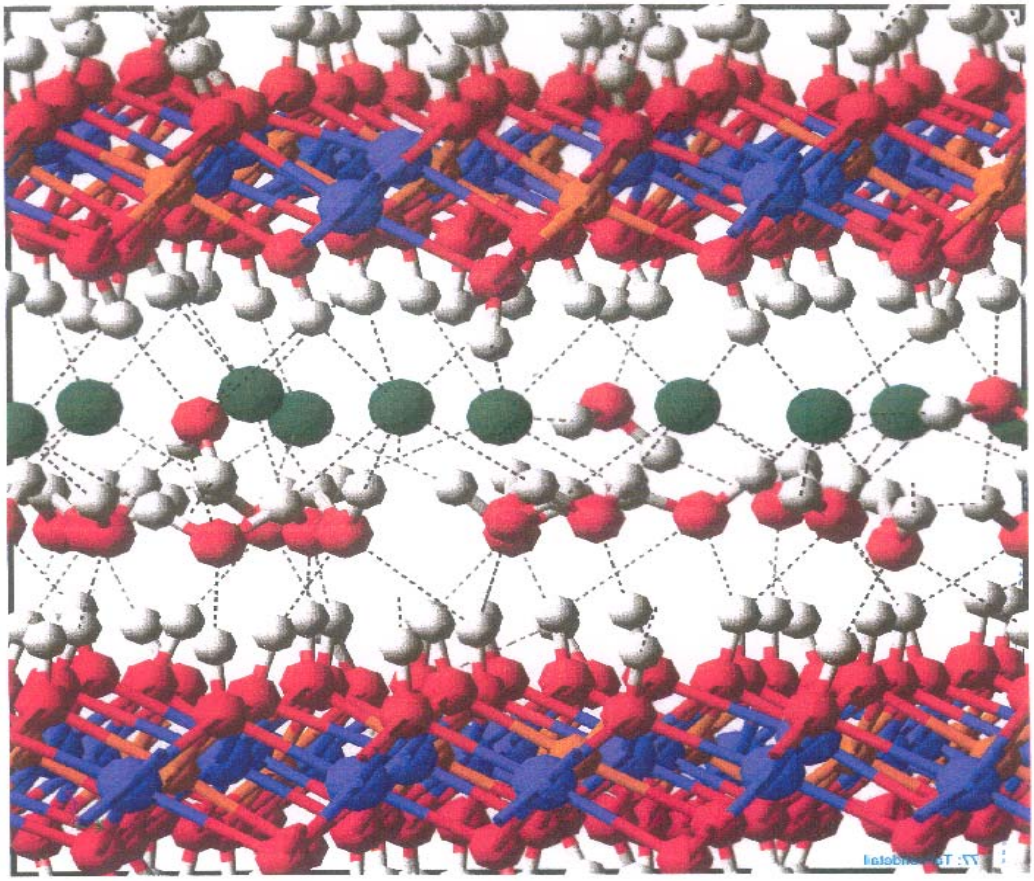

Figure 1.2: Molecular model of $Mg_2Al(OH)_6Cl \bullet 2H_2O$ showing two adjacent LDH sheets held together by interlayer water and chlorides (green).

The metals within the lattice framework for an ideal divalent/trivalent LDH are presumably, except (as we describe in Chapter 6) in some freshly prepared materials, positioned in such a way that the trivalent metal cations cannot be adjacent to one another.

This positioning of the trivalent cations is similar to Lowenstein's rule for the aluminosilicates,[20] which in both cases, are undoubtedly related to Pauling's adjacent charge principle.[21] For every trivalent metal cation in LDH, a partial positive charge will be found in that area. Keeping the trivalent metal cations positioned away from one another ensures that the positive charges will not be localized but spread throughout the

lattice sheets. This separation of positive charges is very important for anionic uptake, in that it keeps the charge-balancing anions from aggregating together in just one area.

One important topic for LDH, with respect to anionic uptake, is charge density. Due to the net positive charge development within the LDH sheets, the unit charge per area can be used to show the potential amounts of anions that LDH with various divalent to trivalent metal ratios can incorporate (relative to one another). The formula for calculating charge density (C_d):

$$C_d = xe/a^2\sin 60^\circ \quad \text{or} \quad C_d = 12.0xe/nm^2$$

The variables in this formula correspond to: x is the ratio of the trivalent metal to the total metals amount, a is the distance between adjacent metal ions in the layer, e is the electronic charge and sin 60° is a geometrical factor describing the angle between the a and b axes.

For example, a 2:1 Mg-Al LDH and a 3:1 Mg-Al LDH should have different charge densities, simply based of the different values for x. Using the simplified formula, the 3:1 Mg-Al LDH has a trivalent metal to total metals amount of 1/4, and the 2:1 Mg-Al LDH has a trivalent metal to total metals amount of 1/3. One can easily calculate charge densities of 4.0 e/nm^2 for a 2:1 Mg-Al LDH and 3.0 e/nm^2 for a 3:1 Mg-Al LDH. The importance of this formula should now be clear; a 2:1 Mg-Al LDH has more positive charge, per unit area, and should then be capable of more anionic incorporation. Although the above calculation was done for a Mg-Al LDH, the charge density formula should produce similar results for other divalent-trivalent metal arrangements. Only the lattice parameter, a, will be different (but not greatly different than in the Mg-Al LDH materials).

1.4 LDH History

The earliest records show that hydrotalcite, the most common naturally occurring mineral of the LDH family, was discovered in Sweden, back in 1842. LDH have been known as mixed-metal hydroxides since the early 20th century,[22,23] but the initial attempts to describe their structure were not correct.

The early investigators noticed differences in the pH of controlled precipitations of mixtures of magnesium and aluminum compounds, by alkali, with respect to both magnesium hydroxide and aluminum hydroxide. Undoubtedly, without the invention of the pH meter some time earlier, these investigators would not have made such profound observations. The early investigators, knowing that they have obtained something unique, described their product as either a surface adsorption complex or as an alternation of $Mg(OH)_2$ and $Al(OH)_3$ compounds.[24,25]

It was not until the 1960s that x-ray diffraction shed some insight about this unique material.[26,27] The x-ray diffraction pattern of the mineral, hydrotalcite, was already known, so by comparison with this synthesized material, the relationship was identified. This ultimately led to the synonym, hydrotalcite-like compounds or the evolved layered double hydroxides, or the less widely used, double layered hydroxides. Throughout the remainder of the 20th century, and up to this day, powder x-ray diffraction remains an integral characterization technique for any synthesized LDH.

1.5 Practical Uses for LDH

As previously mentioned, LDH are anion-exchanging materials, by nature. This has remained their primary practical use,[28-31] and the types of anions that have been investigated with LDH constitute the vast majority of articles published. Since so many types of anions have been explored, there should be an order of preference, based on the anion's size, charge, electronegativity, etc. Back in the 1970s-1980s, a ground-breaking survey on anionic preference was accomplished.[32,33] This survey showed that, of the simple inorganic and organic anions, carbonate is the easiest to intercalate and the most difficult to exchange within LDH. On the opposite end, the halides and nitrate are just as easy to intercalate but the easiest to exchange. Most, if not all of the other anions lie between these two extremes. As a result, for typical anion exchange, most LDH materials are prepared with chloride or nitrate as the initial anion, and then replaced with whatever anion is desired. The key to anion exchange is to never start out with carbonate because it is too difficult to replace by other anions (unless removed by acidification, risking destruction of the entire layer system; carbonate has however been shown to be exchanged with chloride during a dilute HCl(aq)/concentrated NaCl workup of 2:1 Mg-Al and Zn-Al LDH materials).

Other practical uses include, but are nowhere limited to LDH as antacids,[34] drug-delivery systems,[35,36] modified electrodes,[37,38] polymer stabilizers,[39,40] flame retardants,[41,42] adsorbents,[43] electro-photoactive materials,[44] catalysts/catalyst precursors,[45-52] and as a possible template in the origins of life.[53,54] There is no doubt that with time, many more will be discovered.

1.6 Preparation of LDH

1.6.1 Synthesis Methods

Just as there are many practical applications for LDH, there are many pathways for their synthesis. The most common procedure is by the precipitation of an aqueous solution of the divalent/trivalent metal salts with a base (NaOH or NH_4OH). Within this procedure, there are two routes: By the addition of the base to the metal salts solution (variable pH or direct precipitation method)[55] or by the co-addition of the base and metal salts solution, such that a constant pH is held (constant pH or coprecipitation method).[56]

In the addition of the base to the metal salts route, the metal with the lowest solubility, in terms of hydroxide formation, usually will precipitate out first (exceptions have been shown with LDH containing Cr(III)). In the case of a Mg:Al LDH, the aluminum will precipitate out, as aluminum hydroxide, while the magnesiums will remain in solution (equation 1). It is not clear what happens next, when more additions of base are added. It is possible that further hydroxide additions will result in an aluminum hydroxide complex ($[Al(OH)_4]^-$, aluminate), which will then take in the available magnesium ions (equations 2 or 3):

1) $2Mg^{2+} + Al^{3+} + 3OH^- \rightarrow Al(OH)_3(s) + 2Mg^{2+}$

2) $2Mg^{2+} + Al(OH)_3(s) + 3OH^- \rightarrow [Mg_2Al(OH)_6]^+$

or

3) $2Mg^{2+} + Al(OH)_3(s) + 3OH^- \rightarrow [Al(OH)_4]^- + 2OH^- + 2Mg^{2+} \rightarrow [Mg_2Al(OH)_6]^+$

In the above equations, water molecules are left out, for simplicity, and the LDH would also precipitate out as a white solid (but with an appropriate counter-anion). In either case for equations 2 or 3, the leading theory holds that the aluminum hydroxide solid

will undergo some sort of dissolution or modification in order to accommodate six hydroxides, to be shared with neighboring magnesiums.

Titration curves have proven to be helpful when using the variable pH route for LDH synthesis. In the case of a 2:1 Mg-Al LDH, the generated titration curve can be broken down into three main regions of interest. When the magnesium and aluminum salts are dissolved in water, the pH of the solution is usually around 3.5-3.8, if enough of the metal salts are used for the preparation of 1.0 g of LDH. This low pH range is indicative of the acidic properties, inherent in aqueous aluminum. When the first additions of base are added, the aluminum ions will precipitate out first (region 1), until three molar amounts of hydroxide are added. When this stoichiometric amount is reached, all aluminum exists in the solid hydroxide form (region 2). Further additions of hydroxide result in the formation of the LDH (region 3). Figure 1.3 shows a generated titration curve of a 2:1 Mg-Al LDH-Cl.

The generation of complete titration curves for a 2:1 Mg-Al LDH-A (A = chloride, nitrate or carbonate) takes several hours. The pH values for the formation of aluminum hydroxide, from each NaOH addition, equilibrates rapidly, but during the LDH formation, the pH values spike up rapidly, decline rapidly, then slowly equilibrate.

This observation may be evidence of the complex mechanism of LDH formation, from equations 1-3, but is not enough to assume an aluminate intermediate. There is no doubt that the rise, then drop in pH values are due to the incorporation of hydroxide into the forming LDH structure.

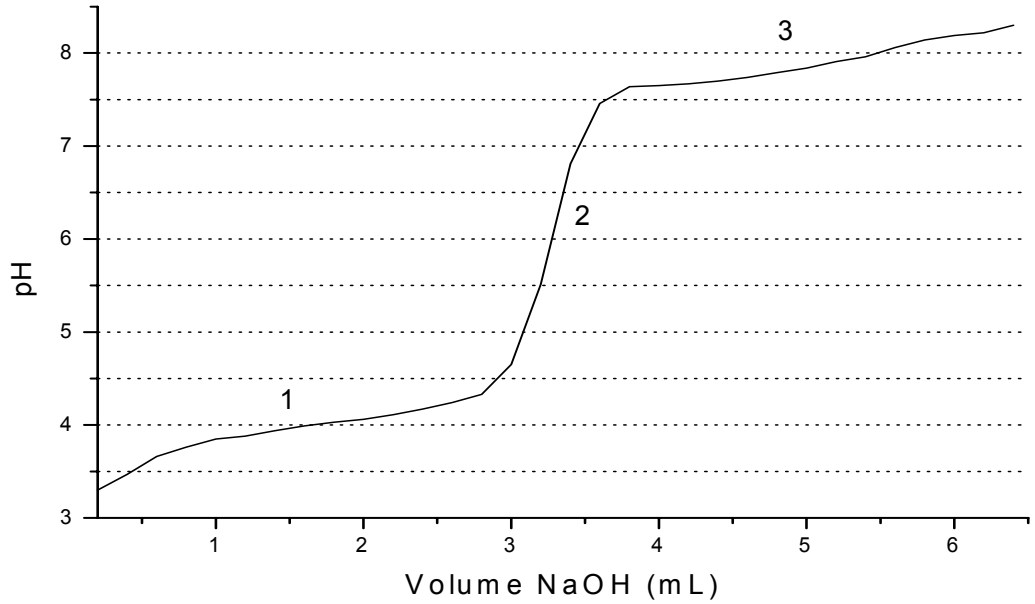

Figure 1.3: Titration Curve of a 2:1 Mg-Al LDH-Cl, starting with a 0.3M $MgCl_2$ and 0.1M $AlCl_3$ solution, then titrating with a diluted 50% NaOH solution (6 moles OH^- for every 1 mole Al^{3+}).

From the titration curve, the aluminum will begin precipitating out at pH values far from the neutral 7.00 mark and show a gradual increase in pH (1). Once the three molar stoichiometric amount of NaOH is added, the curve will sharply increase up to the neutral pH mark (2).

After point (2) is reached, further hydroxide additions result in another fairly smooth increase in pH values (3). The end point of the titration shows a basic material with a pH above the neutral 7.00 mark.

The purpose of staring out with a 3:1 molar ratio of magnesium to aluminum is to use the excess magnesium as a buffer. The excess magnesium will ensure that the overall precipitation pH will be lower than that with a stoichiometric amount. This is useful because a lower pH will mean less uptake of carbon dioxide and any unreacted hydroxides (beyond the stoichiometric amount) will not get incorporated into the LDH.

When generating titration curves for LDH containing both acidic divalent and trivalent metals, the pH values for these three regions will be considerably lower than that for the magnesium and aluminum case. For instance, a 2:1 Co-Al LDH-Cl has its initial pH around 3.1-3.2, its equivalence point pH around 4.2-4.5, and its endpoint pH around 5.5-5.6.

Other, less common techniques include preparation by both divalent and trivalent (hydr)oxides with anion,[57,58] preparation from metals,[59] the so-called aluminate route,[60] sol-gel techniques,[61] homogeneous precipitation,[62,63] and preparation by intentional oxidation.[64,65]

The key points for successful divalent-trivalent metal LDH synthesis:

1) The metal cations should all conform to being in a six-coordinate environment (D_{3d} symmetry).
2) The selected anion should not interfere with the LDH lattice formation by precipitation with any of the LDH lattice metals (K_{sp} issues).
3) Metal ions that are easily reduced/oxidized should be handled differently.
4) Unwarranted or adventitious carbon dioxide should be excluded from the reaction vessel if LDH-CO_3 is not the desired material and the LDH is basic (*vide infra*).

In all of the above techniques, the most important considerations to make when preparing LDH are that the metals ratio and the amount of base ultimately dictate which form will be produced. Also of note, depending on the types of metals, some LDH materials will be more basic and some will be less basic.

1.6.2 Post-Synthesis Treatment

After the LDH precipitate has been prepared, there are two main techniques for post-treatment. The most common post-treatment technique is to subject the newly formed precipitate to gentle reflux, in its own mother liquor. The reflux is performed under a stream of inert gas, in order to avoid adventitious carbon dioxide, except when carbonate is the desired product. The reflux temperature applied is typically in the range of 90 – 110 °C, for about one day. LDH of this type is known as aged LDH.

The other technique does not reflux the LDH after precipitation. The precipitate is allowed to stir, in its mother liquor, under an inert gas, for one hour, and then stopped. LDH of this type is known as fresh or raw LDH.

In both cases, the precipitate is then separated from its mother liquor, by centrifugation and washed, with a recommended high-purity deionized water (Millipore systems). This washing step is usually performed two to three times in order to ensure that any unreacted cations/anions are removed from the precipitate.

The difference between fresh and aged LDH is in the degree of cation ordering and crystallinity. The aged LDH shows stronger, well resolved, LDH lattice vibrational modes and sharper, more intense diffraction peaks. These two factors can be attributed to Ostwald ripening.[66]

Ostwald ripening is a process that is worth mentioning. It is a process that attempts to describe the favorable energetics of large crystals versus small crystals, based on surface area and volume. When LDH crystals are first formed from solution, they have a larger surface area and a smaller volume. During the aging process, the crystals end up having a smaller surface area and a larger volume. The energetics of

this difference stem from the fact that molecules or ions on the surface of a crystal are less stable than the ones that exist within a crystal lattice. From a kinetic versus thermodynamic point-of-view, the small crystals are kinetically favored, since they form first; the large crystals are thermodynamically favored because they are formed at the expense of the smaller crystals. With this in mind, the Ostwald process is based on a dissolution-precipitation (re-precipitation) mechanism.

The favorable energetics of large versus small crystals can be seen through the preparation of “rock candy” or “rock salt” from hot water solutions, using a piece of string (and preferably a seed crystal).

1.7 Common Characterization Techniques

1.7.1 Fourier-Transform Infrared Spectroscopy

Solid-state Fourier-transform infrared spectroscopy (FT-IR) is one of the principal tools for LDH characterization. Not limited to, but mainly used in the mid-IR region (4000 – 250 cm^{-1}), it is primarily used for functional group identification, but it also has been invaluable in the metal hydroxide lattice region. The success of anion exchange with LDH is usually first seen through FT-IR spectroscopy.

Within the sub-range of the mid-IR region (3000 cm^{-1} to 1000 cm^{-1}), many anions of interest will show up.[67-69] Most anions have vibrational modes below 1000 cm^{-1}, and are also taken into account. It is vital to know that FT-IR spectroscopy is only useful if there is an oscillating dipole associated with a particular vibrational mode.[70] This rules out the LDH halides (Cl^-, Br^-, I^-), because these anions do not have any internal modes of vibration.

Also within this range, the hydroxide stretching modes and water bending modes occur. The hydroxide stretching modes (around 3700 – 3000 cm^{-1}) result from the complicated metal-hydroxide bonds and from water, while the water bending mode is strictly from the water molecules.

Although not as widespread but equally important, FT-IR can describe the LDH lattice vibrations with an excellent degree of validity. Below 1000 cm^{-1}, all of the metal (hydr)oxide stretchings and bendings occur. These vibrations are dependent on the type of metals in the LDH, so different metals will lead to different vibrational mode assignments.[71,72] Figure 1.4 shows a FT-IR spectrum of an aged 2:1 Mg-Al LDH-Cl, within the range from 4000 cm^{-1} to 250 cm^{-1}.

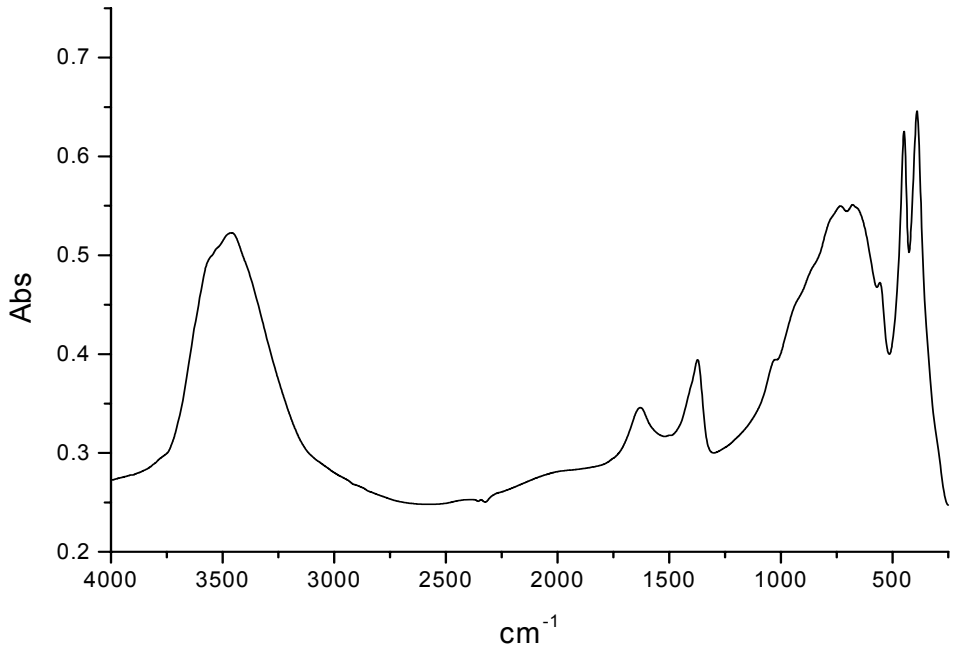

Figure 1.4: Solid-State FT-IR spectrum of aged 2:1 Mg-Al LDH-Cl using CsI optics and background. Abs stands for absorbance.

Important differences exist between 2:1 Mg-Al LDH-Cl materials that have been aged and those that have not. These differences will be presented and discussed in more detail in Chapter 6.

Within the technique of FT-IR spectroscopy, a fairly new method has been used in order to study the possible effects of orientation about the LDH crystals. This method places a few drops of a dilute LDH suspension onto preformed supports (BaF_2, CdTe or polyethylene). This causes the few LDH crystals to lie flat on the selected support, such that all z-polarized vibrational modes will be absent or obscured, leaving only the x,y-polarized modes to be observed. This method was first utilized with LDH-ferrocyanide, which showed a difference between the conventional (KBr) and oriented (BaF_2) spectra in the metallocyanide stretching region (2200 – 2000cm^{-1}).[73] More will be discussed about this particular region in Chapter 2.

1.7.2. Powder X-Ray Diffraction

Powder X-ray diffraction (XRD) is another principal tool for LDH characterization. As previously mentioned, XRD was the tool that linked the synthetic magnesium-aluminum hydroxides to hydrotalcite.

The application of X-ray diffraction is possible through the Bragg equation; $n\lambda = 2d\sin\theta$. This equation must be used to determine which angles are possible for the coherent scattering of X-rays (by diffraction) and the distance between adjacent crystallographic planes. By convention, n is equal to unity, and λ is the wavelength of the material used as the X-ray source (for this work, Cu$K\alpha$ radiation was used, with λ = 1.540562 Å). The diffraction angles are always reported in degrees 2θ, not degrees θ,

because the angles between the incident beam and diffraction beam are always in values of 2θ.

XRD is used to obtain several main pieces of information about LDH: crystallinity, interlayer spacings, particle sizes, repeat layer distances and the distances between nearest neighbors (adjacent metals in the same sheet or hydroxides on the same side of a lattice sheet).

Since LDH studied in this work has a rhombohedral crystal structure, there are only two lattice parameters that are needed. The lattice parameters are: a and c. More will be discussed about these two parameters within this section.

The XRD patterns for LDH are typically scanned from 5° to 70° (2θ), although some scans require a start from 2° (2θ). This is common for LDH that have large intercalated organic or inorganic anions. The other parameters (step-size and dwell time) are up to the user but scans using a step-size of 0.05° and a dwell time of 1.0 seconds produce high-quality patterns. It is advisable that at least 0.1 g of sample (more is preferred) is available, to obtain good intensities in the XRD runs.

Since the LDH that was studied throughout this work has the rhombohedral polytype, the indexing of all patterns follows the simple selection rule for rhombohedral crystal structures: (- h + k + l) = 3n. This means that the reflections will have Miller indices that combine to yield multiples of three. By this rule, the common reflections for a $3R_1$ polytype (based on interlayer spacings) are 003, 006, 009 (0012), 012 and 015. These reflections are generally seen from 2° or 5° (2θ) up to 60° (2θ). After 60° (2θ), depending on the interlayer anion and overall crystallinity, two peaks are commonly

observed. These two peaks are assigned as the 110 and 113 reflections and are based on the actual LDH lattice sheets.

The first piece of information, crystallinity, is observed by the shape and appearance of each peak in the pattern. Aged LDH produce sharp, intense peaks, which correspond to large, well crystalline material. Fresh or raw LDH produce broad, less intense peaks, which correspond to small, less crystalline material (Figure 1.5). Depending on the type of anion, the d_{003} reflection usually shows up as the first reflection between 2° and 12° (2θ) and is given the notation, c_0. The lattice parameter, c, describes the repeat layer distance (3R), and is generally found by multiplying the d_{003} spacing by three: $c = 3d_{003}$ or $c = 3*c_0$.

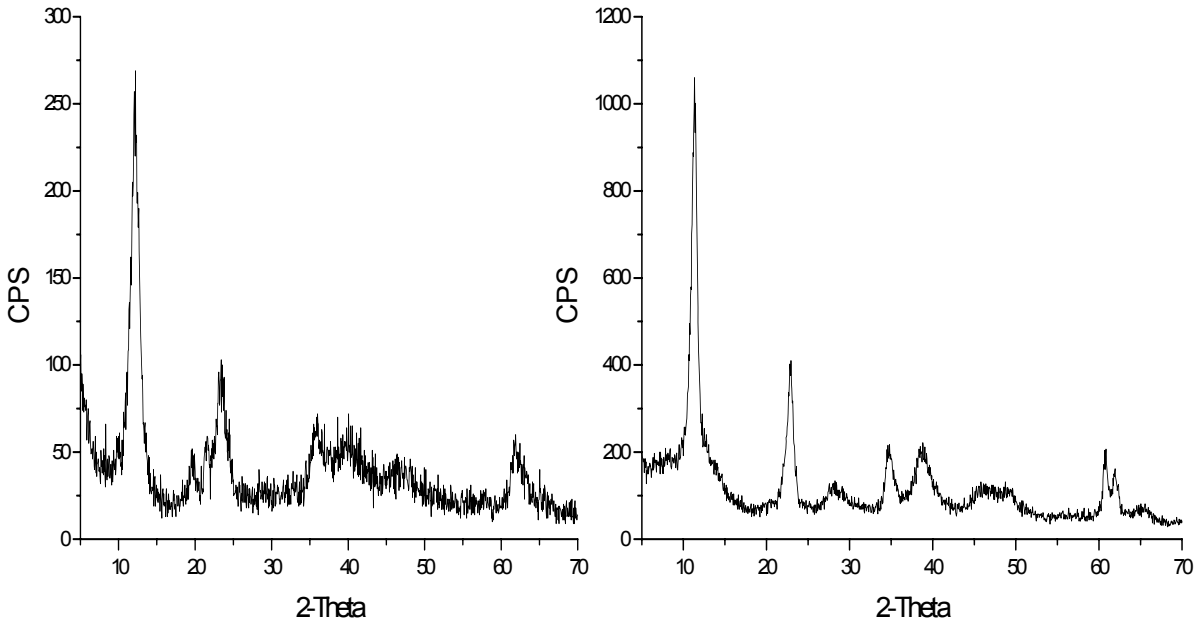

Figure 1.5: PXRD patterns of a 2:1 Mg-Al LDH-Cl. Left: fresh LDH and right: LDH with aging. CPS stands for counts per second.

There is also another way to estimate the repeat layer distance that is based on the intensities of the several (commonly three) reflections (003, 006 and 009). In the aged LDH from Figure 1.5, the 003 reflection (~11° (2θ)) is around twice as intense as the 006 reflection (~22° (2θ)) and around three times as intense as the 009 reflection (~35° (2θ)). This observation is also found by the interlayer spacings for the first three reflections, such that $2*d_{006} = d_{003}$, $3*d_{009} = d_{003}$. From this observation, an estimate of the repeat layer distance, c' notation, can be approximated: $c' = \frac{1}{n}(003 + 2*006 + 3*009 + ... + n*00(3n))$. This approximation is superior to the previous two equations, because it takes into account the interlayer spacings from different Bragg reflection angles.

The second piece of information, interlayer spacing or d-spacing, is found by the information from the 003 reflection. Since each of these reflections has a d-spacing associated with them, by convention they are written as d_{003}, d_{006}, d_{012}, etc. The interlayer spacing is the distance from one LDH sheet to the next LDH sheet. As mentioned before, this is where the intercalated anions reside, and judging by the relative sizes of the anions, the interlayer spacings will be noticeably different. If there are two different sized anions incorporated into separate crystallites in a sample of LDH, two different sets of reflections can be observed (d_{003} for anion A and d_{003} for anion B and d_{006} for anion A and d_{006} for anion B). If the two anions are intercalated in the same layer, the LDH will have a d-spacing dominated by the larger anion; if the two anions are in different layers in the same crystallite, the LDH may have interstratified structures with suitably large c values.

From the interlayer spacing, the actual space that the anion has in the interlayer is determined by calculating what is known as the gallery height. The gallery height is calculated by subtracting the average layer thickness from the interlayer spacing. The reason why this is done is due to the pendant hydroxides that reside in the LDH interlayer. The average thickness of one LDH sheet is the vertical distance from hydroxide to hydroxide (H to H), only if the two hydroxides are on different faces (asterisk to asterisk) of the D_{3d} $M(OH)_6$ structure (Figure 1.6).

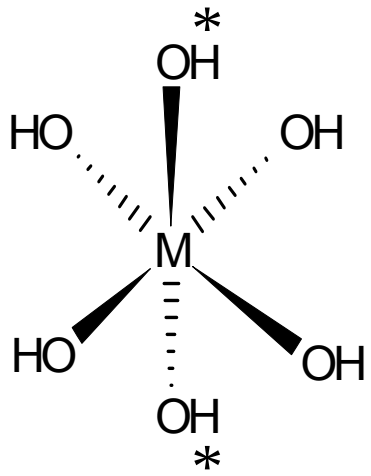

Figure 1.6: Schematic model of a $M(OH)_6$ (D_{3d} symmetry) structure: same sides of a triangular face (all bold or all dashed) or different sides (some bold and some dashed).

The third piece of information, about the lattice hydroxide sheets, is found from the d_{110} and d_{113} reflections. Generally the d_{110} reflection is only used and sometimes the two overlap. These two peaks are usually located at the end of the scan at around 61° and 64° (2θ). The d_{110} reflection provides information about the other lattice parameter, a. This lattice parameter corresponds to the distance between two adjacent hydroxide groups, on the same side of the LDH layer (refer to Figure 1.6) or the average

distance between two nearest metal ions. The lattice parameter, a, is found by multiplying the d_{110} by two ($a = 2*d_{110}$).

There is one other piece of information that the d_{110} reflection can give. When obtaining a XRD pattern, a peak list report should also be produced. A peak list report provides all of the necessary information about a particular sample, such as the peak positions (in degrees 2θ), d-spacings for each peak (in Angstroms) and particle sizes (in Angstroms). LDH researchers obtain the particle size based on the d_{003} and d_{110} reflections, and use that for the average size of the LDH crystals. The d_{003} peak width gives c-axis size (particle thickness), and the d_{110} gives a, b particle size (particle diameter). The Datascan 3.2™ software program uses the Scherrer equation, $t = \lambda / \beta*\cos\theta_B$, to determine the particle (or crystallite) size, based on their measured widths. In this formula, β is the full-width at one-half of the maximum intensity and θ_B is the angle that is half-way between two angles, whose respective intensities are zero.[74] Although this is not as reliable as using particle size analyzers or the SEM scales, it gives a good enough idea about LDH particle sizes.

Both lattice parameters are dependent by the amount of trivalent metal in the LDH layer. It has been shown that as the amount of trivalent metal increases, both lattice parameters decrease.[75]

An increase in the trivalent metal will affect the lattice parameter, a, because the trivalent ionic radii are typically smaller than the divalent ionic radii. The higher charge and smaller ionic radii will lead to shorter M-OH bond distances, which will result in shorter metal to metal (or same side hydroxide to hydroxide) distances.

An increase in the trivalent metal will affect the lattice parameter c, because more trivalent metal content will result in more positive unit charges. An increase in the amount of positive charges will result in more anionic uptake, which will ultimately increase the electrostatic attraction, thus shortening the distance between layer and interlayer.

1.7.3 Elemental Analysis (Flame Atomic Absorption Spectroscopy) and Combustion Analysis (Carbon, Hydrogen and Nitrogen)

Atomic absorption spectroscopy (AAS) is the last of the principal tools for LDH characterization. This technique takes advantage of each element on the periodic table, absorbing energy characteristic for that particular element (a quantum mechanical effect).[76] Much like a fingerprint being used to identify a certain individual, each element absorbs energy at a specific wavelength, one that all other elements will not.

An element to be tested is dissolved (ionized) in an aqueous acidic solution (matrix), and then the solution is passed through a flame, by a nebulizer. The flame reduces the ions to their respective atoms, in which energy, by a special external lamp containing that same element, is directed through the flame. The energy emitted by the element lamp will, in general, only be absorbed by the same element passing through the flame; all other elements will not absorb this specific energy. Since concentration is directly proportional to absorbance, the concentration (or amount) of the element can easily be calculated.

There are two flame types that are used in AAS, so there are two types of burner heads. The first type uses acetylene as the fuel and air as the oxidizing agent and the second type uses acetylene as the fuel and nitrous oxide (N_2O) as the oxidizing agent. Disregarding the complexities, the nitrous oxide burner head is primarily used for elements that tend to form oxides easily within the standard air/acetylene flame. The majority of elements require the air/acetlyene burner head, while a few need the N_2O/acetylene burner head. With regard to the solvents used for ionizing the elements, some of the elements require different components. Most of the elements are prepared, for testing in a 2-5% HNO_3(aq) solution. Some elements require a combination of HNO_3(aq) and HCl(aq) and some even require dissolution in a HF(aq) solution. The elements that will be tested within this work require a 5% HNO_3(aq) solution and the air/acetylene burner head, except for aluminum, which requires a HNO_3/HCl solution and the N_2O/acetylene burner head.

For carbon, hydrogen and nitrogen content, materials are sent to laboratories that specialize in determining their percent amounts. These laboratories typically place a small amount of sample in a special holder, flush the holder with oxygen gas, and then ignite it. This procedure is designed to make CO_2, N_2, and H_2O quantitatively. These molecules are then separated by chromatography and estimated by thermal conductivity effects.

1.7.4 Thermal Decomposition of LDH

Although not a principal tool for characterization, the thermal decomposition of LDH can yield important information about its chemical formula and decomposition

products. The standard technique is thermogravimetric analysis (TGA). From the TGA traces, the derivative of the weight-loss or mass-loss percent with respect to temperature can also be calculated and is known as DTGA. TGA and DTGA are complementary, because TGA describes the amounts of material lost, per increasing temperature, and DTGA provides the exact temperatures where the maximum amount of loss occurs (known as reduction points).

TGA is a simple technique that basically heats a material within a programmed temperature range, under a variety of gases. A small amount of LDH material is placed in a special holder that rests on the surface of a precision balance. A specific temperature range and heating rate are programmed into the instrument's software and the material is then slowly or quickly pyrolyzed. As the material is being pyrolyzed, it will begin to lose mass, either gradually or sharply, at specific temperatures. If no side reactions are wanted during pyrolysis, inert gases, such as nitrogen, helium and argon are used. Gases such as air are used for oxidation pyrolysis and gases such as hydrogen are used for reduction pyrolysis. A steady stream of cool water is needed to flow through the heating mantle in order to prevent damage to the instrument. For most TGA instruments, nitrogen gas is also passed through the balance chamber at the same rate or faster than the gas in the sample compartment.

The thermal decomposition, or pyrolysis, for many LDH materials have been extensively studied, so that a few points of interest can be explained.[77,78] For the more common LDH-CO_3, within the temperature range of 30 – 110°C, surface (or weakly adsorbed) water is driven off. Proceeding in temperature, from 110 – 250°C, the interlayer water gets driven out. Within this range, the LDH becomes dehydrated, with

the interlayers and intercalated carbonate remaining intact, to the eventual collapse of the LDH interlayers. The final range, from around 300 – 500°C, dehydroxylation of the LDH layers (to form the mixed oxides) and decarbonation (decomposition of the carbonate) occur, resulting in a mixture of oxide products, eventually including spinels. Figure 1.7 shows a TGA and DTGA trace for a 2:1 Mg-Al LDH-CO_3.

LDH containing complex organic anions, or more complex anions than carbonate or the halides will produce TGA/DTGA traces that will be considerably different than the traces shown in Figure 1.7. Most organic anions will have complicated thermal decomposition steps that may be even more complicated when incorporated into LDH. Also of note, most organic anions develop into what is known as a char, which is mostly carbon (soot or ash), during pyrolysis. This char can be burned off by oxidizing gases, such as air or oxygen, but will leave elemental carbon behind, by inert gases, such as nitrogen, helium or argon.

The consequences of the charring ability of LDH with organic anions are important for flame retardation materials research.

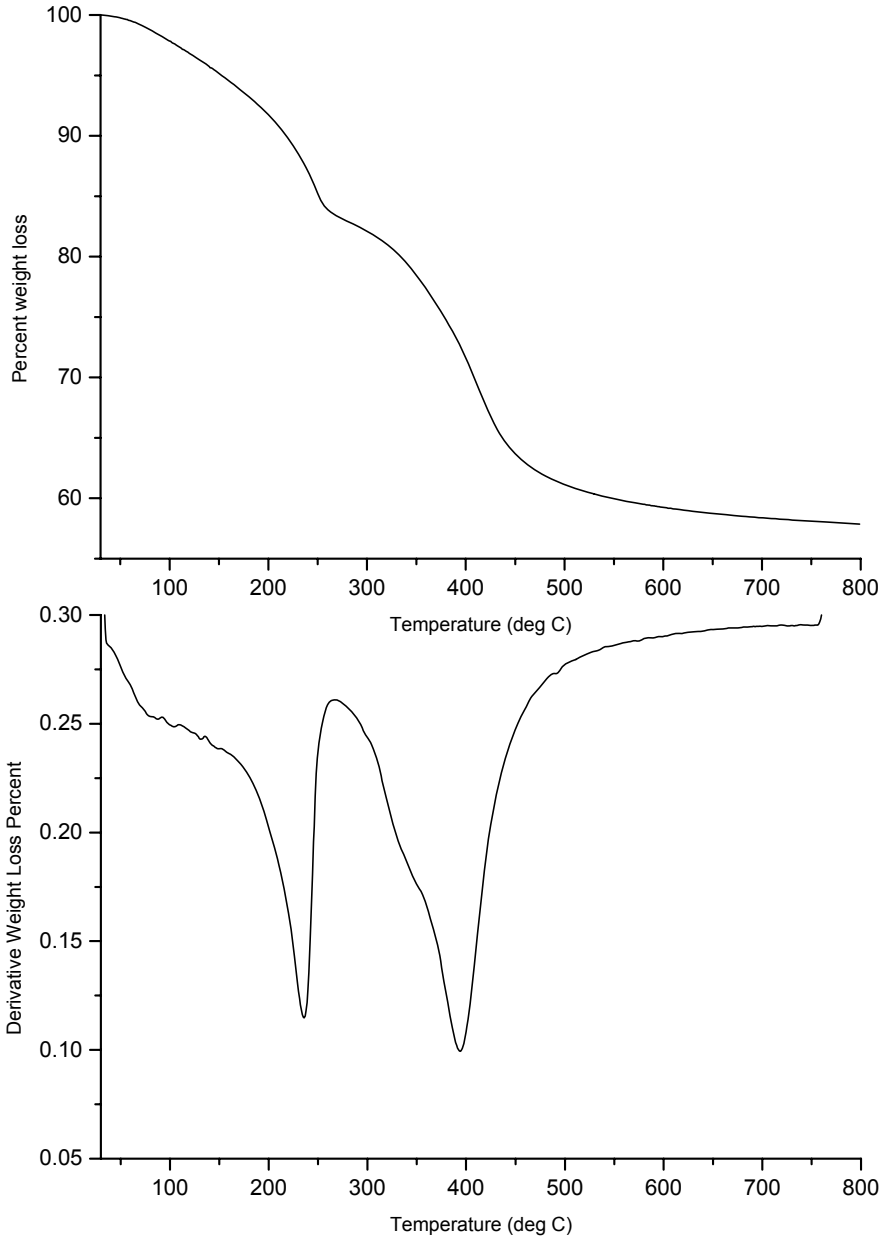

Figure 1.7: TGA (top) and DTGA (bottom) traces for a 2:1 Mg-Al LDH-CO_3.

From the information above, and the TGA/DTGA traces in Figure 1.7, the partly overlapping steps in the thermal decomposition route for a 2:1 Mg-Al LDH-CO_3 (pyrolyzed under nitrogen gas) can be deduced:

Step 1: $[2Mg_2Al(OH)_6](\text{interlayer } 2H_2O)[CO_3](\text{adsorbed } H_2O) \rightarrow$

$[2Mg_2Al(OH)_6](\text{interlayer } 2H_2O)[CO_3] + \text{adsorbed } H_2O$ (30-100 °C)

Step 2: $[2Mg_2Al(OH)_6](\text{interlayer } 2H_2O)[CO_3] \rightarrow [2Mg_2Al(OH)_6][CO_3]$

+ interlayer $2H_2O$ (110-250 °C)

Step 3: $[2Mg_2Al(OH)_6][CO_3] \rightarrow 2Mg_2AlO_6 + 3H_2 + CO + O_2$ (300-500 °C)

The Mg_2AlO_6 is not an actual phase, but a mixture of $MgAl_2O_4$ and oxides of magnesium and aluminum.

Further heating to temperatures up to 1000 °C produces no change other than spinel (Mg_2AlO_4) along with some mixed metal oxides. The formation of spinel, from metal oxides cannot be observed in the TGA/DTGA traces because it involves no change in weight loss. Characterization techniques such as FT-IR, SEM/TEM and XRD are used to identify the existence of spinel.

One interesting point about the formation of Mg-Al spinel is warranted. The spinel structure can be seen at temperatures around and exceeding 500 °C, but when rehydrated in water (with an appropriate anion), LDH can be re-formed. This is known as the memory effect.[79,80] Although the memory effect will not result in 100% conversion back to LDH, it is a very effective technique that many researchers use when they want to exchange carbonate for other anions. Spinel formed at temperatures around 1000°C will not convert back to LDH by the memory effect, regardless of how hard one tries to rehydrate it. These properties of Mg_2AlO_4 closely resemble the properties of α-Al_2O_3.

LDH that contain metals susceptible to reduction/oxidation or anions more complicated than carbonate will undoubtedly show different thermal decomposition traces but the main areas of decomposition should still be observed.

Although TGA was discussed as the premier method for obtaining information about the thermal decomposition of LDH, another popular technique is known as Differential Scanning Calorimetry (DSC). This method provides information about energy changes as a function of temperature variations. Unfortunately the cost of a DSC instrument has relegated most LDH research groups to remain using TGA.

1.7.5 Visible-Ultraviolet Spectroscopy (Vis-UV)

UV-Vis (Vis-UV) spectroscopy is similar to TGA in that it is not considered a principal characterization tool for LDH. The possible exception is when transition metals are used for the LDH lattice construction or are intercalated/adsorbed, as complexes. Since most transition metal salts are colored (simple salts and complexes) and have various electronic structures, UV-Vis spectroscopy can be an important tool.[81-83]

Some examples for which UV-Vis spectroscopy should be used, include transition metal complexes that undergo symmetry changes ($O_h \rightarrow D_{3d}$ by trigonal distortion), geometric changes through ligand field strengths (T_d $[NiCl_4]^{2-}$ vs. D_{4h} $[Ni(CN)_4]^{2-}$, electronic structure changes upon oxidation-reduction (d-d transitions, if any), and color changes arising from loss/gain of coordinate-covalently bonded ligands (red, O_h, CoL_6 and blue, T_d, CoL_4). The use of UV-Vis spectroscopy is not only useful in the visible region, due to the colors of most transition metal compounds, but also in UV region, where charge-transfer bands occur (e.g. Fe(III) with OH ligands). The UV-Vis

spectra of LDH materials are commonly collected by diffuse reflectance or transmission, because these materials are solids.

The UV-Vis spectra of transition metals incorporated into LDH are generally interpreted by comparison with known compounds.

1.7.6 Scanning/Transmission Electron Microscopy (SEM/TEM)

SEM/TEM have not been principal characterization tools in the past but they are quickly attaining such status because they can provide important information about the texture and morphology of the LDH crystallites. Improvements in magnification power and resolution over the last couple of decades have resulted in more and more research groups incorporating these microscopes into their research and publications.

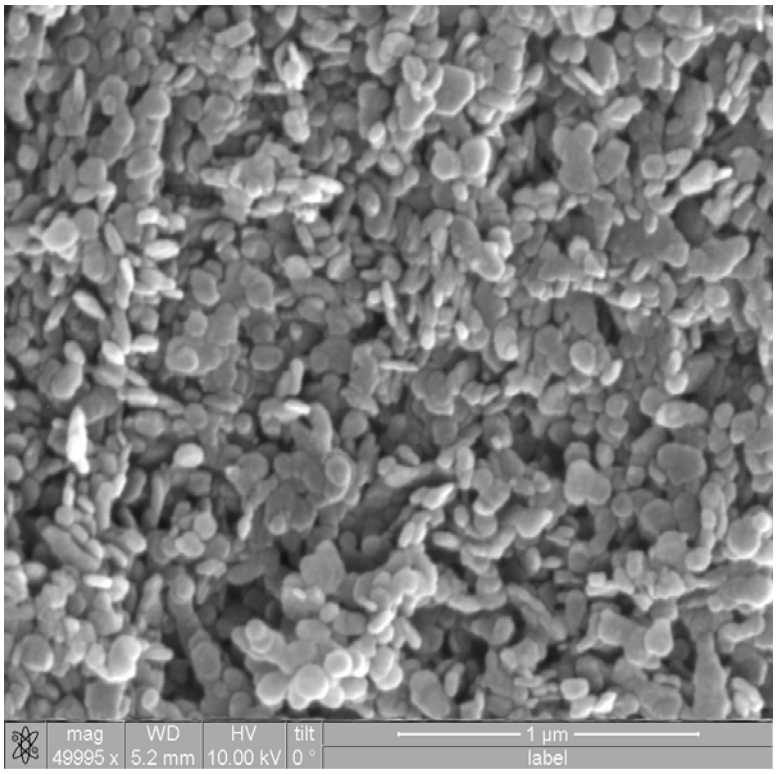

Figure 1.8: SEM image of an aged 2:1 Mg-Al LDH-Cl (magnification at 50,000X)

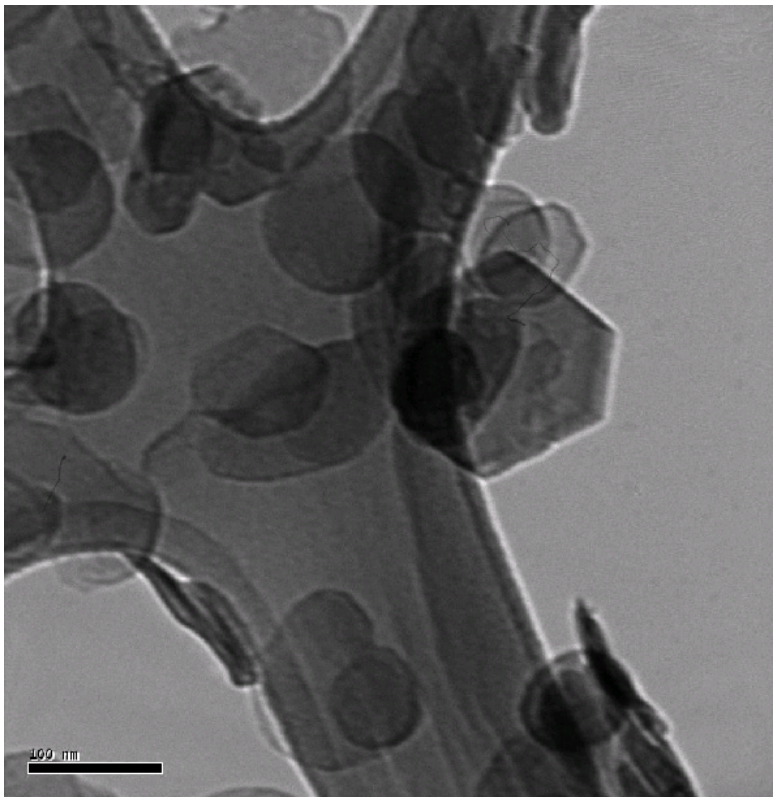

Figure 1.9: TEM image of an aged 2:1 Mg-Al LDH-Cl with zinc (magnification at 47,000X)

As stated in the XRD section earlier, LDH has a rhombohedral crystal polytype. When viewed by SEM, the LDH crystals appear as hexagonally shaped platelets[84] (Figure 1.8)**,** but the actual hexagonal shape is more clearly seen by the TEM image (Figure 1.9).

This is not a contradiction, because the rhombohedral polytype refers to the layer stacking sequence and the hexagonal platelets refer to overall crystal growth. The hexagonal platelets are the most common image for LDH with simple anions (halides, nitrate and carbonate), but LDH has been observed to have quite different morphologies with certain organic anions.[85]

Also previously stated in the XRD section, LDH prepared by contrasting post-synthesis techniques (aging versus fresh) have different particle sizes. SEM/TEM have been used to physically observe the much smaller LDH crystals, obtained without aging, compared to the much larger LDH crystals, obtained by aging. The fresh LDH materials appear as clumps or aggregates, with some resemblance to the more refined hexagonal platelets.

SEM preparation involves placing a small amount of sample (typically a diluted suspension) on carbon or copper tape on the top of specially made SEM mounts. The sample is then placed in a vacuum chamber, pumped down to low pressures, and then sprayed with a conductive coating (gold or a gold/palladium mixture). The gold or gold/palladium coating helps dissipate the negative charge of the impinging electrons, which would build up on such non-conductive materials, such as LDH and degrade the imaging.

1.7.7 Other Notable Characterization Techniques

Other techniques that have been used in LDH study have included Neutron diffraction, Raman spectroscopy, XANES (x-ray absorption, near-edge structure), XPS (x-ray photoelectron spectroscopy), EXAFS (extended x-ray absorption, fine structure), Mössbauer Spectroscopy, EPR (electron paramagnetic resonance spectroscopy) and NMR (nuclear magnetic resonance spectroscopy) and BET (Brunauer, Emmett and Teller, for surface area and pore size). None of these methods were used for any of the projects in this work, so they will not be discussed further.

One notable technique that deserves mentioning is single crystal X-ray diffraction. Under normal circumstances, this technique is one of the most powerful and accurate tools for determining atomic positioning, bond distances and bond angles. Unfortunately, this technique requires crystals that are relatively large and pure (a single crystal). Synthetic LDH crystals so far prepared are too small and aggregated in order to use this technique, but single crystal X-ray diffraction has been successfully used on hydrotalcite and many related minerals.[86] Perhaps with time, improvements in the single-crystal x-ray instrumentation and in preparative technique will result in the successful elucidation of such small crystals.

1.8 References

(1) de Roy, A.; Forano, C.; El Malki, K.; Besse, J.P. In Synthesis of Macroporous Materials; Occelli, M.L., Robson, H.E., Eds., Van Nostrand Reinhold: New York, 1992; Vol. 2, p108.

(2) Trifio, F.; Vaccari, A. in Comprehensive Supramolecular Chemistry; Atwood, J.L., Manicol, D.D., Davies, J.E.D., Vogtle, F., Eds.; Pergamon: Oxford, 1996; Vol. 7, p251.

(3) Layered Double Hydroxides: Present and Future; Rives, V., Ed.; Nova Science Publishers: Huntington, New York, 2001.

(4) Braterman, P. S.; Xu, Z. P., Yarberry, F. In *Handbook of Layered Materials*; Auerbach, S. M., Carrado, K. A., Dutta, P. K., Eds; Marcel Dekker: New York, 2004; p373.

(5) Taylor, H.F.W. *Miner. Mag*. **1973**, *37*, 338.

(6) Hoffmeister, W.; von Platen, H. *Cryst. Rev*. **1992**, *3*, 3.

(7) Besserguenev, A.V.; Fogg, A.M.; Francis, R.J.; Price, S.J.; Isupov, V.P.; Tolochko, B.P.; O'Hare, D. *Chem. Mater*. **1997**, *9*, 241.

(8) Nayak, M.; Kutty, T.R.N.; Jayaraman, V.; Periaswamy, G. *J. Mater. Chem*. **1997**, *7*, 2131.

(9) Serna, C.J.; Rendon, J.L.; Iglesias, J.E. *Clays Clay Miner*. **1982**, *30*, 180.

(10) Rius, J.; Allmann, R. *Z. Kristallog*. **1984**, *168*, 133.

(11) Song, Y.; Moon, H.S. *Clay Miner*. **1998**, *33***,** 285.

(12) Rives, V.; Kannan, S. *J. Mater. Chem*. **2000**, *10*, 489.

(13) Bellotto, M.; Rebours, B.; Clause, O.; Lynch, J.; Bazin, D.; Elkaiem, E. *J Phys. Chem*. **1996**, *100*, 8527.

(14) Mortland, M.M.; Gastuche, M.C. *Compt. Rend.* **1962**, *225*, 2131.

(15) van Oosterwyck-Gastuche, M.C.; Brown, G.; Mortland, M.M. *Clay Miner*. **1967**, *7*, 177.

(16) Bookin, A.S.; Drits, V.A. *Clays Clay Miner.* **1993**, *41*, 551.

(17) Bookin, A.S.; Cherkashin, V.I.; Drits, V.A. *Clays Clay Miner.* **1993**, *41*, 558.

(18) Newman, S.P.; Jones, W.; O'Connor, P.; Stamires, E.N. *J. Mater. Chem.* **2002**, *12*, 153.

(19) Johnson, T.E.; Martens, W.; Frost, R.L.; Ding, Z.; Kloprogge, J.T. *J. Raman. Spectrosc*. **2002**, *33*, 604.

(20) Lowenstein, W. *Am. Mineral*. **1954**, *39*, 92.

(21) Pauling, L. The Nature of the Chemical Bond. 3rd ed: Cornell University Press, New York, 1960.

(22) Flink, G. *Arkiv Kemi. Min. Geol*. **1910**, *3*, 1.

(23) Flink, G. *Z. Kryst. Min.* **1914**, *53*, 409.

(24) Treadwell, W.D.; Bernasconi, E. *Helv. Chim. Acta* **1930**, *13*, 500.

(25) Feichnecht, W.; Gerber, M. *Helv. Chim.Acta* **1942**, *25*, 131.

(26) Ingram, L.; Taylor, H.F.W. *Mineral Mag*. **1967**, *36*, 465.

(27) Allmann, R. *Am. Mineral*. **1968**, *53*, 1057.

(28) Ulibarri, M.A.; Hernandez, M.J.; Cornejo, J. *J. Mater. Sci*. **1991**, *26*, 1512.

(29) Kang, M.J.; Rhee, S.W.; Moon, H.; Neck, V.; Fanghanel, T. *Radiochimica Acta* **1996**, *75*,169.

(30) Constantino, U.; Casciola, M.; Massinelli, L.; Nocchetti, M.; Vivani, R. *Solid State Ionics* **1997**, *97*, 203.

(31) Crepaldi, E. L.; Pavan, P.C.; Valim, J.B. *Chem. Comm*. **1991**, 155

(32) Miyata, S.; Kamura, T. *Chem. Lett.* **1973**, 843.

(33) Miyata, S. *Clays Clay Miner*. **1983**, *31*, 305.

(34) Beekman, S.M. *J. Am. Pharm. Assoc*. **1960**, *49*, 191.

(35) Gordijo, C.R.; Barbosa, C.A.S.; Ferreira, A.M.D.; Contantino, V.R.L.; Silva, D.D.O. *J. Pharm. Sci*. **2005**, *94*, 1135.

(36) Choy, J.H.; Kwak, S.Y.; Park, J.S.; Jeong, Y.J. *J. Mater. Chem.* **2001**, *11*, 1671.

(37) Itaya, K.; Chang, H.C.; Uchida, I. *Inorg. Chem*. **1987**, *26*, 624.

(38) Qiu, J.B.; Villemure, G. *J. Electroanal. Chem*. **1997**, *428*, 165.

(39) Fisher, H.R.; Geilgens, L.H.. Nanocomposite Material. U.S. Patent 6,372,837, April 2, 2002.

(40) Miyata, S.; Kuroda, M.. Method of Inhibiting the Thermal or Ultraviolet Degradation of Thermoplastic Resin and Thermoplastic Resin Compositions having Stability to Thermal or Unltraviolet Degradation. U.S. Patent 4,299,759, November 10, 1981

(41) Soma, I.; Wakano, H.; Takahashi, H.; Yamaguchi, M. . Flame-Resistant Vinyl Chloride Resin Compositions. Jap. Patent 50,063,047, May 29, 1975

(42) Zammarano, M.; Massimiliano, F.; Bellayer, S.; Gilman, J.W.; Meriani, S. *Polymer* **2005**, *46*, 9314.

(43) M.C. Hermosin, I. Pavlovic, M.A. Ulibarri, J. Cornejo *J. Environ. Sci. Health* **1993**, *A28*, 875.

(44) Robins, D.S.; Dutta, P.K. *Langmuir* **1996**, *12*, 402.

(45) Corma, A.; Fornes, V.; Martinaranda, R.M.; Rey, F. *J. Catal.* **1992**, *58* ,134.

(46) Suzuki, E.; Ono, Y. *Bull. Chem. Soc. Jpn.* **1988**, *61*, 1008.

(47) Laycock, D.E.; Collacott, R.J.; Skelton, D.A.; Tchir, M.F. *J. Catal*. **1991**, *130*, 354.

(48) Roelofs, J.C.A.A.; van Dillen, A.J.; de Jong, K.P. *Catal. Today* **2000**, *60*, 297.

(49) Bhattacharyya, A.; Chang, V.W.; Schumacher, D.J. *Appl. Clay Science* **1998**, *13*, 317.

(50) Finta, Z.; Hell, Z.; Balan, D.; Cwik, A.; Kemeny, S.; Figueras, F. *J. Molec. Catal. A: Chem.* **2000**, *161*, 149.

(51) Padmasri, A.H.; Venugopal, A.; Kumari, V. D.; Rama Rao, K.S.; Kanta Rao, P. *J. Molec. Catal. A: Chem.* **2002**, *188*, 255.

(52) Peppley, B.A.; Amphlett, J.C.; Kearns, L.M.; Mann, R.F. *App. Catal. A: General* **1999**, *179*, 21.

(53) Pitsch, S.; Eschenmoser, A.; Gedulin, B.; Hui, S.; Arrhenius, G. *Origins Life Evol. Biosphere* **1995**, *25*, 294.

(54) Boclair, J.W.; Brister, B.D.; Jiang, J.; S. Lou, S.; Wang, Z.; Yarberry, F.; Braterman, P.S. *Origins of Life Evol. Biosphere* **2001**, *31*, 53.

(55) Ross, G.J.; Kodama, H. *The Am. Mineral.* **1967**, *52*, 1036.

(56) Constantino, V.R.L.; Pinnavaia, T.J. *Inorg. Chem*. **1995**, *34*, 883.

(57) Ogawa, M.; Asai, S. *Chem. Mater*. **2000**, *12*, 3253.

(58) Mascolo, G.; Marino, O. *Mineralogical Magazine* **1980**, *43*, 619.

(59) Ona-Nguema, G.; Abdelmoula, M.; Joran, F. *Environ. Sci. Technol.* **2002**, *36*, 16.

(60) Yarberry, F. Layered Double Hydroxides via Aluminate. Ph.D. Dissertation, University of North Texas, Denton, TX, 2002.

(61) Lopez, T.; Bosch, P.; Ramos, E.; Gomez, R.; Novaro, O.; Acosta, D.; Figueras, F. *Langmuir* **1996**, *12*, 189.

(62) de A.A. Soler-Illia, G.J.; Candal, R. J.; Regazzoni, A.E.; Blesa, M.A. *Chem. Mater*. **1997**, *9*, 184.

(63) Iyi, N.; Maksumoto, T.; Kaneko, Y.; Kitamura, K. *Chem. Lett.* **2004**, *33*, 1122.

(64) Refait, P.; Genin, J.M.R. *Hyperfine Interact.* **1991**, *69*, 827.

(65) Xu, Z.P.; Zeng, H.C. *Chem. Mater*. **2001**, *13*, 4555.

(66) Ostwald, W. *Z. Phys. Chem*. **1897**, *22*, 289.

(67) Kloprogge, J.T.; Wharton, D.; Hickey, L.; Frost, R.L. *Am. Mineral*. **2002**, *87*, 623.

(68) Newman, S.P.; Jones, W. *New J. Chem*. **1998**, *22*, 105.

(69) Twu, J.; Dutta, P.K. *Chem. Mater.* **1992**, *4*, 398.

(70) Atkins, P.W. Physical Chemistry, 6th ed: W.H. Freeman and Co., New York, 1998

(71) Clause, O.; Gazzano, M.; Trifiro, F.; Vaccari, A.; Zatorski, L. *Appl. Catal*. **1991**, *73*, 217.

(72) Hansen, H.C.B.; Koch, C.B.; Taylor, R.M. *J. Solid State Chem*. **1994**, *113*, 46.

(73) Tan, C.; Zhao, J.; Braterman, P.S. *Mater. Res. Bull*. **1994**, *29*, 1217.

(74) Cullity,B.D.; Stock, S.R. Elements of X-Ray Diffraction 3rd ed, Prentice Hall: Upper Saddle River N.J., 2001.

(75) Brindley, G.W.; Kikkawa, S. *Am. Mineral.* **1979**, *64*, 836.

(76) Robinson, J.W. Atomic Spectroscopy: 2nd ed: Marcell Dekker, New York, 1996.

(77) Lopez-Salinas, E.; Torres-Garcia, E.; Garcia-Sanchez, M. *J. Phys. Chem. Solids* **1997**, *58*, 919.

(78) Pesic, L.; Salipurovic, S.; Markovic, V.; Vucelic, D.; Kagunya, W.; Jones, W. *J. Mater. Chem.* **1992**, *2*, 1069.

(79) Beres, A.; Palinko, I.; Bertrand, J.C.; Nagy, J.B.; Kiricsi, I. *J. Mol. Struct.* **1997**, *410- 411*, 13.

(80) Kooli, F.; Depege, C.; Ennaqadi, A.; de Roy, A.; Besse, J.P. *Clays Clay Miner.* **1997**, *45*, 92.

(81) Lindon, J.C.; Tranter, G.E.; Holmes, J.L. Encyclopedia of Spectroscopy and Spectrometry. New York: Academic Press, 2000.

(82) Evans, J.; Pillinger, M.; Zhang, J.J. *J. Chem. Soc., Dalton Trans.* **1996**, *14*, 2963.

(83) Velu, S.; Shah, N.; Jyothi, T.M.; Sivasanker, S. *Microporous Mesoporous Mater.* **1999**, *33*, 61.

(84) Reichle, W. *Solid State Ionics* **1986**, *22*, 135.

(85) Hu, G.; O'Hare, D. *J. Am. Chem. Soc.* **2005**, *127*, 17808.

(86) Allman, R.; Jepsen, H.P. *Neues Jahrb. Mineral. Monatsh.* **1996**, 12, 544.

CHAPTER 2

TRANSITION METALLOCYANIDE EXCHANGE WITH CARBONATE IN LDH

2.1. Anionic Preference in LDH

Several decades ago, Miyata and colleagues established a general range of preference for the uptake of small anions by layered double hydroxides (LDHs). This range is far from complete, in fact, not a single LDH research group has volunteered to undergo a more extensive project dealing with a much larger range of anions for any sort of preference studies. It is doubtful that this will ever happen, even in light of the continuation of LDH being used to intercalate or adsorb more and more different anions, within the realm of anion exchange.

In light of this shortfall, the small lists that are available are informative because they show which anions can be easily replaced and which ones are more difficult to replace. The small list below (compiled from a larger list, by Miyata) showing only the most commonly used anions can be used as a strategy guide for preparing LDH with various anions:

$$NO_3^- < Br^- < Cl^- < OH^- < SO_4^{2-} < CO_3^{2-}$$

This preference list shows that LDH containing nitrate or the halides will be easily replaced by anions such as sulfate or carbonate. More importantly, this list shows that carbonate in LDH will not be effectively replaced by any of the anions listed. The two words, easily and effectively do not mean completely. It has been shown that LDH containing chloride can be easily replaced by carbonate but some residual chloride

remains.[1] This can be understood due to some of the interlayer chloride remaining trapped between adjacent carbonate anions. If anion exchange took place by one of the preferential anions "sweeping through" the interlayer, in one direction, then complete exchange would result. This scenario is unlikely to happen. Instead the carbonate anions will diffuse through the interlayers, from all possible directions. When carbonate anions travel through the LDH interlayer in opposing directions, some of the chloride anions can become trapped between them.

2.2. Anion Exchange Attempts of Carbonate with Selected Transition Metallocyanides

2.2.1 Purpose of Experiment

Since carbonate is the most strongly held anion for Mg-Al LDH materials, some selected transition metallocyanides, having the general formula: $[M(CN)_6]^{n-}$, were used for simple competition studies. The resulting possibilities are intercalation, surface adsorption or no uptake in any form.

The five selected transition metallocyanide complexes were hexacyanoferrate ($[Fe(CN)_6]^{4-}$), hexacyanoruthenate ($[Ru(CN)_6]^{4-}$), hexacyanocobaltate ($[Co(CN)_6]^{3-}$), hexacyanochromate ($[Cr(CN)_6]^{3-}$) and hexacyanoplatinate ($[Pt(CN)_6]^{2-}$).

The choice of these selected complexes was based mostly on the size and charge of each complex, and to a lesser extent, availability. All of the above metallocyanide complexes were used in the form of aqueous solutions of potassium salts, in order to bring them into contact with the insoluble LDH suspensions.

2.3 Experimental Procedure

The final LDH products were prepared through a two-part anionic exchange procedure. The first part exchanged chloride with carbonate and the second part exchanged (or attempted to exchange) carbonate with each metallocyanide complex.

2.3.1 Parent LDH Preparation

In order to prepare 1.0g batches of 2:1 Mg-Al LDH-Cl, a solution containing 0.3 M [Mg^{2+}] (2.357 g $MgCl_2 \bullet 6H_2O$), 0.1M [Al^{3+}] (1.004 g $AlCl_3 \bullet 6H_2O$), and 1.0 M total [Cl^-] (0.2431 g NaCl used in addition to the chlorides from the magnesium and aluminum salts) (salts supplied by Sigma Aldrich) were dissolved in a 250 mL three-necked flask with 42 mL of deionized water (Millipore MilliQ, 18 MΩ cm^{-1}). The three-necked flask was then placed in a heated oil bath, under a constant flow of nitrogen gas (ultra high-purity grade). Once a bath temperature of 40 °C was reached, NaOH was added to the metal salts solution (1.3 mL of supplied 50% w/w NaOH solution, Alfa Aesar; 6 mol OH^- for every 1 mol Al^{3+}). The white precipitate was then allowed to stir, under a reflux temperature (100 °C), overnight.

After reflux, the solution was removed from the oil bath and allowed to cool. The LDH suspension was then transferred to 50 mL centrifuge tubes and centrifuged for twenty minutes. The supernatant was decanted and the precipitate washed with deionized water, then centrifuged for ten more minutes. The decanting, washing and centrifuging step was repeated, for a total of two more washes. The initial separation, followed by two subsequent washes is standard operating procedure for all synthesized LDH materials, in our research group.

After the washing of the 2:1 Mg-Al LDH-Cl, the precipitate was transferred into another 250 mL three-necked flask, along with 50 mL of deionized water. A 50 mL solution of 0.1 M Na_2CO_3 (0.530 g, supplied by Fisher) was prepared in 50 mL of deionized water (two-fold excess carbonate based on a ½ : 1 molar ratio of CO_3^{2-} : Al^{3+}, from the general formula from Chapter 1). The Na_2CO_3 solution was then added to the LDH-Cl solution and allowed to stir for one hour. After one hour of mixing, the LDH suspension was separated and washed, as described above.

After washing the newly formed 2:1 Mg-Al LDH-CO_3, the white precipitate was placed in a vacuum desiccator, to dry under room temperature. The vacuum desiccator uses a vacuum to reduce the pressure inside the desiccator, which expedites the evaporation of water from the LDH precipitate. The desiccator also contains drying agents (molecular sieves and drierite) that absorb the water that evaporates out of the LDH material.

Since five different metallocyanide complexes will be studied, five more 1.0 g samples of 2:1 Mg-Al LDH-CO_3 were prepared by the exact same procedure. All 2:1 Mg-Al LDH-CO_3 samples were fully dried before any metallocyanide salts were added.

Once all of the 2:1 Mg-Al LDH-CO_3 samples were dry, they were ground to a fine powder, using a mortar/pestle. The dried samples were weighed, and then re-suspended, in 50 mL of deionized water, using an ultrasonic cleaner (Fisher Scientific). The re-suspended LDH samples were transferred to 250 mL three-necked flasks, along with 25 mL of deionized water.

2.3.2 Metallocyanide Exchange Procedure

Each of the five potassium metallocyanide salts (supplied by Sigma Aldrich, except for potassium hexacyanoruthenate(II), by Alfa Aesar) was dissolved in deionized water, but the concentrations were varied. For the hexacyanoferrate and hexacyanocobaltate complexes, 50 mL of 0.1 M solutions were prepared by dissolving 2.11 g $K_4Fe(CN)_6 \bullet 3H_2O$ and 1.66 g $K_3Co(CN)_6$, in deionized water. For the hexacyanoruthenate and hexacyanochromate complexes, 25 mL of 0.05 M solutions were prepared by dissolving 0.585 g $K_4Ru(CN)_6 \bullet 3H_2O$ and 0.407 g $K_3Cr(CN)_6$ in deionized water. For the hexacyanoplatinate complex, 50 mL of a 0.04 M solution was prepared by dissolving 0.859 g $K_2Pt(CN)_6$ in deionized water.

The concentration differences are based on the amounts of each metallocyanide needed for the effective exchange of carbonate. Since the hexacyanoferrate and hexacyanoruthenate complexes carry a minus four charge (4-), it takes 2 moles of each to be equivalent with the carbonate in LDH (1/4 $[M(CN)_6]^{4-}$: 1/2 CO_3^{2-}). For the hexacyanocobaltate and hexacyanochromate complexes, their minus three charges (3-) requires 1.5 moles of each to be equivalent with carbonate (1/3 $[M(CN)_6]^{4-}$: $1/2\, CO_3^{2-}$). For the hexacyanoplatinate complex, its minus two charge (2-) has a 1:1 molar ratio with carbonate (1/2 $[M(CN)_6]^{4-}$: 1/2 CO_3^{2-}).

Since we doubted that exchange of carbonate will occur, we decided to go with much smaller amounts of each metallocyanide. If extensive exchange had been observed, we would have then planned on performing another round of exchange experiments, using an excess amount of each metallocyanide, with respect to their stoichiometrically equivalent amounts.

The exchange reactions were performed as followed: two separate samples containing approximately 1.0 g of 2:1 Mg-Al LDH-CO_3 were allowed to stir with the $K_4Fe(CN)_6$ and $K_3Co(CN)_6$ solutions for fifteen and thirty minutes. At the fifteen-minute mark, one-half of the solutions were removed from mixing and centrifuged/washed, as previously described. At the thirty-minute mark, the rest of the solutions were removed from mixing and centrifuged/washed. After washing, the 2:1 Mg-Al LDH-CO_3/$[Fe(CN_6]^{4-}$ and 2:1 Mg-Al LDH-CO_3/$[Co(CN)_6]^{3-}$ samples were dried in the same vacuum desiccators as the parent LDH-CO_3 materials.

Three separate 0.50 g batches of 2:1 Mg-Al LDH-CO_3 were allowed to stir with the, $K_3Cr(CN)_6$, $K_4Ru(CN)_6$ and $K_2Pt(CN)_6$ solutions. The smaller amounts of LDH used were due to the availability of these three metallocyanide salts. These samples were also removed after fifteen and thirty minutes of mixing, with similar washing and drying.

2.3.3 Characterization of Products

All FT-IR spectra were collected using a Perkin-Elmer 1760X spectrometer with KBr (Aldrich) as the background. Depending on the procedure, each sample was scanned from 4000 cm^{-1} down to 700 cm^{-1} or 400 cm^{-1}, for an average of forty scans each, at a resolution of 4 cm^{-1}.

The conventional spectra were performed by first scanning a background disc with only KBr (0.2000 g, self-pressed disc). After the background spectrum has been obtained, each sample was prepared by weighing out approximately 0.001 g sample, then adding KBr, such that the total disc weight totaled 0.2000 g. The materials were

then ground to a fine powder and pressed into discs. The spectra of the LDH samples with KBr were all scanned from 4000 – 400 cm^{-1}.

We have found that by preparing sample discs that differed by 0.5 mg or greater, from the 0.2000 g weight of the KBr background disc, small, sharp peaks would show up in the spectra near the base of the hydroxide stretching peaks (3000 cm^{-1}). These peaks match the peaks of the KBr background disc and are not due to the LDH samples or disc contamination.

The oriented spectra were obtained using BaF_2 supports. The BaF_2 discs (by Thermo Spectra-Tech) were already pre-formed, so no weighing of any samples was needed. In order to prepare the samples for oriented IR, dilute suspensions of each sample were placed onto the BaF_2 disc surface (2-3 drops), and then the water was evaporated off in a vacuum desiccator. The oriented spectra of the LDH samples (including a BaF_2 disc, as the background) were all scanned from 4000 cm^{-1} down to 700 cm^{-1}. BaF_2 does not have the spectral range that KBr has; as a result, 700 cm^{-1} is typically as low as one can go.

Oriented spectra could not be obtained for the 2:1 Mg-Al LDH-CO_3/hexacyanochromate and 2:1 Mg-Al LDH-CO_3/hexacyanoplatinate samples. As will be described, with the aid of the actual IR spectra, these two samples did not have strong enough metallocyanide stretching peaks to be adequately observed.

All XRD patterns were collected using a Siemens F-series or D500 X-ray diffractometers. All patterns were scanned from 5° to 70° (2θ), with a step size of 0.05° and a dwell time of one second using CuKα radiation (λ=1.54056Å). The patterns were

recorded and obtained using Data Scan 3.2™, without internal standards, since the sample material was required for characterization by AAS, C,H,N and TGA/DTGA.

Elemental analysis was conducted on all samples, except for the ruthenocyanide. For the metal determinations, AAS was performed using a Perkin-Elmer AAnalyst 300 flame atomic absorption spectrometer, with each element lamp and standard provided by Perkin-Elmer. For carbon, hydrogen and nitrogen analysis, Atlantic Microlab and M-H-W Laboratories performed the combustion analysis and provided the results.

TGA was also performed for each sample, under nitrogen gas. Approximately 20 mg of each LDH sample was weighed, placed in the sample holder, and then pyrolyzed from 30 – 760 °C at 10 °C/min increments. All TGA and DTGA traces were recorded and obtained using Pyris software.

2.4 Results

Figure 2.1 shows the full range or conventional IR spectra of each 2:1 Mg-Al LDH-CO_3/metallocyanide sample, along with a spectrum of 2:1 Mg-Al LDH-CO_3, as reference. By comparing the reference 2:1 Mg-Al LDH-CO_3 spectrum with the spectrum of the 2:1 Mg-Al LDH-Cl, from Chapter 1, we can easily see the carbonate contamination previously discussed. One noticeable difference between these two materials is the broad shoulder present at the base of the hydroxide stretching peaks (around 3000 cm^{-1}). This shoulder has been attributed to carbonate, hydrogen-bonded to the LDH hydroxides.[2] The more carbonate present in the LDH, the stronger this shoulder appears. Back to the IR spectrum of the 2:1 Mg-Al LDH-Cl, there is no

shoulder at the base of the hydroxide stretching peaks, and the carbonate peak is much weaker, so we can describe our carbonate contamination as minor.

All of the IR spectra look the same, except within the transition metallocyanide-stretching region (2200 – 2000 cm^{-1}). This is the "fingerprint" region for each of the metallocyanide complexes. Since this region is the most important for this project, it has been expanded for more appropriate viewing.

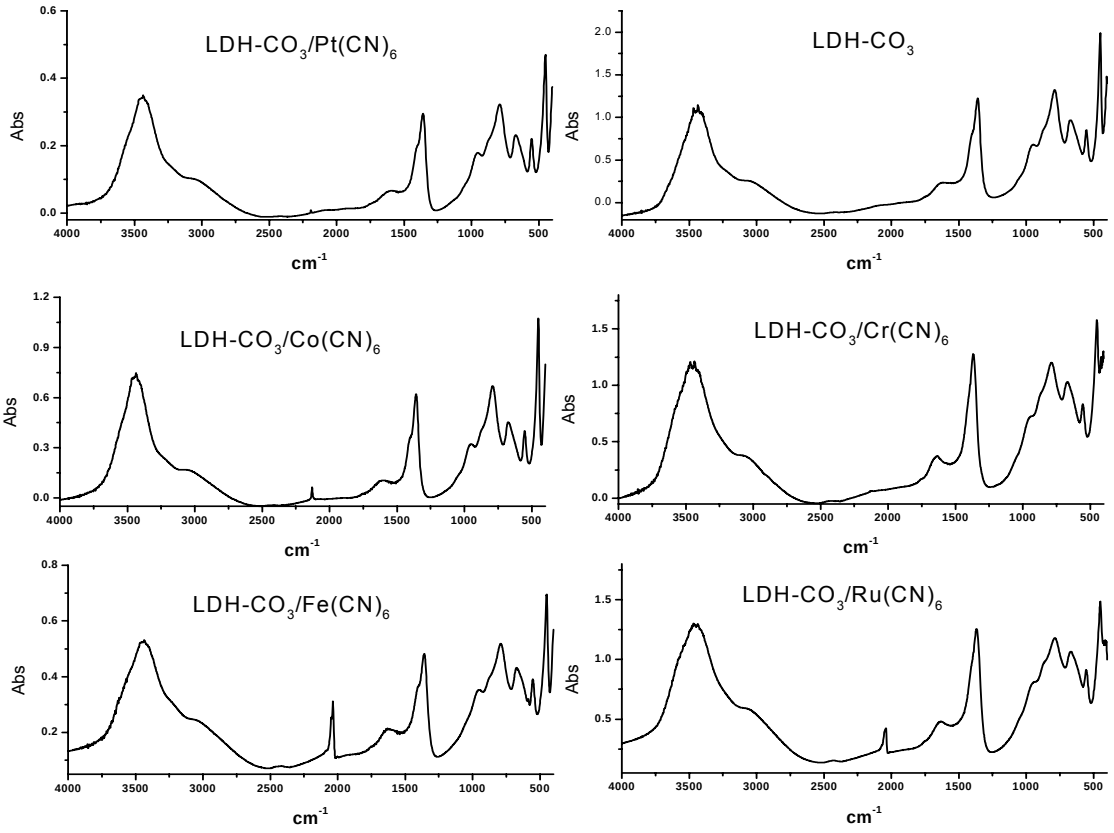

Figure 2.1: Conventional IR spectra for each of the five LDH-metallocyanide samples, along with the parent 2:1 Mg-Al LDH-CO_3 as reference.

From Figure 2.1, it is apparent that the spectra for the 2:1 Mg-Al LDH-CO_3 samples with hexacyanochromate and hexacyanoplatinate show extremely weak peaks in the metallocyanide stretching region.

Expanding the spectra to only contain the metallocyanide stretching region clearly shows the respective peaks for hexacyanochromate and hexacyanoplatinate. Figure 2.2 shows the expanded IR spectra for each of the metallocyanide samples, within the 2200 – 2000 cm^{-1} range.

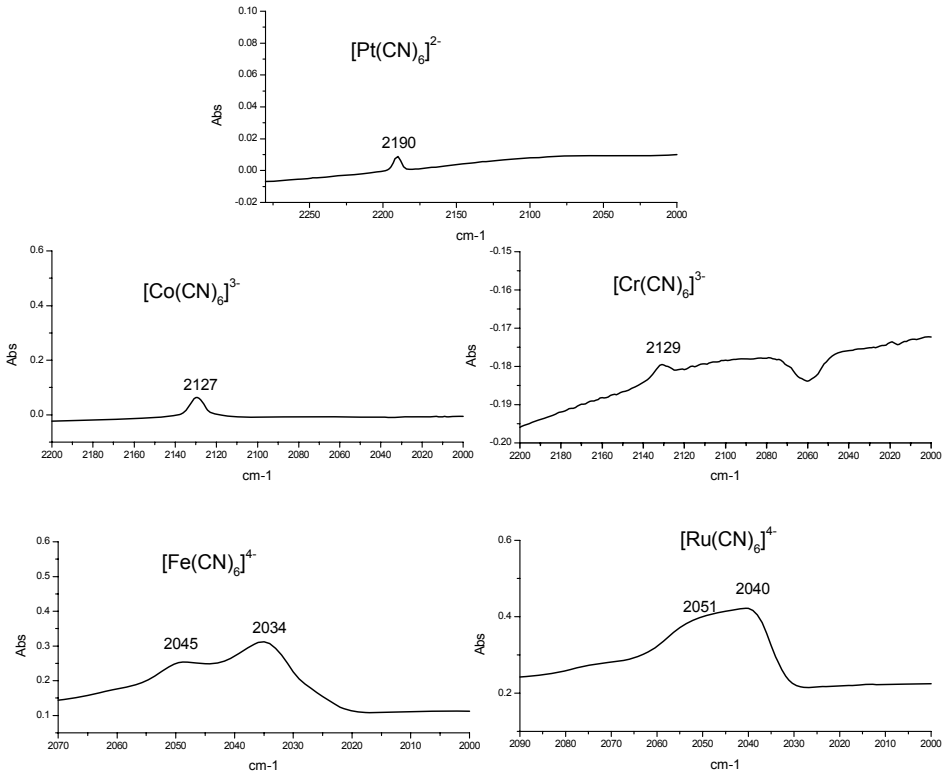

Figure 2.2: Conventional IR spectrum, expanded within the metallocyanide stretching region for each of the five LDH-metallocyanide samples.

From Figure 2.2, the 2:1 Mg-Al LDH-CO_3 with hexacyanoferrate and hexacyanoruthenate shows splitting of the metallocyanide stretching peaks ($[Fe(CN)_6]^{4-}$ at 2034 cm^{-1} and 2045 cm^{-1}; $[Ru(CN)_6]^{4-}$ at 2040 cm^{-1} and 2051 cm^{-1}). The splitting of these peaks has been previously observed with LDH materials containing hexacyanoferrate(II) or hexacyanoruthenate(II), where in both cases, the

metallocyanides were intercalated in the LDH.[3,4] For the rest of the samples, no such splitting has occurred, so only one peak is observed ($[Co(CN)_6]^{3-}$ at 2127 cm^{-1}, $[Cr(CN)_6]^{3-}$ at 2129 $cm^{-1}$and $[Pt(CN)_6]^{2-}$ at 2190 cm^{-1}).

The oriented IR spectra for the 2:1 Mg-Al LDH-CO_3 with hexacyanoferrate, hexacyanoruthenate and hexacyanocobaltate are shown in Figure 2.3. The spectrum for the hexacyanocobaltate sample does not look any different than in the conventional spectrum, but for the hexacyanoferrate and hexacyanoruthenate samples, the lower energy peak is noticeably absent, leaving the higher energy peak observable.

Oriented spectra could not be obtained for the 2:1 Mg-Al LDH-CO_3 samples containing hexacyanochromate and hexacyanoplatinate. The full range and expanded spectra for these two metallocyanides showed peaks that were barely visible. These spectra had more sample amounts, per disc, than the amounts used for the BaF_2 supports. As a result of the smaller sample amounts used for the oriented procedure, the characteristic metallocyanide stretching peaks, for hexacyanochromate and hexacyanoplatinate were not observed.

Placing more sample on the BaF_2 discs would have alleviated the problem of observing the hexacyanochromate and hexacyanoplatinate metallocyanide stretching peaks, but we would have run the risk of losing any possible orientation effects.

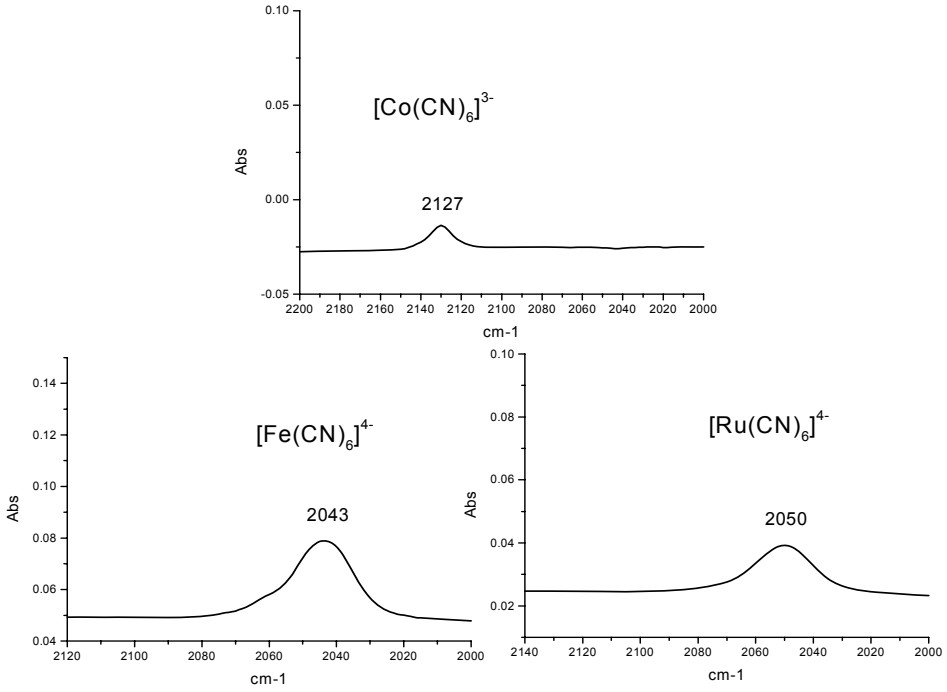

Figure 2.3: Oriented IR spectra for three of the five LDH-metallocyanide samples. The spectra for the LDH samples with hexacyanochromate and hexacyanoplatinate could not be observed.

The XRD patterns for each of the 2:1 Mg-Al LDH-CO_3/$M(CN)_6$ samples, along with 2:1 Mg-Al LDH-CO_3, as reference, are shown in Figure 2.4. The seven observed peaks are typical for LDH, with the Miller indexing labels: 003, 006, 012, 015, 018, 110 and 113. All of the samples resemble the pattern for the parent 2:1 Mg-Al LDH-CO_3, but in one particular case, some of the hexacyanoferrate appears to have been intercalated (Figure 2.5), henceforth described as the special LDH-hexacyanoferrate sample.

We believe that some hexacyanoferrate was able to get into the LDH interlayer by the slow evaporation of water by the drying from two different vacuum pumps. The stronger Welch pump dried the samples faster, in which no hexacyanoferrate was

observed in the LDH interlayer. The weaker Precision pump dried the samples more slowly, in which case some hexacyanoferrate was observed in the LDH interlayer.

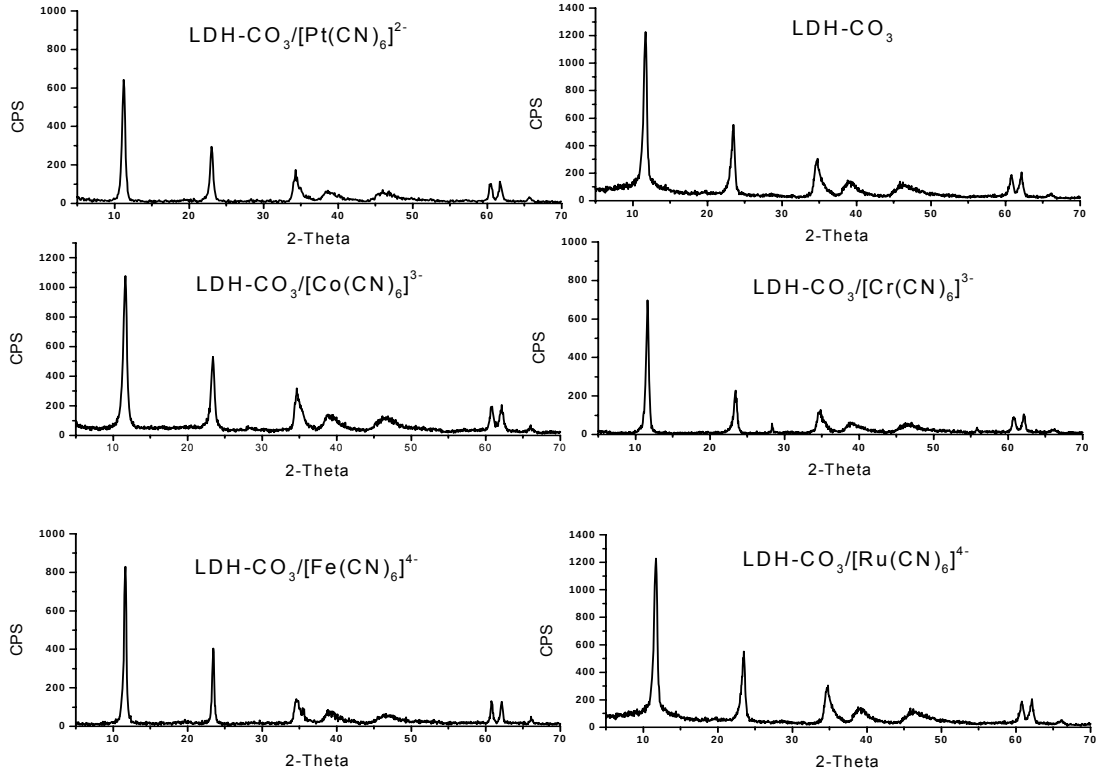

Figure 2.4: XRD patterns for each of the five LDH-metallocyanide samples, along with the parent 2:1 Mg-Al LDH-CO_3 as reference. The common Bragg reflections (from Chapter 1) are seen in all samples.

These two samples were prepared using identical procedures, except that during the drying phase different pumps happened to be available. This apparently did not work. It was believed that there would not be any differences in the drying power between these two pumps, but there was a difference between the vacuum strengths between the two (Welch pump at 0.05 mm Hg; Precision pump at 0.6 mm Hg). Unfortunately, we have not been able to reproduce these intercalation results.

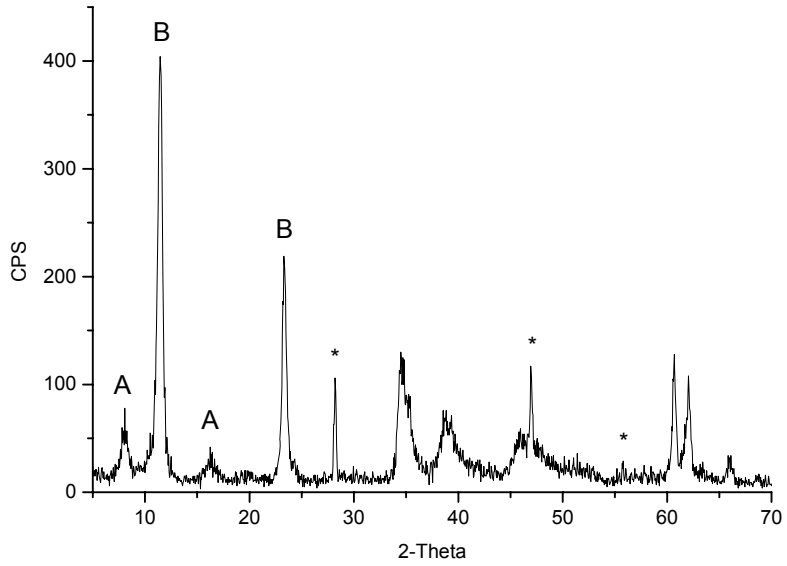

Figure 2.5: XRD pattern of the special hexacyanoferrate sample, dried using the weaker Precision pump. This pattern shows two types of anions within the LDH interlayer. Peaks labeled A represents the 003 and 006 reflections for hexacyanoferrate, B represents the 003 and 006 reflections for carbonate, and * represents CaF_2 standard.

All relevant XRD data for all samples, including the parent 2:1 Mg-Al LDH-CO_3 and the special hexacyanoferrate sample appear in Table 2.1. All five of the LDH-CO_3/$[M(CN)_6]^{n-}$ samples have d-spacings and gallery heights too close to the parent 2:1 Mg-Al LDH-CO_3 for any intercalation to have occurred. The special hexacyanoferrate sample shows a d-spacing larger than all of the others, by 3 Å. This calculates to a gallery height of around 6 Å, which is too large for carbonate. The d-spacing for the special hexacyanoferrate sample agrees with previous reports on LDH intercalated with hexacyanoferrate,[5,6] so we can conclude that it is due to hexacyanoferrate, but it is not known if the hexacyanoferrate is in the same interlayer (or same crystallite) as the carbonate.

Table 2.1: The interlayer spacings (uncorrected) and gallery heights for the five LDH-metallocyanide samples, along with 2:1 Mg-Al LDH-CO_3 as reference. The special LDH-hexacyanoferrate case* is also shown.

Sample	Interlayer Spacing (Å)	Gallery Height (Å)
LDH-CO_3	7.59	2.79
LDH-CO_3/$Fe(CN)_6$	7.61	2.81
LDH-CO_3/$Ru(CN)_6$	7.59	2.79
LDH-CO_3/$Co(CN)_6$	7.62	2.82
LDH-CO_3/$Cr(CN)_6$	7.82	3.02
LDH-CO_3/$Pt(CN)_6$	7.59	2.79
LDH-CO_3/ferrocyanide*	10.91	6.11

Table 2.2: Elemental analysis for each of the five LDH-CO_3/$[M(CN)_6]$ samples. The semi-quantitative results are shown in parentheses.

LDH-$[M(CN)_6]^{n-}$	%Mg	%Al	%C	%H	%N	Mg:Al	M:Al
$[Fe(CN)_6]^{4-}$	13.81	8.24	3.54	4.03	1.56	1.86	0.086 (0.150)
$[Ru(CN)_6]^{4-}$	11.32	6.85	3.32	3.80	1.41	1.84	N/A (0.095)
$[Co(CN)_6]^{3-}$	16.40	9.11	3.67	3.93	1.50	2.00	0.059 (0.043)
$[Cr(CN)_6]^{3-}$	11.78	6.96	3.71	4.36	0.32	1.88	0.048 (N/A)
$[Pt(CN)_6]^{2-}$	9.06	5.39	3.25	3.93	0.67	1.87	0.018 (0.141)

The full elemental analysis results appear in Table 2.2. The percentages of carbon and nitrogen are worth examining. If all of the carbonate were exchanged by each metallocyanide, then the two percentages would be in the ratio of their atomic weights, giving more nitrogen than carbon. The higher percent carbon is clearly due to the presence of metallocyanide and carbonate. If no metallocyanide were incorporated with the LDH, there would be no nitrogen present. Since a small amount of nitrogen is present, some metallocyanide was incorporated.

Since the ruthenium analysis could not be obtained, a semi-quantitative approach was attempted, based on the area under the curve for the CN stretching peak of the $[M(CN)_6]^{n-}$ complex. We chose to validate the method using $K_3Co(CN)_6$ because

within the CN stretching region, only one peak is observed (2127cm^{-1}) and the potassium salt is more simple than the LDH material.

We prepared 0.2000 g $K_3Co(CN)_6$/KBr sample discs by weighing 1.0 mg, 1.2 mg, 1.4 mg, 1.6 mg,1.8 mg and 2.0 mg of $K_3Co(CN)_6$, and adding the difference with KBr. The IR spectra were obtained for each of these six samples, with the hope that we would be able to see increasing absorbance values, due to an increase in the salt amounts. This did not occur, so this method cannot be considered reliable. One of the major pitfalls with trying to use this method, for a solid-state sample, is due to the scattering of the IR energy upon striking the sample disc. Since the IR energy will scatter when striking the disc, the transmittance or absorbance values will be affected. The attempt to estimate the amount of $[Ru(CN)_6]^{4-}$ in this way was therefore abandoned.

The TGA/DTGA traces are shown in Figures 2.6 and 2.7. Similar to the results for XRD, all LDH-CO_3/$M(CN)_6$ traces resemble the parent LDH-CO_3 sample (Figure 1.7, Chapter 1). Only a few minor points of difference are observed, mainly small differences in the final percent weight loss between each of the LDH-CO_3/$M(CN)_6$ samples. We would expect greater weight loss from samples containing more metallocyanide, but, since each sample had only small amounts of metallocyanide present, with respect to carbonate, only small differences are observed.

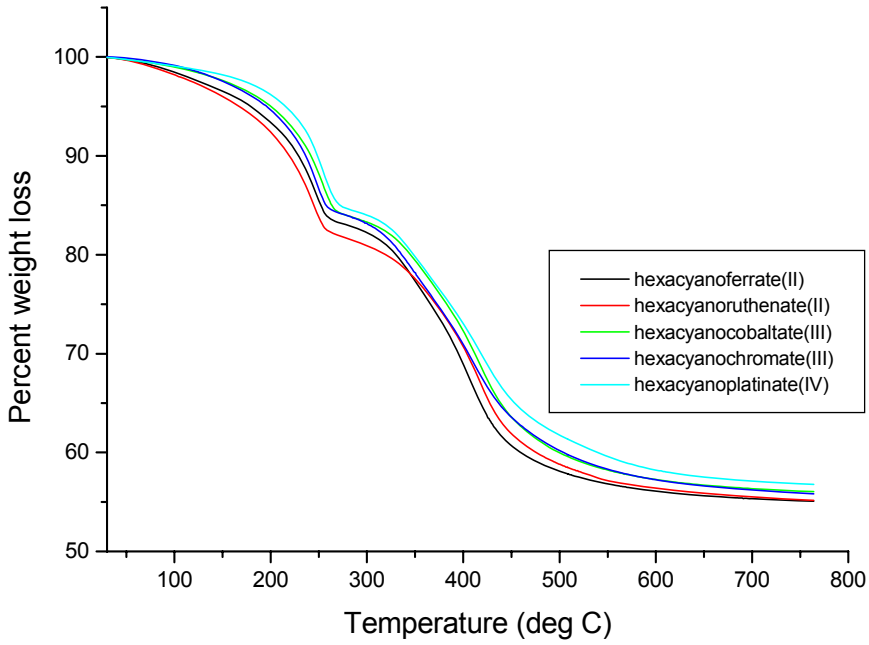

Figure 2.6: TGA traces (under nitrogen gas) for the five LDH-CO_3/$M(CN)_6$ samples.

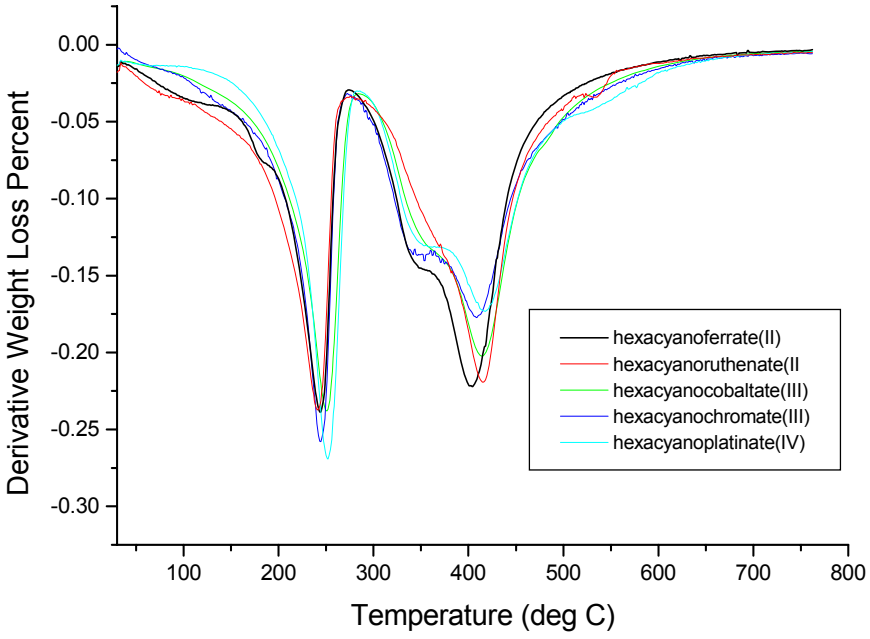

Figure 2.7: DTGA traces (under nitrogen gas) for the five LDH-CO_3/$M(CN)_6$ samples.

The DTGA traces show only minor differences in the five samples. Three weight loss peaks are present (two major and one shoulder). The peak around 250 °C is due to interlayer water being driven out, and the shoulder and peak around 350 – 400 °C are due to decomposition of the adsorbed/intercalated anions (metallocyanide and carbonate) and dehydroxylation of the LDH layers, respectively.[7,8]

2.5 Discussion

The splitting for the 2:1 Mg-Al LDH-CO_3/$[Fe(CN)_6]^{4-}$ peaks have been observed before and are common. The single peak for the 2:1 Mg-Al LDH-CO_3/$[Co(CN)_6]^{3-}$ sample has also been observed before.[9] The rest of the samples have never been synthesized before, but their respective cyano-stretching peaks agree with previously documented results for their respective potassium salts.[10]

The question then arises as to why some of the 2:1 Mg-Al LDH-CO_3/$[M(CN)_6]^{4-}$ complexes show such splitting and the others do not? The use of group theory can aid in the interpretation of such differences, when or if there are modifications in the symmetry of each metallocyanide complex. For any model $[M(CN)_6]^{n-}$ complex, with octahedral (O_h) symmetry, group theory predicts only one active infrared mode in the metal cyanide stretching region,[11] denoted as $\tilde{\nu}$ (MC-N). This seems to be the case for all of the metallocyanide samples, except for the ones having hexacyanoferrate and hexacyanoruthenate. Since these two samples show splitting, it is unlikely that their respective complexes have maintained an overall local O_h symmetry. The most likely scenario is by octahedral distortions.

Distortions from O_h symmetry are common among inorganic complexes, with the most famous of all, copper(II) complexes and Jahn-Teller distortions.[12] The Jahn-Teller distortions are mainly electronic, which should not apply to any of the five LDH metallocyanide samples, because of equal occupation of the electrons in the t_{2g} levels in all five cases ($[Fe(CN)_6]^{4-}$, $[Ru(CN)_6]^{4-}$: low spin d^6; $[Co(CN)_6]^{3-}$: low spin d^6; $[Pt(CN)_6]^{2-}$: low spin d^6; $[Cr(CN)_6]^{3-}$: d^3).

From a geometry perspective, several distortions from O_h symmetry are possible. These include: tetragonal distortion ($O_h \rightarrow D_{4h}$, the copper(II) case), trigonal distortion ($O_h \rightarrow D_{3d}$)[13], rhombic distortion ($O_h \rightarrow D_{2h}$)[14] and prismatic distortion ($O_h \rightarrow D_{3h}$).[15] Figure 2.8 shows the four possible scenarios (M= central metal and L= ligand). From these four possible scenarios, group theory should assist in either eliminating or maintaining them.

The above distortions are not the only ones that can result. There are also many structures that could exist between such point groups (i.e., structures somewhere between O_h and D_{3d}). For simplicity, these structures will not be considered, but realistically cannot be ruled out. Factors, such as the chemical interactions between these transition metallocyanide complexes and the chemical environment of the LDH (interlayer/surface carbonate, interlayer/surface water and the pendant hydroxides from the LDH layers) can further complicate such octahedral distortions, much in a similar manner that crystal packing factors can.

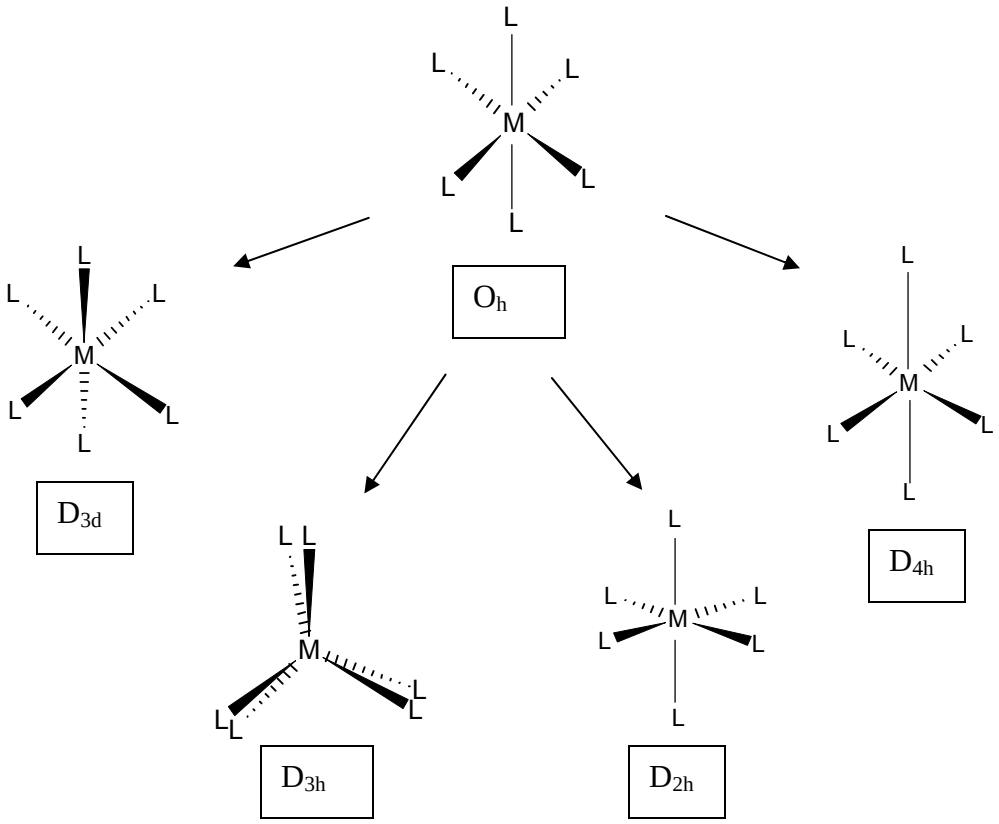

Figure 2.8: Octahedral ML_6 complex and some of the possible distortions that it can undergo. The D_{3h} structure is shifted so all six ligands are shown.

The results using group theory, for the M-CN stretch, are shown in Table 2.3. For the O_h case, only one IR active mode should be observed. For the D_{4h}, D_{3h}, and D_{3d} cases, two IR active bands should be observed. For the D_{2h}, three IR active bands should be observed.

The distinction from one, two and three IR active bands, with respect to the observed metallocyanide stretching regions, should now be clear.

Table 2.3: The IR active modes, for the above five point groups, determined by group theory.

Point Group	Reducible Representations (IR Active modes)
O_h	$\Gamma(MC\text{-}N) = T_{1u}$
D_{3d}	$\Gamma(MC\text{-}N) = A_{2u} + E_u$
D_{4h}	$\Gamma(MC\text{-}N) = A_{2u} + E_u$
D_{2h}	$\Gamma(MC\text{-}N) = B_{1u} + B_{2u} + B_{3u}$
D_{3h}	$\Gamma(MC\text{-}N) = E' + A''$

Group theory was able to eliminate the rhombic distortion structure, due to the three IR active modes, but the other structures show either one or two active IR modes. For the hexacyanoplatinate, hexacyanocobaltate and hexacyanochromate samples, group theory predicted one IR active mode, for an O_h point group, and the IR spectra showed one IR active mode. We can therefore be confident that these three complexes have suffered no major distortions from their O_h symmetry.

For the hexacyanoferrate and hexacyanoruthenate samples, three different point groups are possible. Group theory cannot be used in order to decide which of these three possible point groups the correct ones are. Another characterization tool is needed, and such a tool that is suitable is XRD.

As discussed before, XRD is used to determine the interlayer spacings in LDH. These interlayer, or d-spacings provide information on the size of an intercalated anion. The d-spacings will clearly be different for the remaining three possible point groups, because of their relative sizes. Unfortunately, for this project, only a small amount of hexacyanoferrate was intercalated, as seen in Figure 2.5. Regardless of the small amounts, enough is there to register a d-spacing measurement.

Some of the earlier work with $[Fe(CN)_6]^{4-}$ and LDH was done using a 2:1 Mg-Al LDH-Cl, in which the chloride anions were easily exchanged. The interlayer spacing (d_{003} peak) was around 11 Å, much larger than the 7 Å, typical for interlayer chloride. From this 11 Å d-spacing, the $[Fe(CN)_6]^{4-}$ complex was deduced to exist in a D_{3d} symmetry, with its principal C_3 rotation axis perpendicular to the LDH sheets.[16] This determination rules out the D_{4h} and D_{3h} point groups.

From these results, $[Fe(CN)_6]^{4-}$ and $[Ru(CN)_6]^{4-}$ are most likely to exist having a D_{3d} symmetry with the 2:1 Mg-Al LDH-CO_3/$M(CN)_6$ samples, even though $[Ru(CN)_6]^{4-}$ was not intercalated and only a small amount of $[Fe(CN)_6]^{4-}$ was.

The elemental analysis was the “weak-link” in this project. The magnesium and aluminum ratios were close enough to the ideal 2:1 Mg:Al ratio to be satisfactory, but the metals analysis for each of the transition metals, was not reliable. The main problem in attempting to determine transition metal content, in $[M(CN)_6]^{n-}$ complexes, is that these complexes are robust enough to survive, intact, in the acidic matrices used in AAS. Most likely these complexes passed through the flame, still strongly bonded to their respective cyano ligands. This would seriously hinder the effective absorbance of the specific energy for each of the transition metals in question. The C,H,N analysis was just as unreliable as the metals analysis. The same explanation, in terms of metal-cyano bonding may or may not also apply. The fact of the matter is that the samples were sent off to two different companies, in which two different results were sent back. We used the results from Atlantic Microlab, because they were the closest to the theoretical amounts. This problem of differing results was only observed for this project. All of the other times that C,H,N analysis was required, both companies produced

nearly identical results. Perhaps good metal analyses could be obtained after total decomposition of the complexes by powerful reagents, but this would not help with the carbon and nitrogen problem.

The thermogravimetric analysis results produced thermal decomposition traces that were too close to the parent 2:1 Mg-Al LDH-CO_3 for any further remarks. One interesting note did come about after these five materials were pyrolyzed. The colors of each sample were different, which directly reflects the type of transition metal that each contained. The product initially containing $[Fe(CN)_6]^{4-}$ had a pale-yellow appearance, the product initially containing $[Ru(CN)_6]^{4-}$ had a light-brown appearance, the product initially containing $[Co(CN)_6]^{3-}$ had a light-blue appearance, the product initially containing $[Cr(CN)_6]^{3-}$ had a light-green appearance and the product initially containing $[Pt(CN)_6]^{3-}$ had a dark-brown appearance.

The IR spectra suggests much less uptake of $[Cr(CN)_6]^{3-}$ than of $[Co(CN)_6]^{3-}$, which seems strange since size and charge are comparable. However, the integrated absorption coefficients for $K_3[Cr(CN)_6]$ is 2,100 $mole^{-1}$ cm^{-2} and for $K_3[Co(CN)_6]$ is 18,300 $mole^{-1}$ cm^{-2}.[17] What this means is that the hexacyanochromate complex does not absorb IR radiation as strongly as hexacyanocobaltate, so that even with comparable uptake, the latter will give much weaker IR absorption. Based on the green color of the pyrolyzed 2:1 Mg-Al LDH-CO_3/$[Cr(CN)_6]$, there is more hexacyanochromate in the LDH sample than the interpretation based on the simple IR intensities.

2.6 Conclusions/Future Directions

When used together, FT-IR spectroscopy and powder XRD were able to determine that the five transition metallocyanide complexes were primarily adsorbed onto the LDH surface. This was expected because of the known difficulty in removing interlayer carbonate by anion exchange. Of the five metallocyanide complexes studied, the two with the largest negative charge ($[Fe(CN)_6]^{4-}$ and $[Ru(CN)_6]^{4-}$) showed splitting in their respective metallocyanide stretching regions. We attributed this to the two complexes undergoing deformations, from local O_h symmetry. It may be possible that both of these complexes underwent O_h distortions, in order to effectively spread out their charges for compensation with four positive charges in the LDH lattice sheets. This tentative explanation may be understood through hydrogen bonding.

The actual transition metal-cyanide bonds should be strong enough to resist any deformations in geometry, but strong hydrogen bonding between the LDH and the metallocyanide complexes could result in deformations that would be directional (directional towards the location containing positive charge).

The elemental analysis proved unreliable, presumably because of the robust nature of the metallocyanide complexes.

These results can be used to supplement the earlier list of anion preference:

$$NO_3^- < Cl^- < [M(CN)_6]^{n-} < CO_3^{2-}$$

How these metallocyanide complexes will fit into a much larger list remains unknown, but suffice it to say that each of the metallocyanide complexes should be able to replace nitrate or the halides. The fact that carbonate was not exchanged, will keep it at the top of the list, so the above list is partially adequate.

Each of the five metallocyanide complexes were subjected to LDH materials having a Mg:Al ratio of 2:1, although Mg:Al ratios of 3:1 are more familiar and more extensively studied. Any future work, along similar lines of what was achieved with this project, would clearly have to include LDH having various Mg:Al ratios.

More importantly, the Mg-Al LDH that was used as the parent material was a more basic LDH. Other LDH materials, containing different metals would be worth exploring. Other lattice metal combinations could produce LDH having less or more basic properties, which may influence how well carbonate remains intercalated, or how well any of the $[M(CN)_6]^{n-}$ complexes interact. For example, a Co-Al LDH, which is a less basic LDH, may be more inclined to release carbonate during exchange with any of the aforementioned metallocyanide complexes. These exchange reactions may possibly be pH dependent.

Another interesting variable is temperature. All of the attempted exchange reactions were performed at room temperature. By increasing the solution temperature, the intercalated carbonate may be forced out and replaced with any one of the five metallocyanide complexes more expeditiously, due to the fact that CO_2 evolution is thermodynamically more favored at higher temperatures. These exchange reactions may possibly be thermodynamically controlled.

It is doubtful that extending the times of the reactions would change anything. What was achieved after fifteen or thirty minutes of mixing should be the same after one day or three weeks of mixing. It is unlikely that these exchange reactions can be kinetically controlled, but it may be worth looking into.

The five-metallocyanide complexes chosen are not the only ones that exist. Further experiments with transition metallocyanides containing Mo, W, Os, Rh and Ir could be attempted, but would ultimately depend on the availability, price, and stability of each one. It is doubtful that any of these metallocyanide complexes would be any more or less successful than the ones that were actually tested. Of the ones listed above, the $[Os(CN)_6]^{4-}$ complex would be the most interesting, because of its charge. Hexacyanoferrate and hexacyanoruthenate both showed splits in their respective metallocyanide stretching region, so hexacyanoosmate may also.

These materials may have some potential catalytic use[18-24], especially when used as a source of mixed oxides, in the case of bifunctional catalysis. They were shown to have small amounts of transition metal incorporated, which would be considered ideal. Most notably would be the samples containing ruthenium and platinum. These transition metals would occur free (Pt metals) or be readily reduced to metal by substrate (as in carbonylation or hydrogenation).

2.7 References

(1) Braterman, P. S.; Xu, Z. P., Yarberry, F. In *Handbook of Layered Materials*; Auerbach, S. M., Carrado, K. A., Dutta, P. K., Eds; Marcel Dekker: New York, 2004; p 373.

(2) Kloprogge, J.T.; Frost, R.L. *J. Solid State Chem.* **1999**, *146*, 506.

(3) Boclair, J.W.; Brister, B.D.; Wang, Z.; Yarberry, F.; Braterman, P.S. *J. Solid State Chem.* **2001**, *161*, 249.

(4) Richardson, M.C.; Ambadapadi, S.; Braterman, P.S. unpublished results.

(5) Crespo, I.; Barriga, C.; Rives, V.; Ulibarri, M.A. *Solid State Ionics* **1997**, *101-103*, 729.

(6) Roto, R.; Villemure, G. *J. Electroanal. Chem.* **2006**, *588*, 140.

(7) Ulibarri, M.A.; Labajos, F.M.; Rives, V.; Trujillano, R.; Kagunya, W.; Jones, W. *Inorg. Chem.* **1994**, *33*, 2592.

(8) Holgado, M.J.; Rives, V.; Sanroman, M.S.; Malet, P. *Solid State Ionics* **1996**, *92*, 273.

(9) Boclair, J.W.; Brister, B.D.; Yarberry, F.; Braterman, P.S. *Chem. Mater.* **1999**, *11*, 2199.

(10) Sharpe, A.G. The Chemistry of Cyano Complexes of the Transition Metals: Academic Press, London, 1976.

(11) Cotton, F.A. Chemical Applications of Group Theory 3rd ed: John Wiley & Sons, New York, 1990.

(12) Modern Coordination Chemistry: J. Lewis and R.G. Wilkins eds.; Interscience Publishers, New York, 1960.

(13) Davis, P.H.; Wood, J.S. *Inorg. Chem.* **1972**, *11*, 812.

(14) Borromei, R.; Cavalli, E.; Oleari, L. *Inorg. Chim. Acta* **1993**, *204*, 159.

(15) Cozar, O.; David, L.; Chis, V.; Damian, G.; Todica, M.; Agut, C. *J. Molec. Struct.* **2001**, *563*, 371.

(16) Kikkawa, S.; Koizumi, M. *Mater . Res. Bull.* **1982**, *17*, 191.

(17) Nakamoto, K. Infrared and Raman Spectra of Inorganic and Coordination Compounds, 5th ed: Wiley, New York (1997)

(18) Shen, J.; Guang, B.; Tu, M.; Chen, Y. *Catalysis Today* **1996**, *30*, 77.

(19) Kaneda, K.; Yamashita, T.; Matsushita, T.; Editani, K. *J. Org. Chem.* **1998**, *63*, 1750.

(20) Palomares, A.E.; Lopez-Nieto, J.M.; Lazaro, F.J.; Lopez, A.; Corma, A. *Appl. Catal.* **1999**, *B20*, 257.

(21) Cavani, F.; Trifiro, F.; Vaccari, A. *Catal. Today* **1991**, *11*, 173.

(22) Srinivas, S.T.; Sai Prasad, P.S.; Madhavendra, S.S.; Kanta Rao, P. *Recent Advances in Basic and Applied Aspects of Industrial Catalysis* **1998**, *113*, 835.

(23) Basile, F.; Basini, L.; Fornasari, G.; Gazzano, M.; Trifiro, F.; Vaccari, A. *J. Chem. Soc., Chem. Comm.* **1996**, 2453.

(24) Basile, F.; Fornasari, G.; Gazzano, M.; Vaccari, A. *Appl. Clay Sci.* **2000**, *16*, 185.

CHAPTER 3

INCORPORATION OF TETRACYANONICKELATE(II) IN LDH

3.1 Successful Approach for Intercalating a Transition Metallocyanide in LDH

Chapter 2 described a very limited but useful range of anions that have preferential exchange with layered double hydroxides (LDHs), and the unsuccessful attempt of removing carbonate from the LDH interlayer by larger and more highly charged transition metallocyanides.

It was noted that successful intercalations of these metallocyanides were possible by starting out with a parent LDH having either chloride or nitrate in the interlayer.

This lesson was taken into account for the attempt of intercalating the tetracyanonickelate(II) or nickelocyanide complex ($[Ni(CN)_4]^{2-}$), by anion exchange with LDH. initially having chloride or nitrate in the interlayer. As mentioned in chapter 1, the charge density of an LDH is dependent on the ratio of the trivalent metal to the total metals, and was different for LDH having a 2:1 divalent-trivalent or 3:1 divalent-trivalent metal ratios. The LDH having the lower of the two ratios would have more trivalent metal amounts in the lattice sheets, and would potentially incorporate more anions. The two most important points of consideration in dealing with LDH as anion exchangers are: 1) the ease of replacement of the initial anion with one of interest and: 2) the amounts of such anion that can be theoretically incorporated, as determined by the LDH charge density.

3.2 Purpose of Experiment

This experiment was designed to intercalate the square planar $[Ni(CN)_4]^{2-}$ complex in the interlayers of Mg-Al LDH materials, having 2:1 and 3:1 Mg-Al ratios. In order to achieve successful intercalation with these two LDH's, their respective initial interlayer anions were chloride and nitrate.

Assuming successful intercalation of nickelocyanide by exchange of both chloride and nitrate, the amounts of nickelocyanide should be different due to the higher anionic uptake capacities of LDH having larger charge densities. In other words, the 2:1 Mg-Al LDH should be able to incorporate more nickelocyanide than the 3:1 Mg-Al LDH analog. What is equally important but implied in the previous two sentences is the incorporation of more complex in an LDH interlayer may result in a more crowded interlayer environment. The amounts of nickelocyanide will ultimately be governed by the amounts of positive charges, from the LDH sheets. What needs to be taken into consideration is how these complexes will be positioned in the LDH interlayers when more is in the 2:1 LDH type and less is the 3:1 LDH type.

The principal characterization tools (FT-IR, XRD, AAS) were used for all materials, along with C,H,N analysis, TGA/DTGA and bulk pyrolysis for the thermal decomposition characterization, also done using XRD.

The applications for LDH, containing nickel, are immediately evident by the catalytic nature of nickel or nickel oxide.[1-3] Since LDH are renown for their catalytic applications as catalysts or as catalytic precursors (Chapter 1), these LDH-$Ni(CN)_4$ or pyrolyzed LDH-$Ni(CN)_4$ materials may hold some use in the future.

As far as our knowledge is concerned, the interaction of tetracyanonickelate with LDH would be the first reported interaction of any LDH with any square planar transition-metallocyanide.

3.3 Experimental Procedure

The starting materials consisting of 2:1 and 3:1 Mg-Al LDH-Cl ($Mg_2Al(OH)_6Cl$ and $Mg_3Al(OH)_8Cl$) along with 2:1 and 3:1 Mg-Al LDH-NO_3 ($Mg_2Al(OH)_6\ NO_3$ and $Mg_3Al(OH)_8\ NO_3$) were synthesized by the direct precipitation route described in the introductory chapter.

Approximately 2.0 g batches of the four parent LDH materials were prepared by precipitating either metal chlorides solutions or metal nitrates solutions with a 50% NaOH solution.

For the LDH-Cl materials, enough $MgCl_2 \bullet 6H_2O$ was weighed out to make 0.3 M and 0.4 M solutions and enough $AlCl_3 \bullet 6H_2O$ was weighed out to make 0.1M solutions. The same concentrations were used for the $Mg(NO_3)_2 \bullet 6H_2O$, $Al(NO_3)_3 \bullet 6H_2O$ and $NaNO_3$ solutions.

For the preparation of the 2.0 g batches, the actual amounts were: 5.083 g magnesium chloride, 1.938 g aluminum chloride and 2.5 mL 50% NaOH for the 2:1 Mg-Al LDH-Cl; 5.286 g magnesium chloride, 1.570 g aluminum chloride and 2.7 mL 50% NaOH for the 3:1 Mg-Al LDH-Cl; 5.577 g magnesium nitrate, 2.721 g aluminum nitrate and 2.3 mL 50% NaOH for the 2:1 Mg-Al LDH-NO_3; and 6.133 g magnesium nitrate, 2.246 g aluminum nitrate and 2.5 mL 50% NaOH for the 3:1 Mg-Al LDH-NO_3. Once the metal salts were weighed out and placed in separate 250 mL three-necked

roundbottomed flasks, 85 mL of deionized water was added to each flask, even though the stoichiometry amounts were calculated as different for each LDH batch.

The white precipitates were allowed to reflux (around 100 – 105°C), overnight, under a steady stream of ultra-high purity nitrogen gas. The LDH suspensions were then removed from reflux, placed in 50 mL centrifuge tubes, centrifuged, and the solids washed with deionized water (Millipore MilliQ Academic, 18 MΩ cm^{-1}). The centrifuge/wash steps were repeated to ensure all unreacted ions were removed from the LDH solids. The LDH materials were placed in vacuum desiccators, each wrapped in parafilm, but not allowed to dry.

The potassium tetracyanonickelate(II) was prepared by the addition of KCN to $Ni(CN)_2$ by the following combination reaction:

$$2KCN(aq) + Ni(CN)_2(s) \rightarrow K_2Ni(CN)_4(aq)$$

Due to the high pH attained by free cyanide addition (pH ~10), the above reaction was performed under nitrogen gas and then immediately set on a hot plate for the evaporation of water. The orange-red crystals were then placed in a vacuum dessicator for continued drying, under molecular sieves and drierite. The stoichiometric amounts needed to be followed closely due to the ease of $[Ni(CN)_5]^{3-}$ complex formation when excess free cyanide is added. The solution goes from orange to light red and decomposes upon evaporation giving off ammonia gas, which further spikes the pH of the solution and may introduce further contaminants into the recovered nickelocyanide salt. The presence of the $[Ni(CN)_5]^{3-}$ complex can be easily seen by infrared spectroscopy due to its CN stretch at around 2105 cm^{-1}, as opposed to the CN stretch of $[Ni(CN)_4]^{2-}$ at around 2120 cm^{-1}.[4]

Approximately 2.0 g of each “wet” LDH was added to 50 mL solutions containing the tetracyanonickelate(II) complex. The amount of $K_2Ni(CN)_4$ used was based on a 2.5 molar ratio of $[Ni(CN)_4]^{2-}$ for every mol Cl^- or NO_3^-, in order to ensure excess. The exchange reactions took place in an inert environment (nitrogen, ALPHAGAZ 1) glove box, and allowed to stir for one hour. The materials were centrifuged and washed with deionized water. The washed materials were then placed in vacuum dessicators and dried at room temperature.

The infrared spectra were collected using a Perkin-Elmer 1760X spectrometer with FT-IR grade KBr as the background. The spectra were scanned throughout the 400 cm^{-1} to 4000 cm^{-1} range, for an average of 40 scans, per sample, at a resolution of 4 cm^{-1}. Approximately 1 – 2% LDH material was weighed, and incorporated into a 0.200 g sample disk containing the sample and KBr.

The XRD patterns were obtained using a Siemens D500 series diffractometer utilizing Data Scan 3.2™ software. The patterns were scanned from 5° to 70° (2θ) using CuKα radiation (λ=1.54056Å) with a step size of 0.05° and a dwell time of one second. Any smoothing of the patterns that needed to be done for better peak resolution and identification was done using the adjacent averaging methods in the Origin software package.

The elemental analysis of the LDH materials was done by flame atomic absorption (Mg, Al, Ni) using a Perkin-Elmer AAnalyst 300 spectrometer with Perkin-Elmer supplied standards and by commercial combustion (C,H,N) done by M-H-W Laboratories. The metals analysis was not done for the pyrolyzed samples, under the

assumption that the metals amounts should not considerably change, regardless of the temperatures reached during thermal decomposition.

The TGA studies were done with a Perkin-Elmer TGA6 from 30 – 800°C at a heating rate of 10 °C/min, with steady nitrogen flow into the internal balance compartment. Approximately 20 mg of each individual LDH-$Ni(CN)_4$ sample was pyrolyzed under air (hospital breathing grade), nitrogen, hydrogen and helium (all ultra-high purity grade), at steady flow rates.

For bulk thermal decomposition studies, 1.5 g of each LDH-$Ni(CN)_4$ material was pyrolyzed in quartz combustion tubes using a Thermolyne 48000 furnace, at temperatures up to 600 °C (held at 600 °C for fifteen minutes), using the same grade of gases as with the TGA procedure. This technique was used for XRD studies, which needed much larger sample amounts than the 20 mg used for TGA.

The PXRD patterns for the pyrolyzed materials were collected using the same parameters as for the LDH-$Ni(CN)_4$ materials.

3.2 Results

3.4.1 The Parent LDH Materials

The IR spectra and XRD patterns for the 2:1 and 3:1 Mg-Al LDH-Cl and Mg-Al LDH-NO_3 materials are shown in Figure 3.1 and 3.2.

The IR spectra for the 2:1 and 3:1 Mg-Al LDH-Cl materials show some carbonate contamination (around 1360 cm^{-1}). For the 2:1 and 3:1 Mg-Al LDH-NO_3 materials, sharp peaks occur around 825, 1384 and 1763 cm^{-1}, characteristic of the ν_2, ν_3 and the $2\nu_2$ stretching modes of the nitrate anion, respectively.[6,7] In all cases, the 2:1 Mg-Al

LDH materials show a single peak at 447 cm^{-1} (for all 2:1 Mg-Al LDH systems), but no such peak occurs for the 3:1 Mg-Al LDH materials.

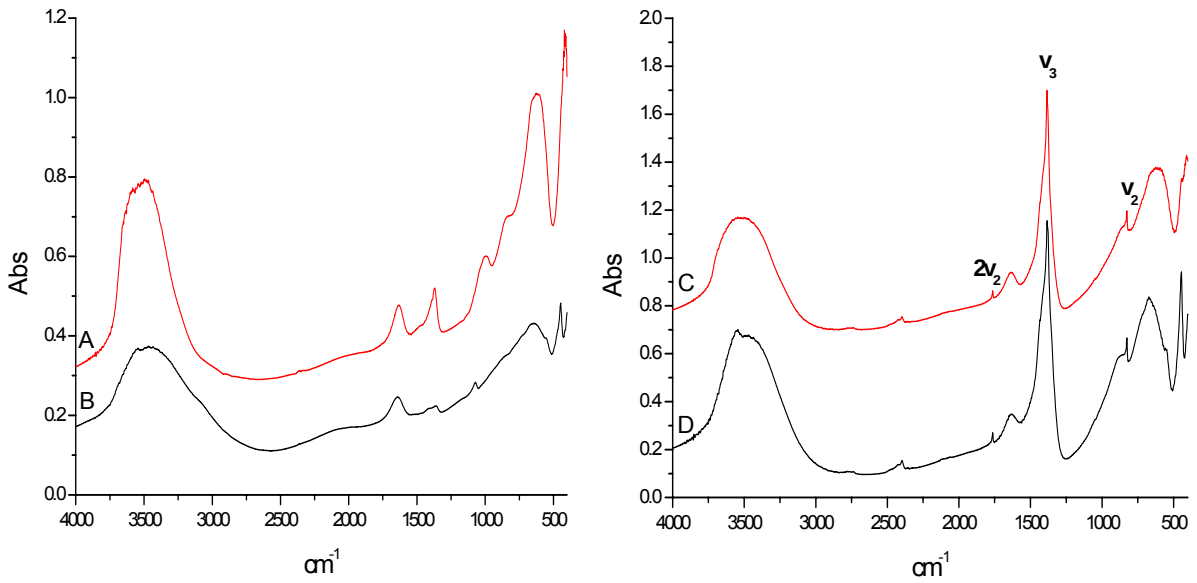

Figure 3.1: Conventional FT-IR spectra of (A) 3:1 Mg-Al LDH-Cl; (B) 2:1 Mg-Al LDH-Cl; (C) 3:1 Mg-Al LDH-NO_3 and (D) 2:1 Mg-Al LDH-NO_3.

The XRD patterns for the 2:1 and 3:1 Mg-Al LDH-Cl materials show a higher degree of crystallinity, with the 110 and 113 reflections well resolved. The 2:1 and 3:1 Mg-Al LDH-NO_3 materials show a lower degree of crystallinity, with the 110 and 113 reflections overlapped.

The interlayer spacings (d_{003} spacings) for the following materials: 3:1 Mg-Al LDH-Cl = 8.05 Å; 2:1 Mg-Al LDH-Cl = 7.69 Å; 3:1 Mg-Al LDH-NO_3 = 9.29 Å; 2:1 Mg-Al LDH-NO_3 = 8.58 Å. These results show that nitrate takes up more space in the LDH interlayer and that the interlayer spacing for the 3:1 Mg-Al LDH materials are larger than the 2:1 Mg-Al LDH materials.

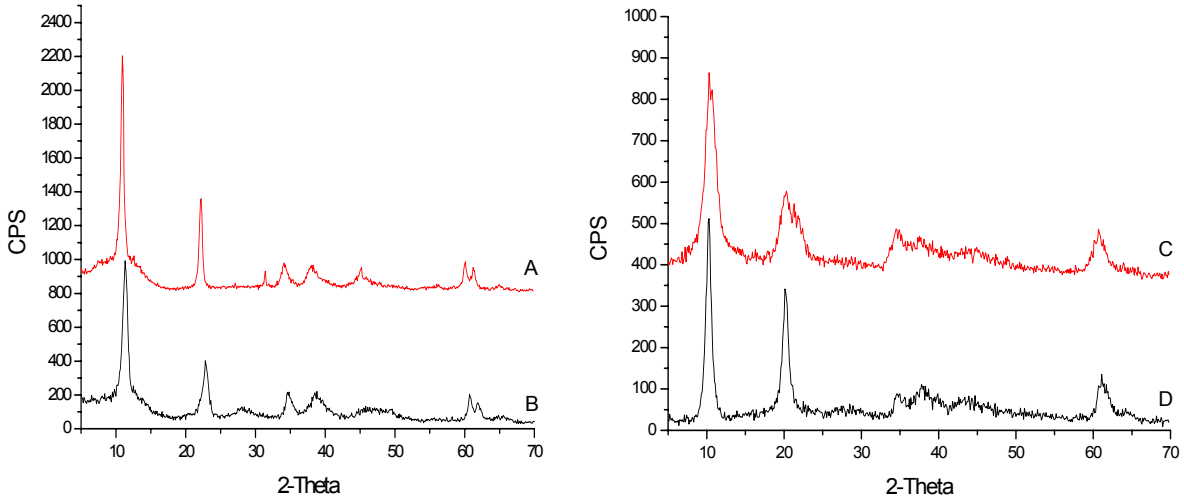

Figure 3.2: XRD patterns for (A) 3:1 Mg-Al LDH-Cl; (B) 2:1 Mg-Al LDH-Cl; (C) 3:1 Mg-Al LDH-NO_3 and (D) 2:1 Mg-Al LDH-NO_3.

3.4.2 The 2:1 and 3:1 Mg-Al LDH-$Ni(CN)_4$ Materials

The IR spectra (Figure 3.1) show some carbonate contamination (around 1360 cm^{-1})[5], which could not be completely eliminated, regardless of our inert glove-box work. The IR spectra do not show an extensive carbonate presence as shown by the absence of the carbonate-hydroxyl interaction peak that is typically seen near the base of the OH stretching peak (around 3000 cm^{-1}). The 2:1 Mg-Al LDH-$Ni(CN)_4$ material from the parent 2:1 LDH-Cl shows a sharp peak around 3620 cm^{-1}, characteristic of a high frequency band that has been previously described for LDH containing ferrocyanide.[8]

It is not known how the nickelocyanide complex caused this peak to show but it does not exist in the IR spectra of the parent LDH materials.

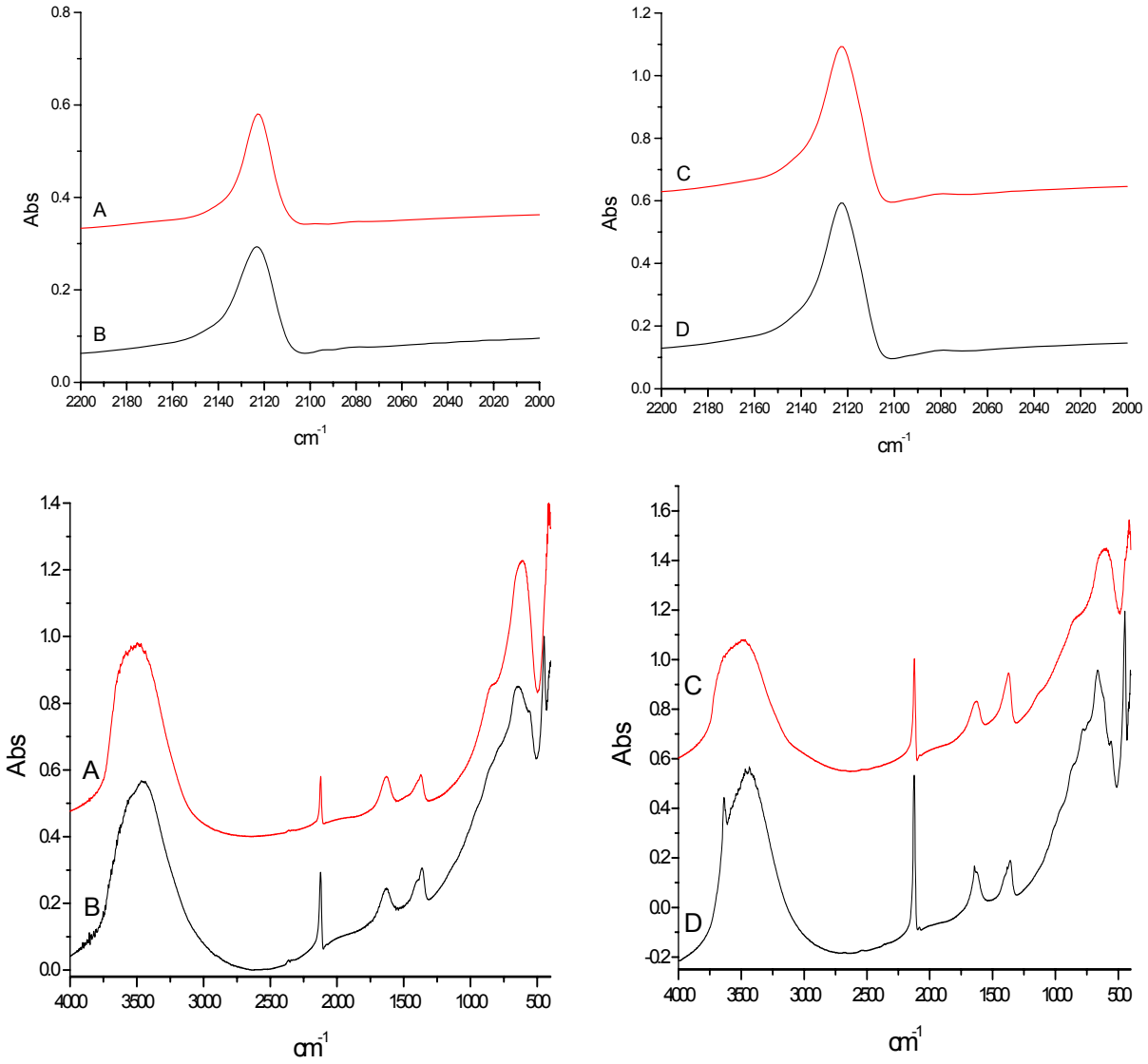

Figure 3.3: Conventional FT-IR (below) and expanded FT-IR (above) spectra of (A) 3:1 Mg- Al LDH-Ni$(CN)_4$ and (B) 2:1 Mg-Al LDH-Ni$(CN)_4$ from exchange with parent LDH-Cl and (C) 3:1 Mg-Al LDH-Ni$(CN)_4$ and (D) 2:1 Mg-Al LDH-Ni$(CN)_4$ from exchange with parent LDH-NO_3.

In all four materials, a single $[Ni(CN)_4]^{2-}$ stretching peak is observed at 2122 cm^{-1}, in agreement with the square planar complex.[9] Both 2:1 Mg-Al LDH samples have the 447 cm^{-1} peak, which is observed for any aged Mg-Al LDH having a 2:1 Mg:Al ratio. On the other hand, the 3:1 Mg-Al LDH samples do not show this 447 cm^{-1} peak. More will be discussed about this observation during Chapter 6. In all four materials, the water-bending mode, at around 1630 cm^{-1}, is also present.[10] There are subtle differences between the materials, based on the metal ratios: the 3:1 LDH samples show a broad peak within the 500 – 800 cm^{-1} range. The 2:1 LDH materials have this peak within the same region, but the peak is sharper, with additional smaller peaks and shoulders. More will be said about this region in Chapter 6, but the differences can be attributed to a higher degree of cation order, for the 2:1 Mg-Al LDH materials.

Aside from the sharp peak at 3620 cm^{-1}, the OH stretching peak in spectrum D is sharper than spectrum C (possibly due to the presence of this 3620 cm^{-1} peak). A closer look at spectrum B shows a more pronounced shoulder than spectrum A. Spectrum C also appears to have such a shoulder.

The XRD patterns show well crystalline particles, for the 2:1 LDH samples, but poorly crystalline particles, for the 3:1 LDH samples (Figure 3.2). The 3:1 LDH patterns had to be smoothed, using the adjacent average method, in the Origin software. Smoothing techniques can be useful if a spectrum or pattern contains a large signal-to-noise ratio or if any peaks are close enough to one another to overlap, but care must be taken because smoothing reduces resolution.

The most notable observation is seen in the pattern for the 2:1 LDH-$Ni(CN)_4$ sample, exchanged from the parent LDH-NO_3. The first two reflections have nearly the

same intensities. As seen from the XRD patterns, from Chapter 1, the second reflection (d_{006}) is usually less in intensity than the first reflection (d_{003}). This is typically seen for any LDH material, regardless of the type or size of the interlayer anion. For most LDH materials, the interlayer spacings of the first four reflections show this same trend, in which the c' relation can also be used to determine the repeat layer distance (from Chapter 1).

The pattern for the 2:1 LDH-$Ni(CN)_4$ sample, exchanged from the parent LDH-Cl, does not show the exact same observation because the d_{006} reflection is still much more intense than what is normally observed. The intensities are not what are important, but it is the interlayer spacings. In most cases, the c' formula may have to be shortened due to the overlap of the d_{009} and d_{012} reflections, but it is a more accurate way of determining the repeat layer distance, because it takes into account more of the Bragg reflections in a rhombohedral crystal system.

The unusually strong d_{006} reflections ($2\theta = 15 – 16°$) are not indicative of any contamination, nor are they indicative of materials that are no longer LDH. In these cases, it is simply understood that there are strong reflections, of the nickelocyanide, in the 006 plane. There are other examples of the higher angle reflections being just as strong, as or stronger than the lower angle reflections.11, 12

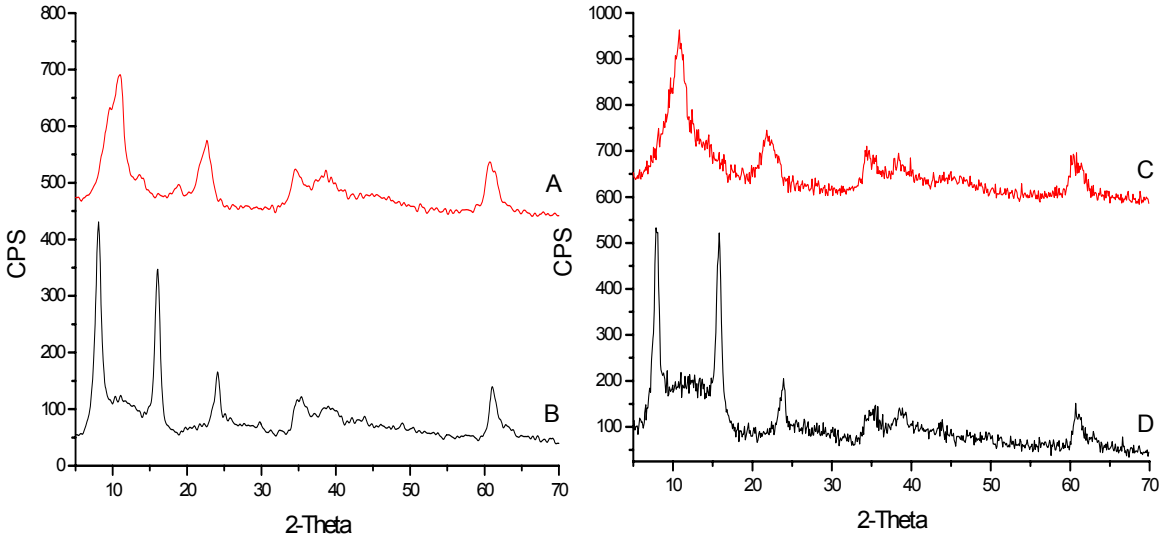

Figure 3.4: XRD patterns for (A) 3:1 Mg-Al LDH-Ni$(CN)_4$ and (B) 2:1 Mg-Al LDH-Ni$(CN)_4$ from exchange with parent LDH-Cl and (C) 3:1 Mg-Al LDH-Ni$(CN)_4$ and (D) 2:1 Mg-Al LDH-Ni$(CN)_4$ from exchange with parent LDH-NO_3.

Now that the XRD patterns have been obtained, the interlayer spacings will then be used to calculate the gallery heights. Once the gallery heights have been determined, we will have an idea of the space that the nickelocyanide complex occupies. Based on the concept of charge density, we would expect more nickelocyanide in the 2:1 LDH material than the 3:1 LDH material, and we may then be able to see differences in the gallery heights.

Once any differences in the gallery heights are observed, we can, if we know the dimensions of the anion, use simple trigonometry (the theorem of Pythagorus and the definition of the sine angle) to determine how these complexes are positioned, within the LDH gallery heights, relative to the LDH layers.

Table 3.1 shows the interlayer spacings, gallery heights and the nickelocyanide tilt angles for each of the four LDH samples. From these data, we can see differences between the 2:1 LDH-Ni$(CN)_4$ samples and the 3:1 LDH-Ni$(CN)_4$ samples.

Table 3.1: XRD data (uncorrected) and angles of tilt calculated for each LDH-$Ni(CN)_4$ sample. The calculated tilt angles: H-bond distance on the left and the van der Waals radius of nitrogen on the right.

Starting Material	d_{003} (Å)	Gallery Height(Å)	Tilt Angle (°)
2:1 Mg-Al LDH-Cl	10.91	6.11	66.8 / 71.9
2:1 Mg-Al LDH-NO_3	11.05	6.25	70.0 / 76.3
3:1 Mg-Al LDH-Cl	9.21	4.41	41.6 / 43.4
3:1 Mg-Al LDH-NO_3	8.15	3.35	30.2 / 31.4

The tilt angle, for each nickelocyanide complex was calculated as follows:

1) The gallery height dictates how much space the nickelocyanide occupies, which was determined by subtracting the layer thickness from the interlayer spacing.
2) The size of the nickelocyanide complex, itself, was determined, with the following bond lengths[13]: NiC =1.86 Å, CN = 1.14 Å, also using the computational method and basis set described in 5).
3) The lengths from opposite side cyanides and adjacent side cyanides are: opp = 6.00 Å, adj = 4.24 Å.

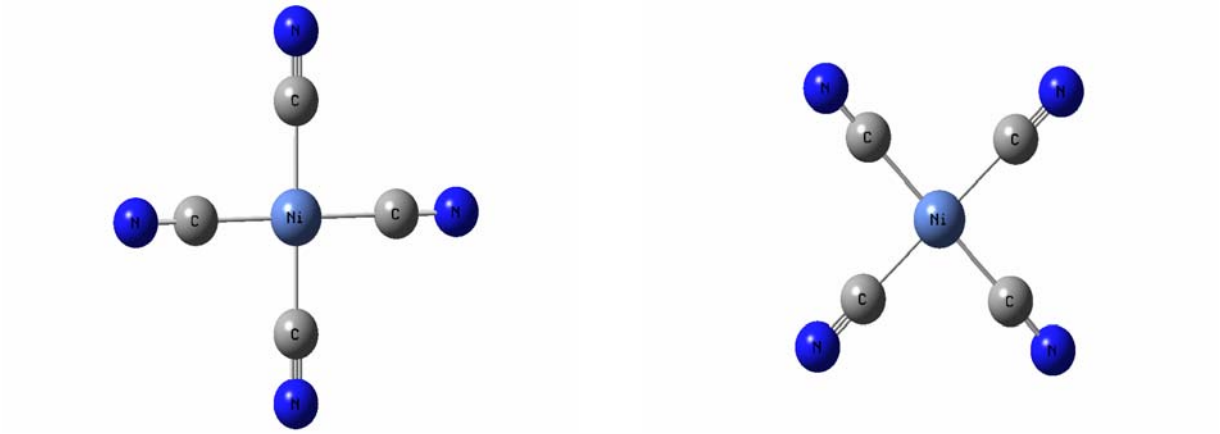

Figure 3.5: Tetracyanonickelate(II) complex (drawn using GaussView 3.08).

The distance from the opposite cyanides would be too large for the complex to fit in the gallery height, upright (we also have to take into account the hydrogen bonding distance from the LDH layer hydroxides and the nickelocyanide nitrogens). Instead, the complex positions itself in the LDH interlayer as seen by the structure on the right in Figure 3.3.

4) The nickelocyanide complex must then tilt itself in order to fit into the gallery height.
5) The hydrogen bonding distance between one water molecule and one of the nitrogens on the tetracyanonickelate complex was calculated to be 1.697 Å, using the B3LYP/LANL2DZ (DFT method and basis set).[14,15] The alternative to this bond distance is the use of the van der Waals radius of nitrogen, which is 1.55 Å.

The length of the complex, in the upright position can now be calculated as: 2*(1.86 Å + 1.14 Å + 1.70 Å or 1.55 Å). This 9.39 Å or 9.10 Å distance is now the full length of the opposite ends of the complex. Only one-half of these values are needed, since the nickelocyanide complex is not in an upright position in the LDH interlayer. By the definition of a right triangle, the distance from adjacent cyanide groups (hypotenuse) is either 6.43 Å or 6.65Å.

6) From the definition of the sine angle: sin θ = opposite/hypotenuse, the tilt angle, θ, can then be found: $\theta = \sin^{-1}$(opposite/hypotenuse).

Depending on whichever value was used, the hydrogen bond or the van der Waals radius, the calculated results clearly show larger angles for the 2:1 LDH-$Ni(CN)_4$ samples.

The elemental analysis appears in Table 3.2. The magnesium to aluminum ratios are in good agreement with either their respective 2:1 or 3:1 ratios, the nickel to aluminum ratios are all close to the theoretical 0.5:1 ratios, the carbon to nitrogen ratios are in very good agreement to the theoretical 1:1 ratio, the carbon (and nitrogen) to aluminum ratios are all close to the theoretical 2:1 ratio ($½Ni(CN)_4]^{2-}$: Al^{3+}), but the carbon (and nitrogen) to nickel amounts are lower than the theoretical 4:1.

Table 3.2: Elemental analysis for each Mg-Al LDH-$Ni(CN)_4$ sample, from their respective starting materials.

LDH Material	Mg:Al	Ni:Al	C:N	C:Al	N:Al	C:Ni	N:Ni
2:1 LDH-Cl	2.17	0.57	1.05	1.81	1.72	3.18	3.01
2:1 LDH-NO_3	2.14	0.58	1.08	1.88	1.74	3.24	3.00
3:1 LDH-Cl	3.17	0.54	1.07	2.07	1.94	3.84	3.59
3:1 LDH-NO_3	3.40	0.52	1.08	1.94	1.80	3.73	3.46

LDH Material	%Mg	%Al	%Ni	%C	%H	%N
2:1 LDH-Cl	16.89	8.63	10.70	6.95	3.59	7.69
2:1 LDH-NO_3	19.92	8.67	10.94	7.26	3.18	7.82
3:1 LDH-Cl	17.80	6.21	7.30	5.73	3.50	6.25
3:1 LDH-NO_3	20.25	6.60	7.47	5.70	3.23	6.17

Since the elemental analysis is in good agreement with the theoretical amounts, there should not be much of a difference between the gallery heights and the calculated tilt angles, for both 2:1 LDH samples and both 3:1 LDH samples, with respect to each other, but differences are noticeable. The two-degree difference between the two 2:1 LDH samples is not large enough to be significant, but the twelve to thirteen degree difference between the two 3:1 LDH samples is large enough to be significant.

We attribute this discrepancy to the poorly crystalline materials of the 3:1 LDH samples, possibly making it difficult for the X-ray diffractometer to determine reliable interlayer spacings. Since the nickelocyanide complexes were nearly positioned

parallel, in the LDH interlayer, this may have resulted in a larger degree of disorder within the LDH interlayer. The following two scenarios may help visualize this concept of disorder: In one case we could have all of the nickelocyanide complexes pointing in the same direction. This would result in a more ordered interlayer environment, which would be observed by a clean XRD pattern. The other case could have the nickelocyanide complexes pointing in all different directions. This would result in a more disordered interlayer, in which the XRD pattern would show small, poorly crystalline peaks.

3.4.3 Thermal Decomposition Studies

Figures 3.4 and 3.5 show the TGA traces and Figures 3.6 and 3.7 show the DTGA traces for each of the four 2:1 Mg-Al LDH-$Ni(CN)_4$ samples.

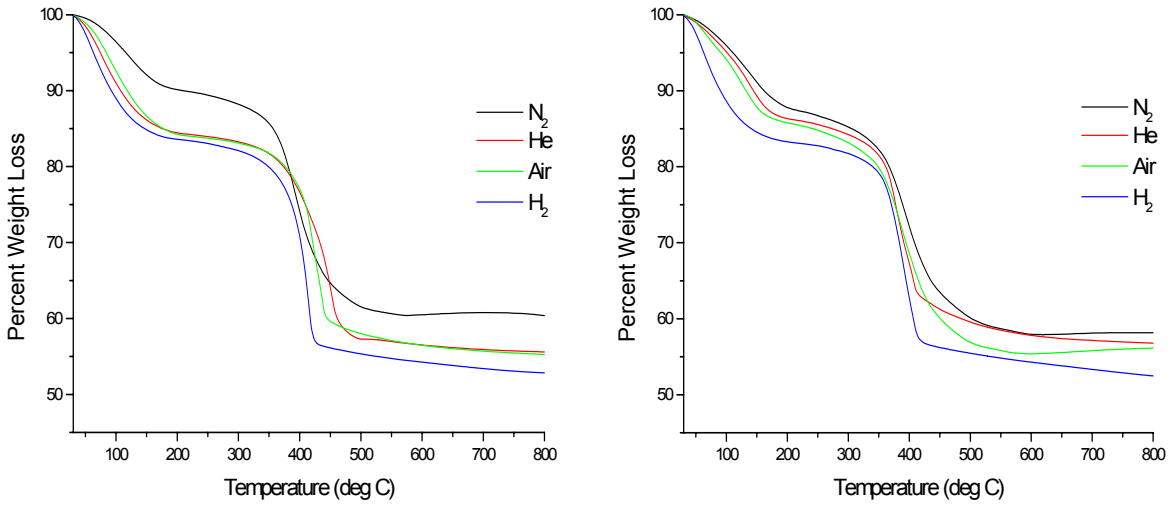

Figure 3.6: TGA traces of 2:1 Mg-Al LDH-$Ni(CN)_4$: left from exchange with parent LDH-Cl and right from exchange with parent LDH-NO_3, under various gases: N_2 (black), air (green), He (red) and H_2 (blue).

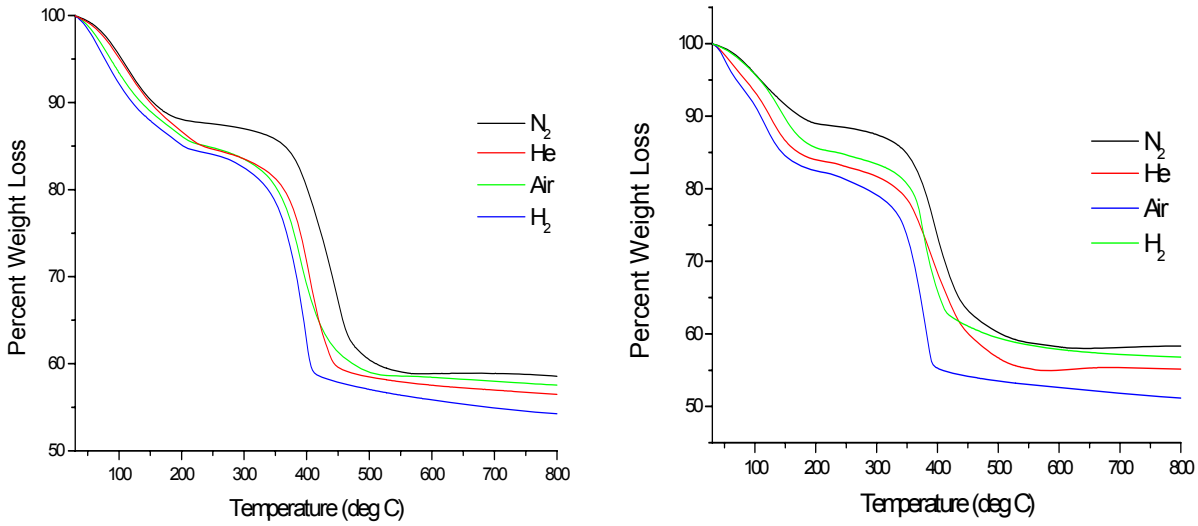

Figure 3.7: TGA traces of 3:1 Mg-Al LDH-$Ni(CN)_4$: left from exchange with parent LDH-Cl and right from exchange with parent LDH-NO_3, under various gases: N_2 (black), air (green), He (red) and H_2 (blue).

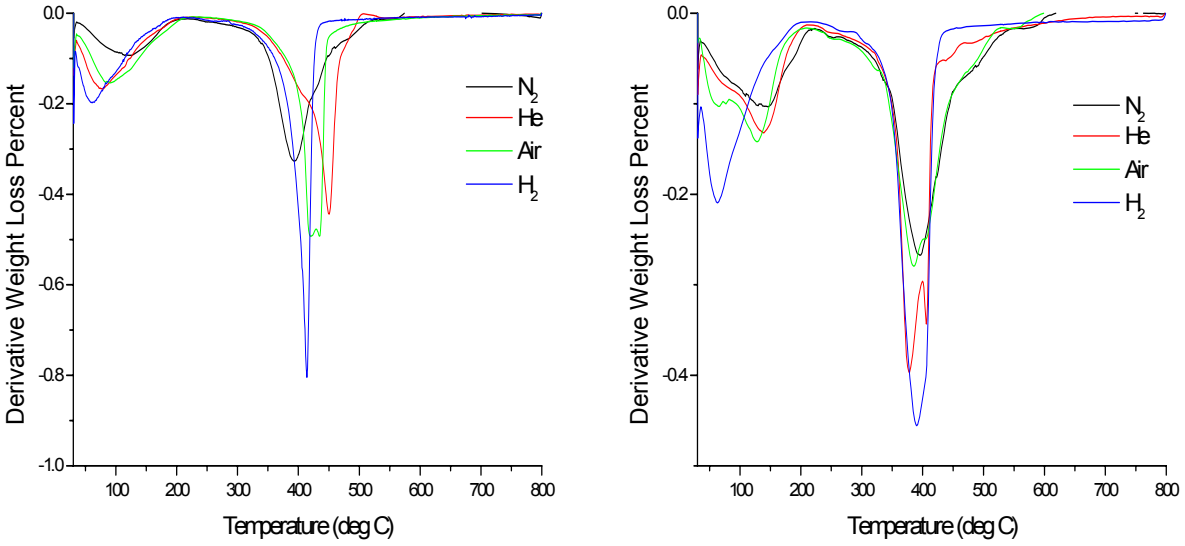

Figure 3.8: DTGA traces of 2:1 Mg-Al LDH-$Ni(CN)_4$: left from exchange with parent LDH-Cl and right from exchange with parent LDH-NO_3, under various gases: N_2(black), air (green), He (red) and H_2 (blue).

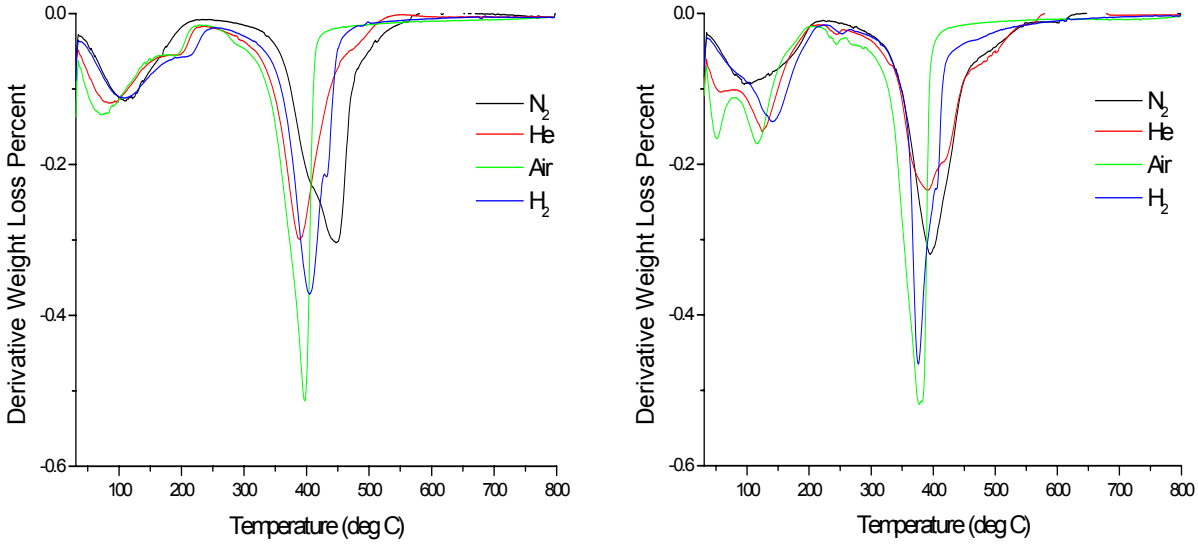

Figure 3.9: DTGA traces of 3:1 Mg-Al LDH-Ni(CN)$_4$: left from exchange with parent LDH-Cl and right from exchange with parent LDH-NO_3, under various gases: N_2 (black), air (green), He (red) and H_2 (blue).

The first set to analyze is the two TGA traces for the 2:1 Mg-Al LDH-Ni(CN)$_4$ samples. It is obvious that the samples pyrolyzed under hydrogen underwent the highest percent weight losses, while the samples pyrolyzed under nitrogen underwent the lowest percent weight losses. The samples pyrolyzed under helium and air lie between these two extremes. The same trend can be observed for the two 3:1 Mg-Al LDH-Ni(CN)$_4$ samples. In all cases, there appears to be some crossing of the traces for the helium and air samples.

Table 3.3 shows the weight loss percents for each of the sixteen samples, grouped according to the parent LDH materials.

Table 3.3: Measured percent weight loss for each pyrolyzed LDH-$Ni(CN)_4$ material under different gases.

LDH-$Ni(CN)_4$ from:	Gas	Percent Weight Loss
2:1 Mg-Al LDH-Cl	Nitrogen	39.66
2:1 Mg-Al LDH-Cl	Air	44.41
2:1 Mg-Al LDH-Cl	Helium	44.75
2:1 Mg-Al LDH-Cl	Hydrogen	47.18
2:1 Mg-Al LDH-NO_3	Nitrogen	41.85
2:1 Mg-Al LDH-NO_3	Air	43.23
2:1 Mg-Al LDH-NO_3	Helium	43.85
2:1 Mg-Al LDH-NO_3	Hydrogen	47.53
3:1 Mg-Al LDH-Cl	Nitrogen	41.44
3:1 Mg-Al LDH-Cl	Air	43.54
3:1 Mg-Al LDH-Cl	Helium	42.46
3:1 Mg-Al LDH-Cl	Hydrogen	45.74
3:1 Mg-Al LDH-NO_3	Nitrogen	41.67
3:1 Mg-Al LDH-NO_3	Air	43.21
3:1 Mg-Al LDH-NO_3	Helium	44.85
3:1 Mg-Al LDH-NO_3	Hydrogen	48.85

From Table 3, we can see anywhere from a 4% to 7% difference between the nitrogen-pyrolyzed materials and the hydrogen-pyrolyzed materials. We attribute this distinction to the reducing power of hydrogen gas[16] upon the nickelocyanide complex, resulting in more complete formation of nickel metal.

The DTGA traces show major reduction steps occurring around 100 – 150°C and around 400 – 450°C. The first step is due to surface and interlayer water. The second step is due to the decomposition of the nickelocyanide complex and the collapse and dehydroxylation of the LDH layers.

Based on the following percent weight losses, some possible thermal decomposition routes can be proposed. The reactions have been greatly simplified, based on the possible reactions of the nickelocyanide complex with the LDH layer hydroxides.

LDH-$Ni(CN)_4$ under air and helium (not charge balanced):

$[Ni(CN)_4]^{2-} + 4OH^- \rightarrow Ni^{2+} + 4HCN + 4O^{2-}$

$Ni^{2+} + 1/2O_2 \rightarrow NiO$ (43-44% average weight loss)

LDH-$Ni(CN)_4$ under nitrogen:

$[Ni(CN)_4]^{2-} + 2OH^- \rightarrow Ni^0(C,N) + 2HCN + 2O^{2-}$

(39-41% average weight loss)

LDH-$Ni(CN)_4$ under hydrogen:

$[Ni(CN)_4]^{2-} + 2OH^- + H_2 \rightarrow Ni^0(C,N) + 4HCN + 2O^{2-}$

(46-49% average weight loss)

All pyrolyzed materials took on a black color, except for the air-pyrolyzed material, which was green. We attribute this black color to finely divided nickel metal and amorphous carbon (which some exists in all samples), but the air sample had much less of it. The green color is presumed to be due to oxides of nickel, such as NiO or $NiAl_2O_4$.

The LDH-$Ni(CN)_4$ samples, pyrolyzed under hydrogen hints at the possibility of an oxidative addition-reductive elimination reaction, which is why we placed H_2 as one of the reactants. This is not surprising because of the high reactivity of hydrogen gas, especially with transition metal complexes at elevated temperatures.

There are no major differences between the 2:1 and 3:1 LDH-$Ni(CN)_4$ samples, with respect to percent weight loss, under any of the gases used.

XRD was performed on the bulk pyrolysis materials, at 600 °C, in order to observe the decomposition products. The same set of parameters was used to obtain the pyrolyzed XRD patterns as with the LDH-$Ni(CN)_4$ materials. Figure 3.8 shows the patterns for the bulk pyrolyzed 2:1 Mg-Al LDH-$Ni(CN)_4$ samples and Figure 3.9 shows the patterns for the bulk pyrolyzed 3:1 Mg-Al LDH-$Ni(CN)_4$ samples.

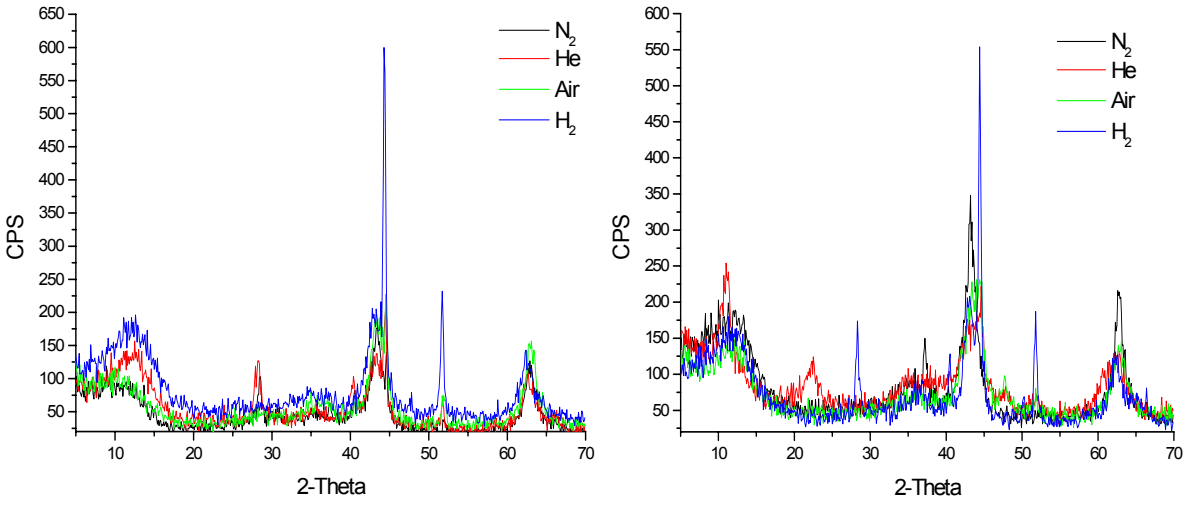

Figure 3.10: XRD patterns of pyrolyzed 2:1 Mg-Al LDH-$Ni(CN)_4$ from parent LDH-Cl (left) and parent LDH-NO_3 (right). The patterns from the different gases: nitrogen (black), helium (red), air (green) and hydrogen (blue).

The materials pyrolyzed under nitrogen, helium and hydrogen ignited, when exposed to the atmosphere while still warm. The black powders were also strongly attracted to an iron magnet, which is indicative of the ferromagnetic properties of nickel metal.[17]

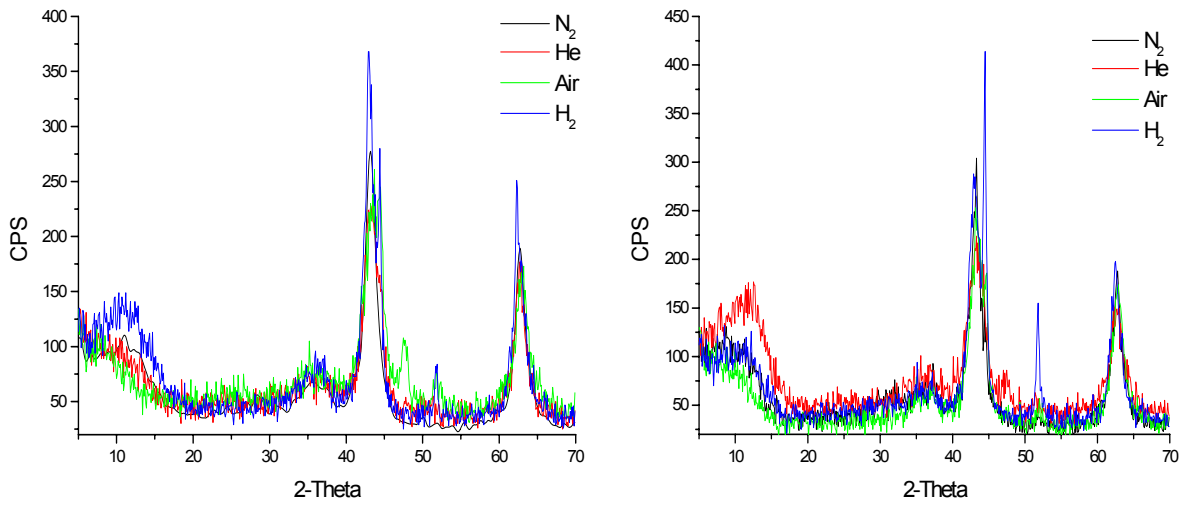

Figure 3.11: XRD patterns of pyrolyzed 3:1 Mg-Al LDH-$Ni(CN)_4$ from parent LDH-Cl (left) and parent LDH-NO_3 (right). The patterns from the different gases: nitrogen (black), helium (red), air (green) and hydrogen (blue).

The pyrolyzed XRD patterns can be difficult to interpret due to the possibility of overlapping peaks from different materials. For instance, the peak around 42 – 43° (2θ), is a result of both spinel ($MgAl_2O_4$) and the Ni (111) reflection, the peak around 62 – 63 ° (2θ) is most likely a combination of MgO and NiO. The peak around 52° (2θ) could be the result of the Ni (200) reflection, γ-Al_2O_3, or a combination of both.

The peaks around 28° (2θ), for the 2:1 LDH-$Ni(CN)_4$ materials could not properly be identified through the use of the ICDD database, but were found to be similar to magnesium chloride. These peaks are not present for the 3:1 LDH-$Ni(CN)_4$ materials, which causes the magnesium chloride guess to be suspect.

Another interesting note is the pattern for the hydrogen-pyrolyzed 2:1 LDH-$Ni(CN)_4$ sample, from the parent LDH-NO_3. This pattern still shows some LDH features, such as a d_{003} and d_{006} reflections (around 11° and 22° (2θ)). This appears to be the result of incomplete decomposition of the LDH-$Ni(CN)_4$, a factor that could have been eliminated with longer pyrolysis times.

The bulk pyrolysis temperatures were not high enough for the spinel structures to be strong enough to revert back to LDH, when re-hydrated in water. According to the memory effect, by hydrating these pyrolyzed materials, in water and anion, we should be able to re-convert these mixed oxides back to LDH. In hindsight, it would have been interesting to see if this would occur, by re-hydrating them in an aqueous solution of $K_2Ni(CN)_4$.

The IR spectra of the bulk-pyrolyzed materials do not show any nickelocyanide present after pyrolysis. It was not possible to perform the IR immediately after the 600 °C temperature was reached, so some presence of water and carbonate are seen each of the sixteen samples. For the pyrolyzed 2:1 Mg-Al LDH materials, there are no 447 cm^{-1} peaks, which indicate that the LDH lattice has been compromised. For the pyrolyzed 3:1 Mg-Al LDH materials, no such 447 cm^{-1} peak would be seen, because it is not present any of the 3:1 Mg-Al LDH materials, regardless of the anion. We can see both a general broadness of the peaks in the low wavenumber region (700 – 400 cm^{-1}) and a weakness of the hydroxide stretching peaks (3500 – 3000 cm^{-1}). The IR spectra for the pyrolyzed materials are shown in Figures 3.10 and 3.11.

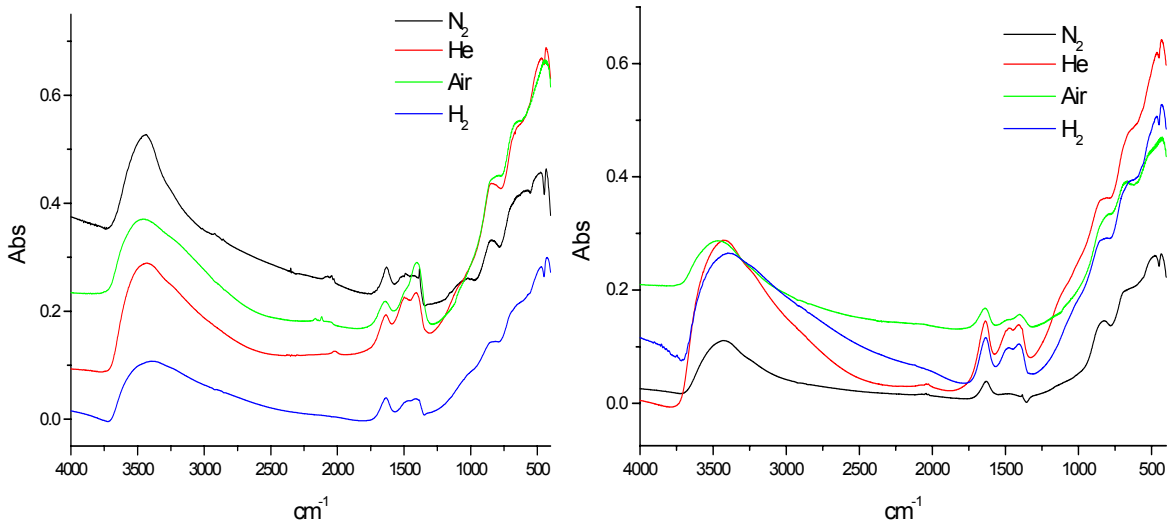

Figure 3.12: FT-IR spectra of pyrolyzed 2:1 Mg-Al LDH-$Ni(CN)_4$ from parent LDH-Cl (left) and parent LDH-NO_3 (right). The patterns from the different gases: nitrogen (black), helium (red), air (green) and hydrogen (blue).

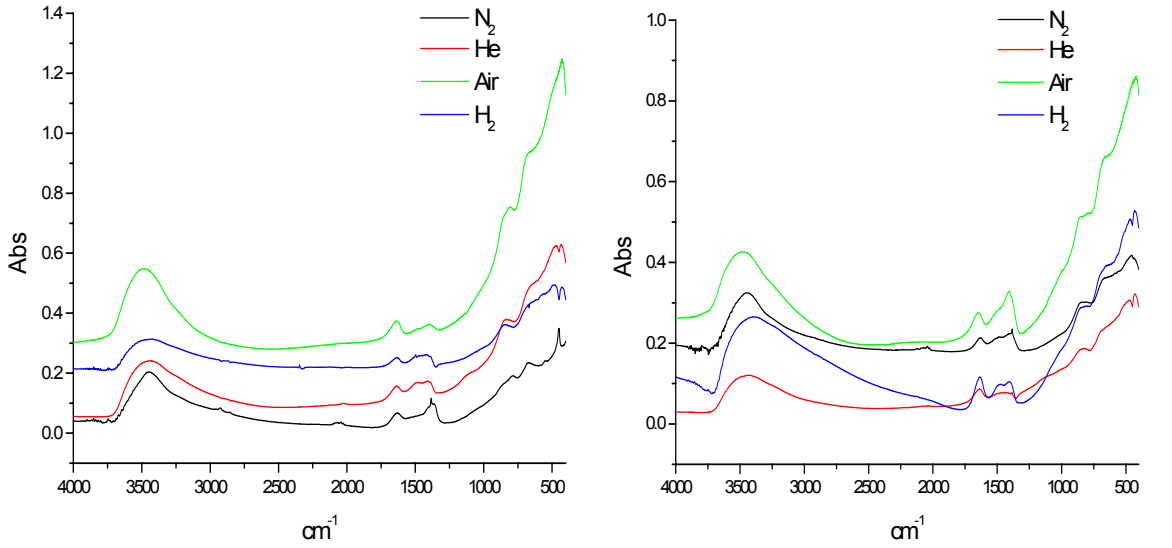

Figure 3.13: FT-IR spectra of pyrolyzed 3:1 Mg-Al LDH-$Ni(CN)_4$ from parent LDH-Cl (left) and parent LDH-NO_3 (right). The patterns from the different gases: nitrogen (black), helium (red), air (green) and hydrogen (blue).

3.5 Conclusions/Future Directions

This project was successful in showing how easy interlayer chloride and nitrate can be exchanged with a transition metallocyanide, in the form of tetracyanonickelate. Depending on the Mg:Al ratio, and consequently the layer charge density, the amounts of nickelocyanide incorporated differed between the 2:1 Mg:Al and 3:1 Mg:Al LDH. There did not appear to be a significant difference between the exchange of chloride or nitrate, in that close to the theoretical amounts of nickelocyanide were shown to exist in all samples.

We attempted to show that as a consequence of layer charge density and the potential amounts of anion that can be intercalated in the LDH interlayer, a crowded interlayer will force the nickelocyanide complexes to position themselves at certain tilt angles. These angles are the consequence of maximizing the amounts of complex, while at the same time minimizing nearest neighbor repulsions. Since a 2:1 LDH incorporates more nickelocyanide, the angles of these complexes is higher than the angles determined for the 3:1 LDH analog. The tilt angles for the 2:1 LDH-$Ni(CN)_4$ samples were almost high enough for the nickelocyanide complexes to be positioned perpendicular to the LDH layers, and the tilt angles for the 3:1 LDH-$Ni(CN)_4$ samples were almost low enough for the nickelocyanide complexes to be positioned parallel to the LDH layers.

Thermogravimetric experiments were conducted in order to gain an understanding of how the LDH-$Ni(CN)_4$ materials thermally decompose, under a variety of gases. In all cases, the samples pyrolyzed under hydrogen gas registered the highest percent weight loss but they did not always register the lowest major reduction temperature.

Depending on the type of gas, the thermal products differed in either their elemental composition or the amounts of amorphous carbon that remained after the pyrolysis. The thermal decomposition products showed a heterogeneous solid-state mixture of Mg,Al oxides, spinel and either NiO or nickel metal. The materials pyrolyzed under nitrogen, helium and hydrogen ignited in the form of burning ambers when introduced to the atmosphere and was strongly attracted to an iron magnet. These two observations are indicative of finely divided nickel metal.

This experiment studied only one type of a square planar $[M(CN)_4]^{n-}$ complex. Other complexes, such as $[Pd(CN)_4]^{2-}$ and $[Pt(CN)_4]^{2-}$ would be of major interest (from a catalytic viewpoint).[18-22] Their larger sizes would clearly be noticed in the LDH interlayer, with tilt angles expected to be different than the $[Ni(CN)_4]^{2-}$ case.

This experiment also focused on magnesium and aluminum as the LDH layer metals, but we would expect to see similar trends with other lattice metals. Once again, the difference between a more basic pH LDH (Mg:Al) and a less basic pH LDH (Co:Al or Co:Cr) may produce different or similar results. The potential possibilities of this type of project are similar to the possibilities discussed at the end of Chapter 2.

There does exist another type of Mg:Al that has not been mentioned previously. As has been stated before, the most commonly studied Mg:Al LDH have their respective divalent-trivalent ratios at 2:1 or 3:1. Since we have shown major differences in the positioning of the nickelocyanide complexes between these two, it would be worth studying the effects of nickelocyanide intercalation with a 4:1 Mg:Al LDH. This high ratio Mg:Al LDH has been studied before,[23] but not near as much as the lower ratio analogs. The main reason is that a 4:1 Mg:Al LDH, having a much lower charge density than the other materials, cannot incorporate as much anion, which makes it a poor subject for anion exchange experiments. This potential to provide more space per nickelocyanide, than the 3:1 Mg:Al LDH, should lead to an even lower tilt angle (one even more close to parallel, if not at parallel) with respect to the LDH layers. Similar studies with tetracyanopalladate and tetracyanoplatinate would increase interest in the relatively neglected low charge density LDH containing a 4:1 divalent-trivalent metal ratio, at least for a little while.

Nickel complexes are also found in tetrahedral point groups ($[NiCl_4]^{2-}$) and have been explored with LDH, although the products do not show any characteristics of tetrachloronickel(II) in them.[24,25] Although more difficult to synthesize, they would be worth exploring with LDH having divalent:trivalent metal ratios of 2:1, 3:1 and possibly 4:1.

3.6 References

(1) Tichit, D.; Medina, F.; Coq, B.; Dutartre, R. *Appl. Catal. A: General* **1997**, *159*, 241.

(2) Chen, Y.; Hwang, C.M.; Liaw, C.W. *Appl. Catal. A: General* **1998**, *169*, 207.

(3) Basile, F.; Fornasari, G.; Poluzzi, E.; Vaccari, A. *Appl. Clay Sci.* **1998**, *13*, 329.

(4) Nakamoto, K. Infrared and Raman Spectra of Inorganic and Coordination Compounds, 5th ed: Wiley, New York (1997)

(5) Labajos, F.M.; Rives, V.; Malet, P.; Centeno, M.A.; Ulibarri, M.A. *Inorg. Chem.* **1996**, *35*, 1154.

(6) Qian, M.; Zeng, H.C. *J. Mater. Chem.* **1997**, *7*, 493.

(7) Xu, Z.P.; Zeng, H.C. *Chem. Mater.* **1999**, *11*, 67.

(8) Boclair; J.W.; Braterman, P.S.; Brister, B.D.; Wang, Z.; Yarberry, F. *J. Solid State Chem*. **2001**, *161*, 249.

(9) Sharpe, A.G. The Chemistry of Cyano Complexes of the Transition Metals: Academic Press, London, 1976

(10) Moroz, T.N.; Arkhipenko, D.K. *Sov. Geol. and Geophys.* **1991**, *32*, 52.

(11) Schutz, A.; Biloen, P. *J. Solid State Chem.* **1987**, *68*, 360.

(12) Beaudot, P.; de Roy, M.E.; Besse, J.P. *J. Solid State Chem.* **2001**, *161*, 332.

(13) Vannerberg, N.G. *Acta Chem. Scand.* **1964**, *18*, 2385.

(14) Becke, A.D. *J. Chem. Phys.* **1993**, *98*, 5648.

(15) Hay, P.J.; Wadt, W.R. *J. Chem. Phys.* **1985**, *82*, 270.

(16) Brown, T.L.; Lemay, H.E.; Bursten, B.E. Chemistry The Central Science: 6th ed: Prentice Hall, New Jersey, 1994

(17) Selwood, P.W.. Magnetochemistry: 2nd ed: Interscience Publishers, New York, 1956

(18) Liu, Y.; Suzuki, K.; Hamakawa, S.; Hayakawa, T.; Murata, K.; Ishii, T.; Kumagai, M. *Chem. Lett.* **2000**.

(19) Kakiuchi, N.; Maeda, Y.; Nishimura, T.; Uemura, S. *J. Org. Chem.* **2001**, *66*, 6620.

(20) Nishimura, T.; Maeda, Y.; Nishimura, T.; Uemura, S. *Chem. Comm.* **2000**, 1245.

(21) Fritz, P.M.; Boelt, H. Catalytic Dehydrogentation of C2-10 Alkanes. Ger Patent 19,858,747, June 21, 2000

(22) Li, Z.; Tu, M.; Shen, J.; Jia, J.; Xu, Z.; Lin, L. *Cuihua Xuebao* **1998**, *19*, 1.

(23) Yun, S.K.; Pinnavaia, T.J. *Chem. Mater.* **1995**, *7*, 348.

(24) Lopez-Salinas, E.; Tomita, N.; Matsui, T.; Suzuki, E.; Ono, Y. *J. Mol. Catal.* **1993**, *81*, 397.

(25) Lopez-Salinas, E.; Ono, Y. *Microporous Mater.* **1993**, *1*, 33.

CHAPTER 4

LAYERED DOUBLE HYDROXIDES AS CATION-EXCHANGING MATERIALS

I. DIVALENT CATION EXCHANGE WITH Mg-Al LDH

4.1 Chemical Properties of LDH

The extensive use of layered double hydroxides (LDH) as anion-exchanging materials has been described in the first three chapters of this work, and still continues to be the main driving force for LDH research. Although this has been the primary definition of LDH, part of being a research scientist is to expand current knowledge and possibly challenge age-old concepts and ideas.

The possibility of LDH in the area of cation exchange has never been fully explored for two good reasons: the first reason is that LDH have a net positive charge that must be balanced by anions. LDH that would take in cations would disrupt the electroneutrality principle and render them positively charged and energetically unstable to exist on their own. The second reason is that the metals in the metal hydroxide layers are thought to be strongly bonded throughout the individual layers and could only be disrupted by heating, acid neutralization or individual metal precipitation with selected anions.

The anionic precipitation scenario is based solely on the comparison of the solubilities of such species with respect to the solubility of the LDH. The pyrolysis and acid treatment scenarios both result in the compromise of the structural integrity of the LDH lattice sheets, with the outcome resulting in either a mixed metal oxide/spinel material or dissolution producing free metal (hydrated) cations. Other than the three scenarios of metal hydroxide disruption, LDH are a fairly robust form of material.

There have been numerous reports of preparing LDH using three different metals, mostly in the forms of LDH containing two different divalent metals and one trivalent metal.[1-8] These materials are prepared by precipitating a solution containing three different metal salts with an appropriate base. The chemistry behind such synthesis is still closely related to the divalent-trivalent metal LDH, with the added feature of the possibility of cationic preference during the precipitation phase.

Another preparatory route for LDH containing several different metals is by the introduction of a transition-metal chelate into the LDH interlayer by intercalation.[9-11]

Ni(II) was found to be taken up by a Mg-Al LDH, with some or no replacement of the LDH magnesiums.[12,13] In one case, the results were attributed to a process known as diadochy (replacement of one metal by another in situ).

We therefore embarked on a project to explore the possibility of partial LDH metal replacement by several candidate metals.

4.2 Purpose of Experiment

Based on what is known about the crystallinity of aged versus fresh LDH, we set out to perform a project that centered on working with LDH materials that were both freshly prepared and aged in their mother liquor solutions. Once these LDH materials were formed, further post-synthesis treatments were conducted on them. Such treatments included stirring these LDH materials in water, sodium chloride solutions and nickel(II) chloride solutions for an extended period of time, and then studying the effects on the improvements in crystallinity, if any such improvements occur.

We were slightly surprised to find that by stirring the freshly prepared LDH in water and NaCl solutions, an increase in crystallinity occurred. But for the fresh LDH in the $NiCl_2$ solution, we were very surprised to find that the nickel(II) cations, in solution, were extensively incorporated into the LDH.

For the aged LDH materials, there were no differences in the crystallinity before and after mixing in water and the NaCl solution, but we discovered that a small amount of nickel(II) cations were also incorporated into the LDH.

The characterization tools used for this project included FT-IR, PXRD, AAS and transmission or diffuse-reflectance (DR)-UV-Vis-NIR.

We then planned on attempting similar experiments with other divalent metal cations, including Co(II), Zn(II), Cu(II), Mg(II) and Mn(II) in order to determine if the results with Ni(II) could be generalized.

4.3 Experimental Procedure

The experimental parameters for all candidate metals were identical to what was done with the nickel incorporation project, with the added characterization tools of DR-UV-Vis-NIR spectroscopy. Since this added characterization tool was not performed on the nickel samples, for the initial submission, the full characterization of these two materials will also be revisited and presented here.

Twelve 2.0g batches of fresh and aged 2:1 Mg-Al LDH-Cl (based on the $Mg_2Al(OH)_6Cl \bullet 3/2H_2O$ formula) were prepared by adding the stoichiometric amounts of 50% NaOH to solutions containing 0.2 M $MgCl_2$ and 0.1 M $AlCl_3$ (6 mole OH^- : 1 mole Al^{3+}) in 250 mL roundbottomed flasks. Six of the LDH materials, designated as fresh,

were allowed to stir in solution for one hour, under a steady stream of ultra-high purity nitrogen gas. The other six LDH materials, designated as aged, were allowed to reflux in solution, under a steady stream of ultra-high purity nitrogen gas, for approximately one day.

All twelve LDH materials were thoroughly washed and separated, after their required mixing times, with Millipore Milli-Q Academic deionized water (18.2 $M\Omega\ cm^{-1}$). Under no circumstances were any of the twelve LDH materials allowed to dry. The fresh LDH-Cl materials were placed in a vacuum desiccator, for storage only (the 50 mL centrifuge tube lids tightly closed, in order to keep CO_2 out and to keep the precipitates hydrated) during the refluxing time for the aged LDH-Cl materials. Since three LDH materials were allowed to reflux at a time, it took two days for the six LDH-Cl materials to be aged.

Once all LDH materials were washed and separated from their respective solutions, they were placed in the MCl_2 solutions and allowed to stir, under a steady stream of ultra-high purity nitrogen gas, for five days.

The amounts of MCl_2 salts needed were based on the anticipated replacement of one-half of the LDH lattice magnesiums. For 2.0 g of each 2:1 Mg-Al LDH-Cl, this equates to: 1.98 g $NiCl_2 \bullet 6H_2O$, 1.98 g $CoCl_2 \bullet 6H_2O$, 1.14 g $ZnCl_2$ (anhydrous), 1.42 g $CuCl_2 \bullet 2H_2O$, 1.69 g $MgCl_2 \bullet 6H_2O$ and 1.05 g $MnCl_2$ (anhydrous).

Each of the MCl_2 salts was dissolved in 50 mL of deionized water, their respective pH recorded, then the wet 2:1 Mg-Al LDH-Cl materials were transferred to these solutions. In order to aid in the wet LDH transfer and to increase the solution

volume for ease of mixing, 50 mL of deionized water was added to the LDH, before transfer to the MCl_2 solutions.

After five minutes of stirring, the pH of the twelve solutions was recorded. After the fifth day of mixing, the pH of each solution was also recorded. As soon as the pH values were documented, all materials were then thoroughly separated and washed, then placed in vacuum desiccators for drying, under mixtures of molecular sieves and drierite.

As a comparison, 1.0g batches of 2:1 M^{II}-Al LDH-Cl (M^{II}= Ni, Co, Zn, Mn and Cu) were prepared. Each of these five LDH materials were prepared by dissolving the following salts amounts in 50 mL deionized water: 1.50 g $NiCl_2 \bullet 6H_2O$, 0.761 g $AlCl_3 \bullet 6H_2O$; 1.49 g $CoCl_2 \bullet 6H_2O$, 0.758 g $AlCl_3 \bullet 6H_2O$; 1.04 g $CuCl_2 \bullet 2H_2O$, 0.736 g $AlCl_3 \bullet 6H_2O$; 0.823 g $ZnCl_2$ (anhydrous), 0.729 g $AlCl_3 \bullet 6H_2O$; 0.810 g $MnCl_2$ (anhydrous), 0.777 g $AlCl_3 \bullet 6H_2O$. To each of these solutions (stirring under a nitrogen gas blanket), 1.0 mL 50% NaOH was added. The suspensions were allowed to mix for one hour, and then 25 mL were removed. These five samples (designated fresh LDH) were then washed/centrifuged, and placed in a vacuum desiccator for drying. The other 25 mL were then placed in a hot oil bath (100 °C) for overnight reflux (also under a nitrogen gas blanket). These five LDH materials were then washed/centrifuged, and placed in a separate vacuum desiccator for drying.

All materials were characterized by FT-IR, PXRD, AAS and transmission or DR-UV-Vis-NIR.

The FT-IR spectra were collected, as CsI pellets (1 – 2% LDH in CsI, for a 0.2500 g total pellet), using a Perkin-Elmer Spectrum One spectrometer, utilizing CsI optics and backgrounds. Each sample was scanned within the mid-IR range (4000 cm^{-1} to 250 cm^{-1}), for an average of forty scans each, and at a resolution of 4 cm^{-1}.

The PXRD patterns were obtained using a Siemens F-series diffractometer, using no internal or external standards. Each diffraction pattern was scanned from 5° to 70° (2θ), using CuKα radiation (λ= 1.54056 Å), with a step size of 0.05° and a dwell time of one second. The patterns and peak list reports were generated using Jade™ software.

Metals analysis was performed by flame AAS, using a Perkin-Elmer AAnalyst 300 spectrometer with Perkin-Elmer supplied standards and element lamps. Each sample was prepared in a 5% nitric acid solution for the first analysis, and then 1 mL aliquots of concentrated hydrochloric acid were added to each LDH solution, and then analyzed again. The aluminum analysis responded to the HCl additions, but the other metals did not. The purpose of using the HCl additions (other than the fact that a HNO_3/HCl solution is recommended for Al) is to complex the aluminums with chlorides, so that it will be more difficult for the aluminums to form refractory oxides within the flame.

The transmission or DR-UV-Vis-NIR spectra were obtained using a Perkin-Elmer Lambda 900 spectrometer. Each spectrum was scanned within the UV-Vis-NIR (near infrared) range, from 200 nm to 1700 nm, at a scan rate of 100 nm/sec and an integration time of 0.12 sec.

4.4 Results

When working with various transition metals, the first observation is due to the numerous colors that each metal may have from their simple salts or more elaborate complexes.

Based on the various colors of transition metals, the samples introduced with the chlorides of magnesium and zinc did not undergo any color changes.

The samples that were introduced with cobalt displayed a pink color throughout the five-day mixing period. Upon drying in the desiccator, the fresh LDH sample maintained its pink color, but the aged LDH sample turned blue.

The samples that were introduced with nickel displayed a green color throughout the five-day mixing period. Upon drying in the desiccator, the fresh LDH sample was deep green, but the aged LDH sample was light green.

The samples that were introduced with copper displayed a blue-green color throughout the five-day mixing period. Similar to the nickel materials, the fresh LDH had a darker blue-green color, but the aged material was lighter.

The samples introduced with manganese displayed unique observations. The $MnCl_2$ solution has a faint-pink color to it. When these solutions were added to the LDH materials, the fresh LDH sample maintained this faint-pink color throughout the five-day mixing period, but within a few seconds of addition to the aged LDH sample, the material turned brown. Upon washing the solids after the mixing stage, the fresh LDH sample immediately took on the similar brown color that the aged LDH sample had.

Another important observation regarding these LDH materials were that the fresh LDH samples separated easily during centrifuge but the aged materials did not fully separate out. After several hours of centrifuge, some of the LDH still remained throughout the solution, but enough solid was recovered, in each sample, for complete characterization.

The difficulty in separation is common for most aged LDH materials, especially after three or four subsequent washes. The aged materials consist of individual well-crystalline particles, but these are smaller than the clumps of less crystalline material in the fresh material, so that centrifuging becomes less effective.

Since twelve total samples were prepared, each one being characterized by several methods, each Mg-Al LDH-M(II) sample will be presented independently, with respect to the divalent metal used.

The range of interest, for the FT-IR spectra, will be from 4000 – 250 cm^{-1}, with special interest in the 1100 – 250 cm^{-1}range, because this range covers the LDH metal hydroxide lattice region (Chapter 6).

For the transmission or DR-UV-Vis-NIR spectra, the range from 200 – 1700 nm will be shown. This range covers the ultraviolet, visible and near-infrared regions.

The pH values for the MCl_2 salt solutions, fresh and aged LDH-Cl samples, after five minutes stirring and after five days stirring with the divalent metal cations are shown in Table 4.1.

Table 4.1: The pH values of the LDH-M(II) materials. Columns below both Fresh and Aged LDH-Cl: Left column (five minutes mixing) and right column (five days mixing).

Metal Salt	Solution	Fresh LDH-Cl			Aged LDH-Cl	
$CoCl_2$	6.18	6.18	6.80		6.90	6.35
$ZnCl_2$	5.58	5.82	5.72		6.27	7.40
$MnCl_2$	6.37	7.46	7.35		7.51	6.91
$CuCl_2$	3.25	4.52	7.25		4.55	4.21
$NiCl_2$	5.82	6.11	6.84		6.70	5.88
$MgCl_2$	6.54	8.01	7.36		8.60	7.58

The pH values show some interesting observations. We would expect the pH values to be high when the divalent metal cations are incorporated into the LDH, because the free divalent cations will not be in solution. This scenario is most evident with the fresh LDH sample treated with copper(II). The aged LDH sample with copper(II) shows low pH values after both five minutes and five days mixing, because the majority of the copper(II) cations may still be in solution.

Other than this single case, data for the other materials are more difficult to interpret because the pH of the parent LDH materials was around 7.30 to 7.50 to start out with. Therefore, the pH studies are inconclusive as to whether or not exchange or uptake has occurred with each of the six divalent metal cations. It is evident that there were pH changes for these materials, somewhere between the five-minute and five-day mixing period.

4.4.1 Mg-Al LDH-Ni(II)

Figure 4.1 shows the FT-IR spectra, XRD patterns and DR-UV-Vis-NIR spectra for the fresh and aged LDH materials after treatment with Ni(II).

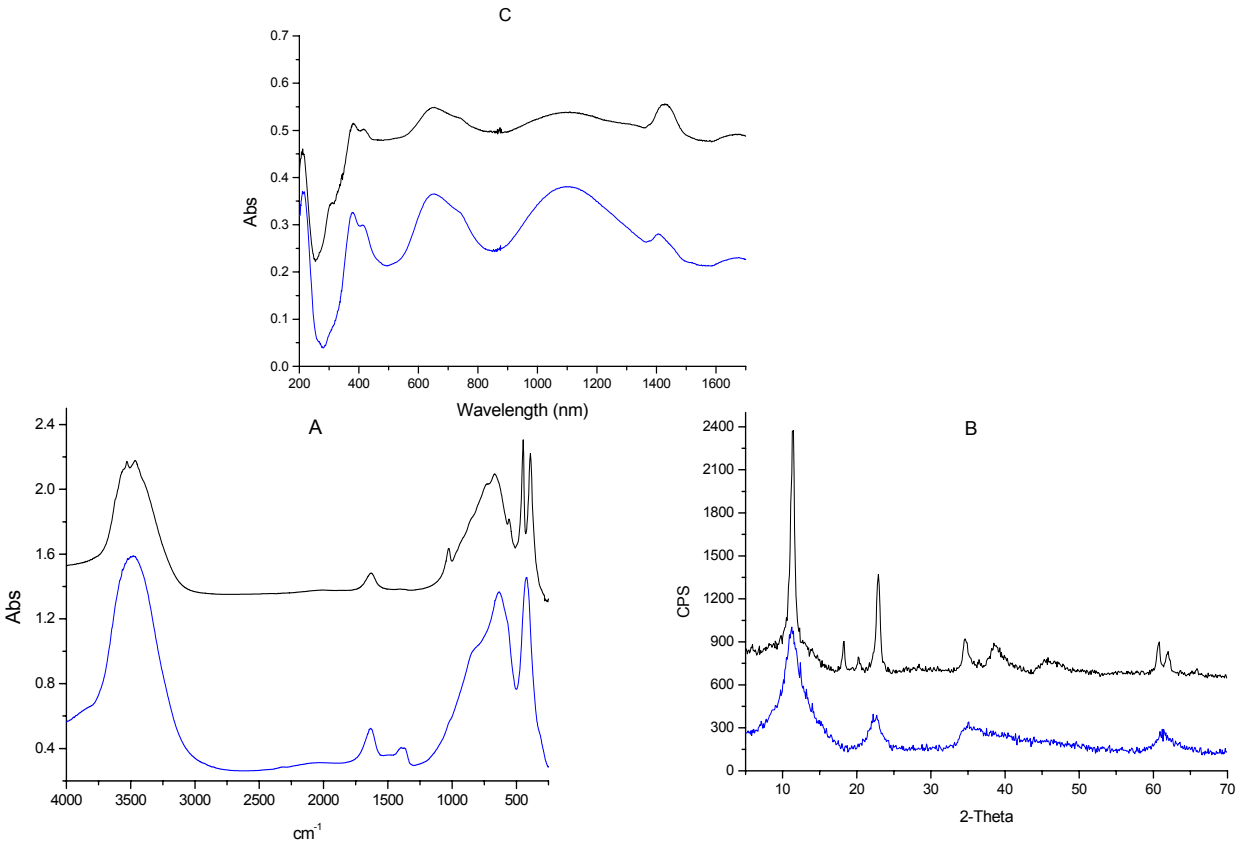

Figure 4.1: A) FT-IR spectra (blue-fresh, black-aged), B) XRD patterns (blue-fresh, black-aged) and C) DR-UV-Vis-NIR spectra (blue-fresh, black-aged) of 2:1 Mg-Al LDH-Cl with Ni(II).

The differences in the IR spectra between the fresh and aged materials are apparent. The aged sample looks similar to an aged 2:1 Mg-Al LDH-Cl (see Figure 1.4, Chapter 1) with peaks at 447 cm^{-1} and 393 cm^{-1}, but the fresh sample shows one strong peak, at 425 cm^{-1}.

The DR-UV-Vis-NIR spectra look similar, but the bands in the fresh sample are stronger and more clearly resolved. These bands have been studied before, and show both spin-allowed and spin-forbidden d-d transitions, with the following assignments in Table 4.2.[14,15]

The single peak around 1380 – 1400 nm has been described as the first overtone of the fundamental hydroxide stretching mode[16] and will appear in all transmission or DR-UV-Vis-NIR spectra.

Table 4.2: DR-UV-Vis-NIR peaks and assignments for both LDH materials with Ni(II).

Wavelength (nm)	Transition
378	$^3A_{2g}(F) \rightarrow {}^1E_g(D)$
416	$^3A_{2g}(F) \rightarrow {}^3T_{1g}(P)$
649	$^3A_{2g}(F) \rightarrow {}^1T_{2g}(D)$
742	$^3A_{2g}(F) \rightarrow {}^3T_{1g}(F)$
1100	$^3A_{2g}(F) \rightarrow {}^3T_{2g}(F)$
1446	NIR

The differences in the XRD patterns are mainly based on the degree of crystallinity. The aged XRD pattern is similar to an aged 2:1 Mg-Al LDH-Cl, with the notable exception of two peaks around 18° (2θ) and 20° (2θ). These two peaks were assigned using the ICCD database to gibbsite ($Al(OH)_3$). The pattern for the fresh material after its exposure to the $NiCl_2$ solution resembles a slightly more crystalline material than its parent fresh 2:1 Mg-Al LDH-Cl (Figure 1.5, Chapter 1). The interlayer spacings for both LDH materials are similar to that found by intercalated chloride, so no nickel, or more probably $[Ni(H_2O)_6]^{2+}$, is in the LDH interlayer.

The metals analysis provides the information needed to conclude whether or not cation exchange has taken place, or simple uptake by adsorption has occurred. From Table 1, the fresh LDH material shows a 1:1:1 ratio of Mg:Ni:Al, but the aged LDH material is close to its original 2:1 Mg:Al ratio, showing a 9:1 Mg:Ni ratio. This is conclusive of a stoichiometric replacement of LDH magnesiums with nickel for the fresh LDH sample, much less complete exchange (probably simple surface or edge adsorption of nickel) for the aged LDH sample.

4.4.2 Mg-Al LDH-Co(II)

From the red and blue colors of the two LDH samples with cobalt, we would expect to see some differences between them during characterization.

When these two color differences were first observed, the first thing that came to mind was their similarity to the commercially available desiccators that are coated with cobalt (II) chloride. When this desiccant is saturated with water, their color is red; when they are dehydrated, their color is blue. It is a well-known fact that the difference is due to a change in local symmetry, from octahedral (red) to tetrahedral (blue). This difference can also be readily seen in the laboratory by dissolving cobalt (II) chloride in both water (red solution) and acetone (blue solution).

Figure 4.2 shows the FT-IR spectra, XRD patterns and DR-UV-Vis-NIR spectra for the fresh and aged samples treated with Co(II). These are the samples that occur in two different colors, so the information from the DR-UV-Vis-NIR (especially the visible region) will be important.

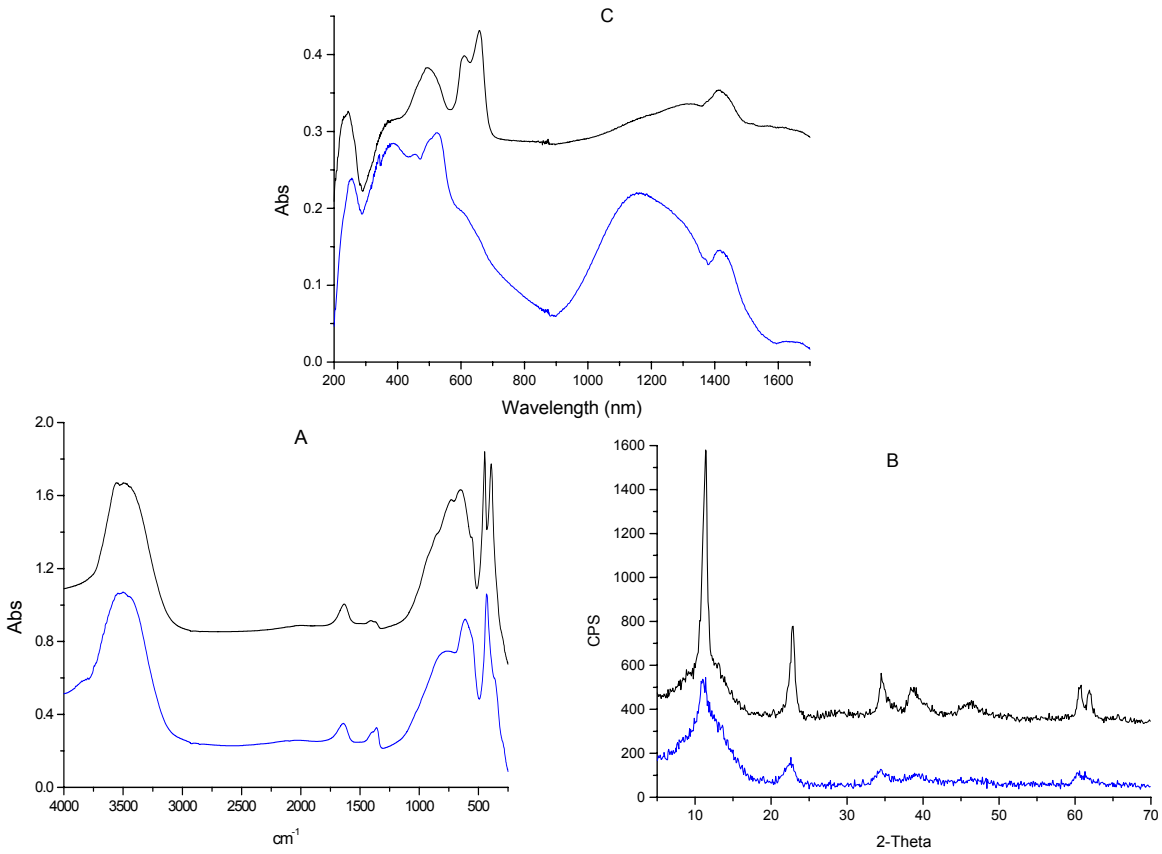

Figure 4.2: A) FT-IR spectra (blue-fresh, black-aged), B) XRD patterns (blue-fresh, black-aged) and C) DR-UV-Vis-NIR spectra (blue-fresh, black-aged) of 2:1 Mg-Al LDH-Cl with Co(II).

The IR spectrum of the aged LDH sample closely resembles that of an aged 2:1 Mg-Al LDH-Cl, with peaks at 447 cm^{-1} and 392 cm^{-1}, but the fresh LDH sample shows one peak at 430 cm^{-1}. These spectra are similar to what was observed for the LDH and nickel case, but the single peak, for the fresh LDH sample, has a different wavenumber.

The differences in the XRD patterns are seen by the broadness of the peaks. The aged LDH sample shows sharper, well resolved peaks, which indicate a greater degree of crystallinity. The fresh LDH sample shows broad peaks that are not very well resolved.

The most profound difference between these two materials is seen in their respective DR UV-Vis-NIR spectra. The fresh LDH sample shows only one band in the visible region, which corresponds to the cobalt(II) ion existing in an octahedral environment. This band has been observed before for O_h Co(II).[17,18] The aged LDH sample shows several bands in the visible region, which corresponds to the cobalt(II) ion existing in a tetrahedral environment. These bands have also been observed before for T_d Co(II).[19] The assignments are listed in Table 4.3.

Table 4.3: UV-Vis-NIR peaks and transitions for both LDH-Co(II) samples. The blue sample on the left and the red sample on the right.

Wavelength (nm)	Transition
488	$^4A_2(F) \rightarrow {}^4T_1(P)$
610	$^4A_2(F) \rightarrow {}^4T_1(F)$
647	$^4A_2(F) \rightarrow {}^4T_2(F)$
1441	NIR

Wavelength (nm)	Transition
520	$^4T_{1g}(F) \rightarrow {}^4A_{2g}(F)$
615	$^4T_{1g}(F) \rightarrow {}^4T_{1g}(P)$
1174	$^4T_{1g}(F) \rightarrow {}^4T_{2g}(F)$
1441	NIR

The metals analysis show a 1:1:1 ratio of Mg:Co:Al for the fresh LDH sample but a 2:1 Mg-Al ratio, and also a 10:1 ratio of Mg:Co for the aged sample. This proves stoichiometric replacement of magnesium for cobalt, for the fresh LDH case and some surface adsorption for the aged LDH case. The blue color for the aged LDH case can now be interpreted as cobalt(II) cations existing on the outside of the LDH layers, where they are susceptible to gain or lose water molecules. This may lead to either octahedral or tetrahedral environments.

4.4.3 Mg-Al LDH-Cu(II)

The LDH materials treated with copper are more difficult to interpret due to the complex chemistry of copper(II). This was anticipated due to the potential Jahn-Teller distortions that O_h copper(II) ions can undergo, and to its ready formation of basic salts.

Figure 4.3 shows the FT-IR spectra, XRD patterns and DR-UV-Vis-NIR spectra for both aged and fresh LDH samples with Cu(II).

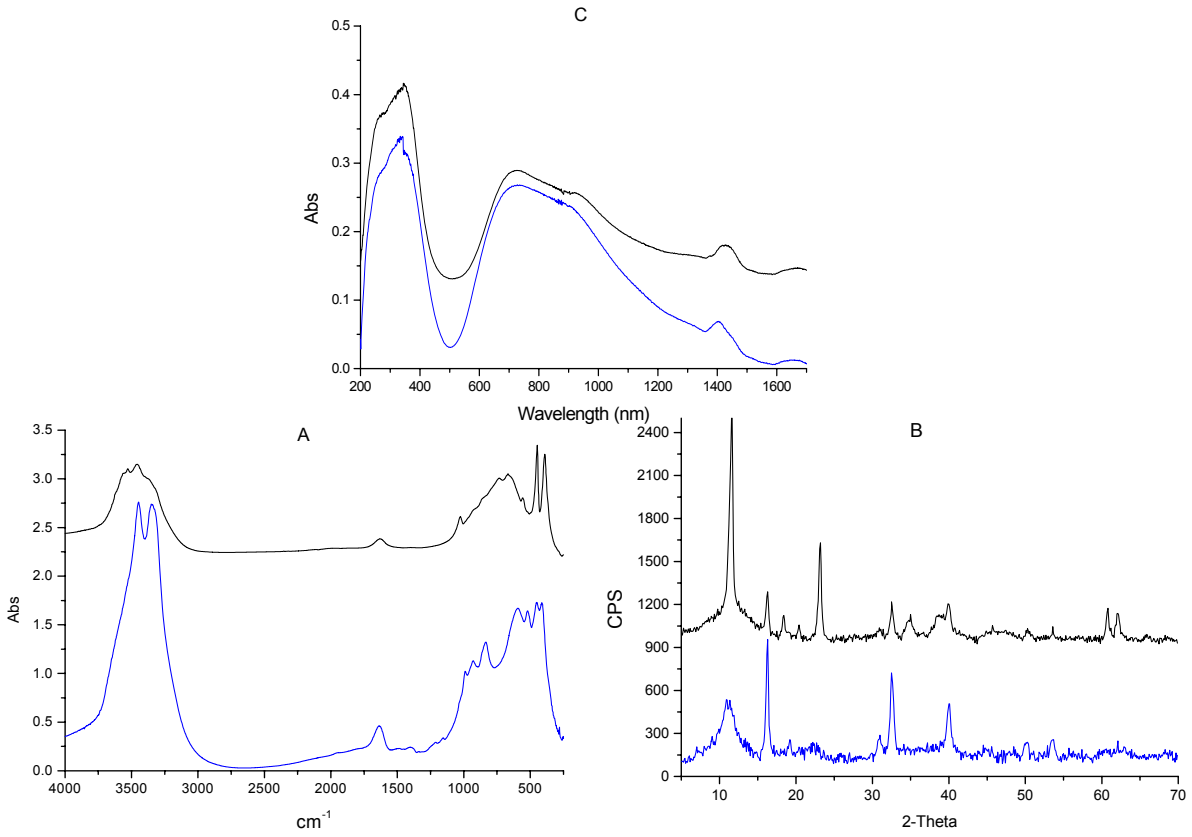

Figure 4.3: A) FT-IR spectra (blue-fresh, black-aged), B) XRD patterns (blue-fresh, black-aged) and C) DR- UV-Vis-NIR spectra (blue-fresh, black-aged) of 2:1 Mg-Al LDH-Cl with Cu(II).

Once again the FT-IR spectrum of the aged LDH sample resembles an aged 2:1 Mg-Al LDH-Cl, with peaks at 447 cm^{-1} and 391 cm^{-1}, but the fresh sample is quite different. There are numerous peaks within the 1000 cm^{-1} to 250 cm^{-1} range, which may or may not all correspond to LDH lattice vibrations.

The XRD patterns are also strikingly different. The aged LDH sample resembles the aged XRD patterns of the two previously described aged LDH materials, but with added peaks. Like the aged LDH sample with nickel, the peaks at around 18° (2θ) and 20° (2θ) are attributed to gibbsite formation. The fresh LDH sample clearly has more than one material. For both materials, there are LDH peaks as well as basic copper chloride peaks present, as identified by the ICDD database.

The DR-UV-Vis-NIR spectra look very similar to each other. In both cases, the d^9 copper(II) ions should produce an observable d-d transition. In a d^9 electronic system, without a Jahn-Teller distortion, we would expect one transition only, t_{2g} to e_g, or ^2E_g to $^2T_{2g}$. With distortion, we may have transitions from a_{1g}, e_g, or b_{1g} (sometimes labeled b_{2g}, depending on choice of axes) to the half-filled b_{2g}. The transitions are weak, independent of the exact ligand identity, and in the red to near IR, so charge transfer is not involved.

The metals analysis show close to a 2:1 Mg:Al ratio and a 8:1 Mg:Cu ratio, indicative of surface adsorption of copper(II)for the aged LDH sample, but a little higher than a 1:1:1 Mg:Cu:Al ratio, for the fresh LDH sample.

In this case, AAS was not as helpful in determining what kind of reaction had occurred, but the XRD pattern for the fresh LDH sample shows a mixture of distinct materials.

4.4.4 Mg-Al LDH-Zn(II)

The LDH materials treated with zinc(II) are easier to understand than the LDH-copper(II) materials. We did not anticipate any chemical or physical complications with zinc, due to its inert nature. One problem that we had, notably with all of the colorless samples, was an apparent negative absorbance in the UV region. We switched from diffuse reflectance to transmission for these samples, which alleviated this problem.

Figure 4.4 shows the FT-IR spectra, XRD patterns and transmission UV-Vis-NIR spectra for the fresh and aged LDH materials with zinc(II).

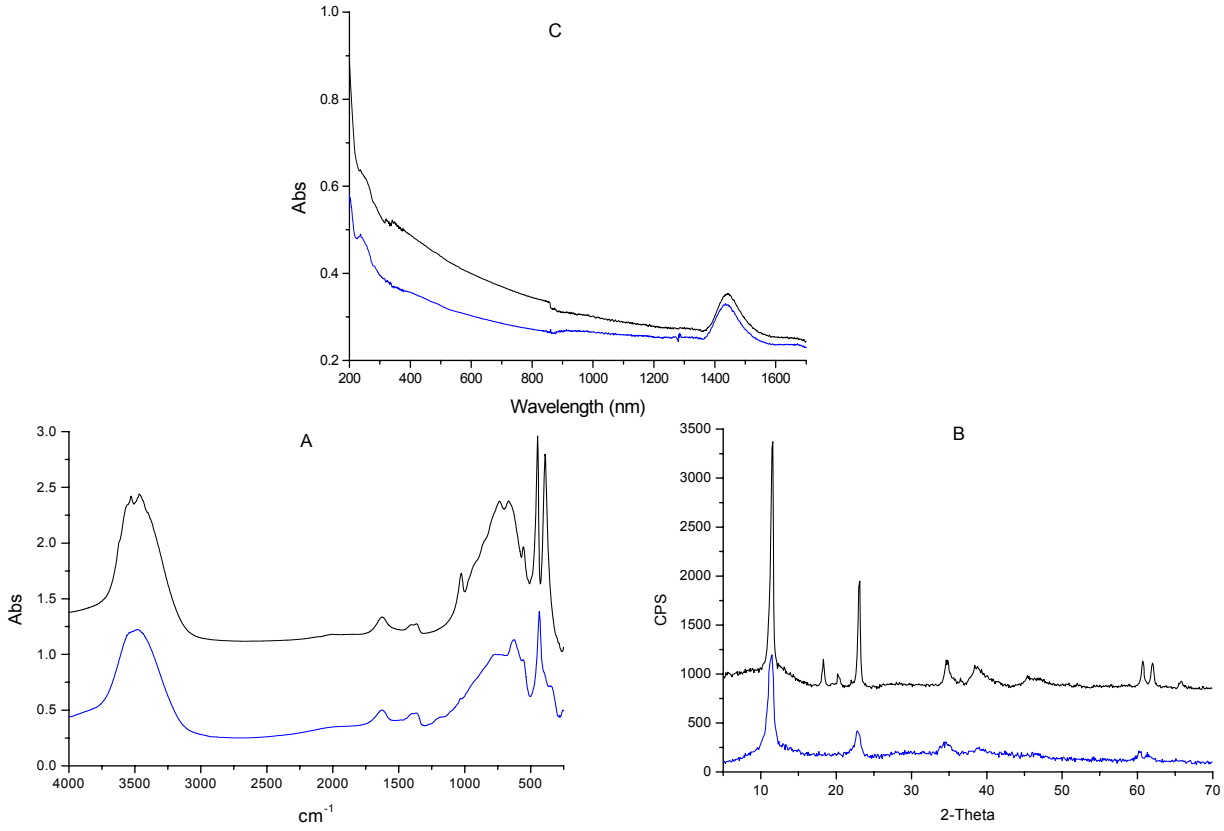

Figure 4.4: A) FT-IR spectra (blue-fresh, black-aged), B) XRD patterns (blue-fresh, black-aged) and C) Transmission-UV-Vis-NIR spectra (blue-fresh, black-aged) of 2:1 Mg-Al LDH-Cl with Zn(II).

What seems to be a recurring theme for the aged LDH-M(II) materials, the FT-IR spectra, for LDH with zinc(II) follow a similar pattern. The aged LDH sample is similar to that of an aged parent 2:1 Mg-Al LDH-Cl, with peaks at 447 cm^{-1} and 391 cm^{-1}. The fresh LDH sample shows one strong peak at 434 cm^{-1}.

The XRD patterns show differences between the two. The aged LDH-Zn(II) sample is similar to the parent aged 2:1 Mg-Al LDH-Cl, but with the added presence of gibbsite peaks. The fresh LDH sample shows broader peaks, but sharper than the fresh LDH-Ni(II) sample.

We anticipated a horizontal spectrum, in the visible region, for both cases due to no d-d transitions within their filled d^{10} configurations. The transmission UV-Vis-NIR spectra are somewhat horizontal, with a slight increase in absorption in the UV region, likely due to charge transfer and/or scattering. As with all samples, there is a peak around 1430 nm, attributed to an O-H stretch combination/overtone.

The metals analysis shows a 1:1:1 Mg:Zn:Al ratio for the fresh LDH sample and a 2:1 Mg:Al and a 17:1 Mg:Zn ratio for the aged LDH sample. This analysis confirms stoichiometric replacement of magnesium by zinc for the fresh LDH sample and some surface adsorption of zinc for the aged LDH sample.

4.4.5 Mg-Al LDH-Mg(II)

We had a different motive for mixing Mg(II) ions with both LDH materials. Instead of determining whether or not replacement or adsorption of Mg(II) ions would occur, which would be a foolish attempt to try to describe, unless we used a magnesium

isotope, we set out to see if an increase in crystallinity for the fresh LDH, while mixing with free Mg(II) ions, would result.

Figure 4.5 shows the FT-IR spectra, XRD patterns and transmission UV-Vis-NIR spectra for the fresh and aged LDH materials, after exposure to Mg(II). In both cases, each IR spectra resemble an aged 2:1 Mg-Al LDH-Cl, with peaks at 447 cm^{-1} and 391 cm^{-1}. The importance with this observation is the appearance of an increase in crystallinity for the fresh LDH sample. The IR spectra for the fresh LDH-Mg(II) sample after such exposure are very different from those of a fresh 2:1 Mg-Al LDH-Cl material (Figure 6.5, Chapter 6).

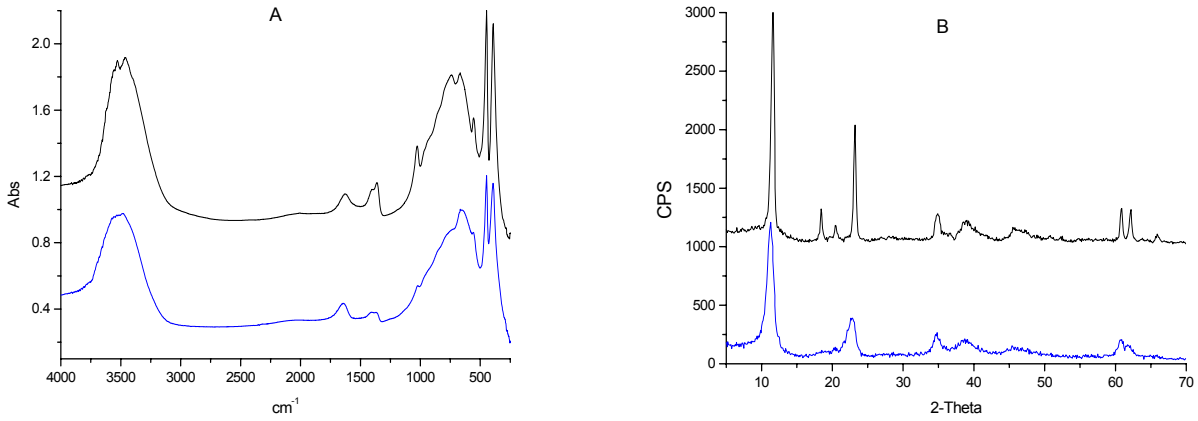

Figure 4.5: A) FT-IR spectra (blue-fresh, black-aged) and B) XRD patterns (blue-fresh, black-aged) of 2:1 Mg-Al LDH-Cl with Mg(II).

The XRD patterns both closely resemble the aged 2:1 Mg-Al LDH-Cl. The aged sample differs from the fresh sample due to the presence of gibbsite.

No UV-Vis-NIR spectra were obtained for these two samples because the spectra were obtained for a fresh 2:1 Mg-Al LDH-Cl and an aged 2:1 Mg-Al LDH-Cl, as the control spectra (Figure 4.6). There would be no differences between these two sets of materials.

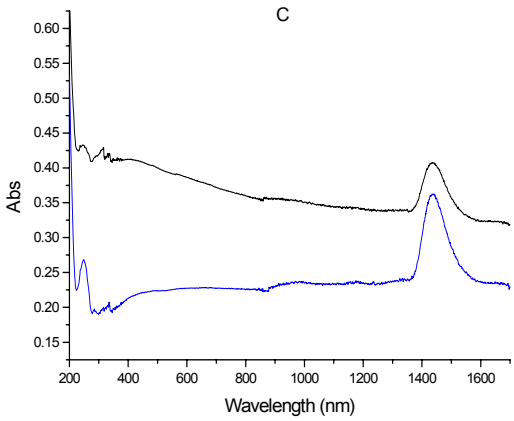

Figure 4.6: Transmission-UV-Vis-NIR of fresh 2:1 Mg-Al LDH-Cl (below) and aged 2:1 Mg-Al LDH-Cl (above).

The metals analysis show close to a 2:1 Mg-Al ratio for both materials. This confirms that no significant increase in magnesium content occurred, whether by incorporation into the LDH lattice framework or by surface adsorption.

4.4.6 Mg-Al DH-Mn(II)

Due to the notable color changes between the fresh and aged LDH samples treated with manganese(II) during the mixing stage, we would have expected to see major differences between these two materials. Unfortunately the fresh LDH sample took on the same color as the aged LDH sample during the washing stage, so we believe that oxidation of Mn(II) has occurred for both LDH materials. The oxidation of Mn(II) to Mn(III) is spontaneous in basic environments, especially in the presences of oxygen. The oxidation to Mn(IV) is unusual in aqueous solution, but is common as solid MnO_2, so we could expect to see it with our materials.

Figure 4.7 shows the FT-IR spectra, XRD patterns and DR-UV-Vis-NIR spectra for both fresh and aged LDH materials with Mn(II).

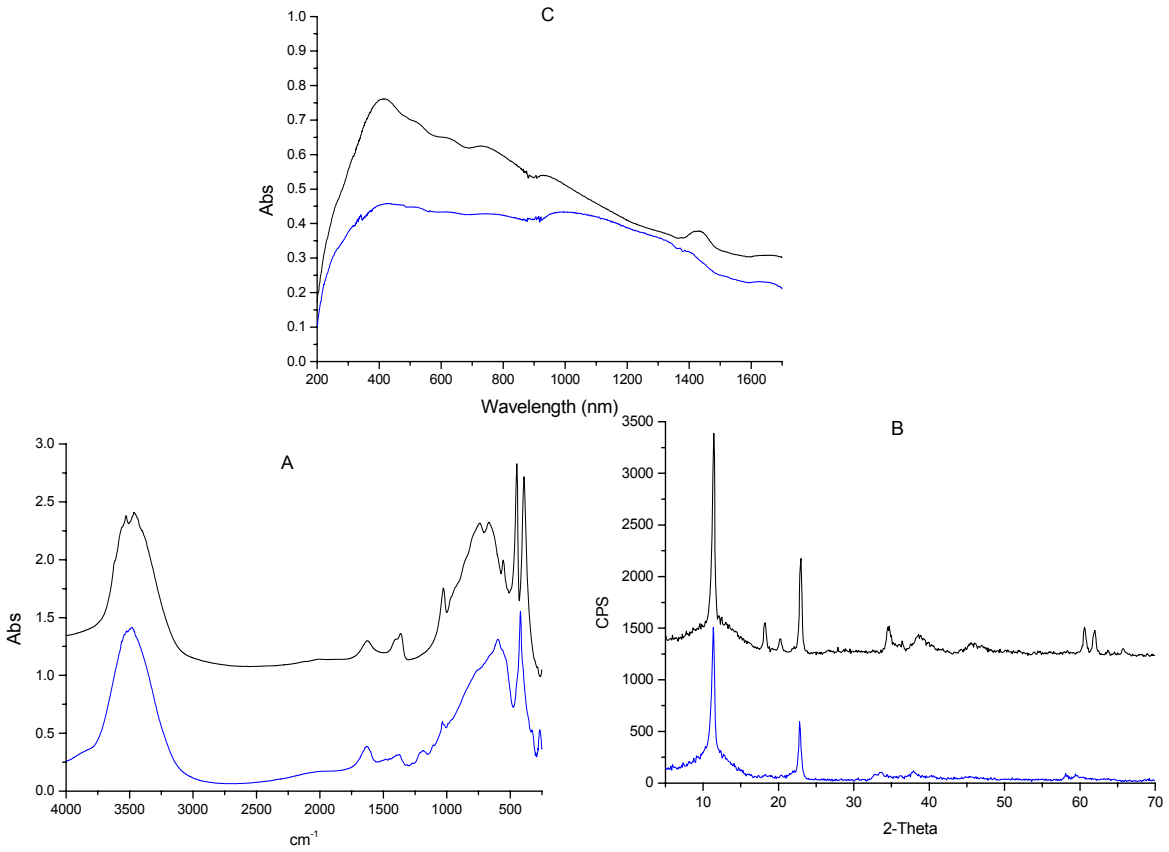

Figure 4.7: A) FT-IR spectra (blue-fresh, black-aged), B) XRD patterns (blue-fresh, black-aged) and C) DR-UV-Vis-NIR spectra (blue-fresh, black-aged) of 2:1 Mg-Al LDH-Cl with Mn(II).

The aged LDH sample is similar to an aged 2:1 Mg-Al LDH-Cl, with peaks at 447 cm^{-1} and 390 cm^{-1}, but the fresh LDH sample shows one strong peak at 419 cm^{-1}. This is a bit puzzling because it is our belief that in order to remain in the LDH lattice framework, as a stoichiometrically exchanged cation, the manganese ion would have to stay in the divalent state. If any oxidation has occurred (to Mn(III) or Mn(IV)), the structural integrity of the LDH lattice would be compromised. We would expect to see something similar to the fresh LDH-Cu(II) case. We do not see anything of this sort, so the LDH structure may have survived. The suggestion that most or some of the manganese remained in the divalent state is plausible; because the dark colors

attributed to higher-valence manganese are so intense that a small degree of oxidation is enough to mask any further changes.

The XRD pattern for the aged LDH sample closely resembles an aged 2:1 Mg-Al LDH-Cl pattern, but once again with gibbsite peaks. The fresh LDH sample shows strong and sharp peaks, not seen as such with any of the fresh LDH materials (exception with the LDH and magnesium). An interesting observation is seen with barely visible 110 and 113 reflections, which appear at angles less than 60° (2θ). These LDH reflections are generally present at 60° and 62° (2θ).[7,21]

The DR-UV-Vis-NIR spectra are not significantly different between the two samples. A very intense and broad band is observed in the visible region for the aged sample, but a less intense and broad band exists for the fresh sample. It is not known what predominate oxidation state the manganese is in, but the DR-UV-Vis-NIR spectra are similar to previously Mn(II) containing LDH materials.[3]

The metals analysis shows some interesting results. There is a 1:1:1 Mg:Mn:Al ratio for the fresh LDH sample, but only a 1:1 Mg:Al and a 19:1 Mg:Mn ratio for the aged LDH sample. We suspect that in the case of the fresh material, Mn(II) is protected by incorporation to the case, while in the presence of aged material, oxidation of Mn^{2+} by air to MnO_2 generates acid, which dissolves up some of the Mg_2Al material. In this case, we may be left with a nominal 1:1 Mg:Al LDH, which is actually a mixture of 2:1 LDH and aluminum hydroxide.

The interpretation of the data and the figures for the LDH-Mn(II) case has shown to be incredibly difficult. One question quickly comes to mind about these materials: If the AAS results show a 1:1 Mg:Al ratio for the aged LDH sample, why does the XRD pattern and the IR spectrum closely resemble an aged 2:1 Mg-Al LDH-Cl?

Table 4.4 shows the 003 reflection angles and the accompanying interlayer spacings for all twelve LDH samples. Each interlayer spacing is approximately the area determined for interlayer chloride, or possibly some residual carbonate. If any of the divalent metals were in the interlayer, Table 4.4 would show larger spacings.

There are differences in the 110 reflections for the samples that have some divalent metal replacement versus full magnesium retention. In every case (except for the samples with magnesium treatment and the fresh 2:1 Mg-Al LDH-Cl/Ni(II) sample), there is an increase in the d-spacing, for the 110 reflection. This is difficult to interpret because all of the divalent metals used are not significantly different, in size, from magnesium.

Table 4.4: Bragg reflection angles and interlayer spacings (uncorrected) for the 003 and 110 reflections in each of the 2:1 Mg-Al LDH-M(II) samples. The 110 reflection could not be resolved for the Fresh 2:1 Mg-Al LDH-Cl/Ni(II) sample.

LDH Material	003 Reflection Angle (2θ)	Interlayer Spacing (Å)	110 Reflection Angle (2θ)	110 d-spacing (Å)
Fresh 2:1 Mg-Al LDH-Cl/Ni(II)	11.39	7.77	61.29	1.51
Aged 2:1 Mg-Al LDH-Cl/Ni(II)	11.40	7.76	60.72	1.52
Fresh 2:1 Mg-Al LDH-Cl/Co(II)	11.19	7.90	60.46	1.53
Aged 2:1 Mg-Al LDH-Cl/Co(II)	11.39	7.76	60.62	1.52
Fresh 2:1 Mg-Al LDH-Cl/Cu(II)	11.10	7.97	60.49	1.53
Aged 2:1 Mg-Al LDH-Cl/Cu(II)	11.58	7.63	60.81	1.52
Fresh 2:1 Mg-Al LDH-Cl/Zn(II)	11.39	7.76	60.30	1.53
Aged 2:1 Mg-Al LDH-Cl/Zn(II)	11.49	7.69	60.78	1.52
Fresh 2:1 Mg-Al LDH-Cl/Mn(II)	11.38	7.77	58.20	1.58
Aged 2:1 Mg-Al LDH-Cl/Mn(II)	11.41	7.75	60.69	1.52
Fresh 2:1 Mg-Al LDH-Cl/Mg(II)	11.30	7.82	60.64	1.53
Aged 2:1 Mg-Al LDH-Cl/Mg(II)	11.60	7.62	60.89	1.52

The full metals analysis, with respect to the Mg:Al, Mg:M(II) and Al:M(II) ratios are shown in Table 4.5. These data support our claim of stoichiometric exchange of LDH magnesium with Co(II), Ni(II) and Zn(II), for the fresh samples. We are not sure about the manganese case, due to the color change indicating oxidation to a higher valence, or to the copper case, because of the likely disruption of the LDH lattice. The aged samples all show close to the theoretical 2:1 Mg:Al ratio, except for the manganese sample.

Table 4.5: Pertinent metals analysis for the LDH-M(II) materials.

LDH Material	Mg : Al	Mg : M(II)	Al : M(II)
Fresh 2:1 Mg-Al LDH-Cl/Co(II)	1.28	1.30	0.99
Aged 2:1 Mg-Al LDH-Cl/Co(II)	2.16	10.15	4.84
Fresh 2:1 Mg-Al LDH-Cl/Zn(II)	1.13	1.04	0.94
Aged 2:1 Mg-Al LDH-Cl/Zn(II)	1.97	16.86	9.96
Fresh 2:1 Mg-Al LDH-Cl/Mn(II)	0.97	0.89	0.92
Aged 2:1 Mg-Al LDH-Cl/Mn(II)	1.06	18.83	20.21
Fresh 2:1 Mg-Al LDH-Cl/Cu(II)	1.42	1.63	0.99
Aged 2:1 Mg-Al LDH-Cl/Cu(II)	1.93	7.62	4.16
Fresh 2:1 Mg-Al LDH-Cl/Ni(II)	0.89	0.80	0.91
Aged 2:1 Mg-Al LDH-Cl/Ni(II)	1.86	9.25	5.54
Fresh 2:1 Mg-Al LDH-Cl/Mg(II)	2.06	---	---
Aged 2:1 Mg-Al LDH-Cl/Mg(II)	1.87	---	---

By multiplying the Mg:M(II) ratio by the inverse of the Al:M(II) ratio, the Mg:Al ratio should be obtained. Comparing these values to the Mg:Al ratios, directly determined by AAS, they are slightly off. We also expected the Mg:M(II) ratios to be double that of the Al:M(II) ratios, but these values are also slightly off. We do not consider these factors significant and they may be due to the potential interference of magnesium and aluminum, with respect to each other, when both are together in the same solution.

4.5 Comparison of Mg-M(II)-Al LDH-Cl with 2:1 M(II)-Al LDH-Cl

In the above sections, an indication that cationic uptake has occurred was based on the positions of the IR peaks below 1000 cm^{-1}. Comparing each spectrum with an aged 2:1 Mg-Al LDH-Cl was easy to do because of the noticeable peaks around 447 cm^{-1} and 393 cm^{-1}. In order to supply more evidence in favor of magnesium replacement, fresh and aged 2:1 LDH-Cl samples containing: Ni-Al, Co-Al, Zn-Al, Cu-Al and Mn-Al were prepared. Each of these materials will produce characteristic IR peaks,

within the 1000 – 250 cm^{-1} range, that can be directly compared to the fresh and aged Mg-M(II)-Al LDH materials.

Along with the IR spectra, XRD patterns and DR-UV-Vis-NIR spectra were also obtained for the ten 2:1 M(II)-Al LDH-Cl samples. These IR spectra, XRD patterns and DR-UV-Vis-NIR spectra are shown in Figures 4.8-4.12.

We did not see any major color differences between the fresh and aged materials, as we did for the Mg-M(II)-Al LDH samples. Both 2:1 Ni-Al LDH-Cl samples were the same green color, both 2:1 Cu-Al LDH-Cl samples were the same blue-green color, both 2:1 Mn-Al LDH-Cl samples were the same brown color, and both 2:1 Co-Al LDH-Cl samples were the same pink-red color.

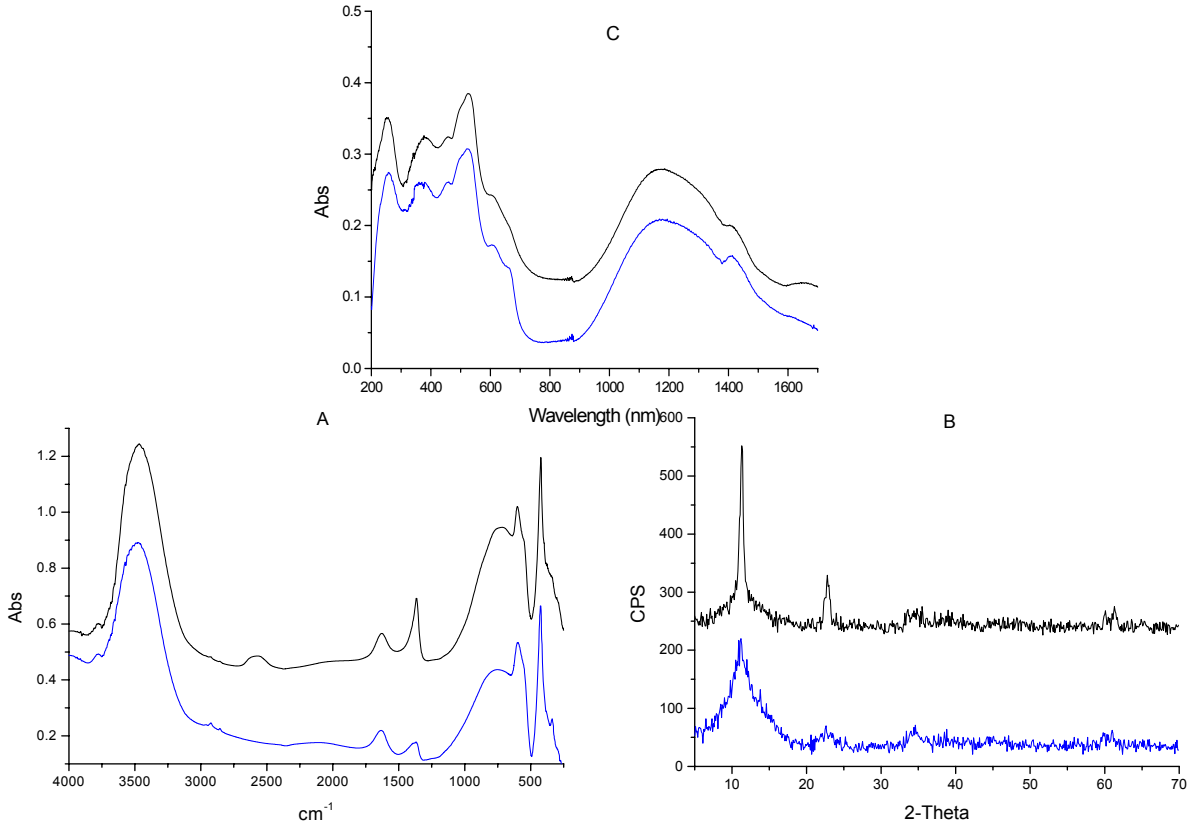

Figure 4.8: A) FT-IR spectra (blue-fresh, black-aged), B) XRD patterns (blue-fresh, black-aged) and C) DR-Vis-NIR spectra (blue-fresh, black-aged) of 2:1 Co-Al LDH-Cl.

For the 2:1 Co-Al LDH-Cl samples,[22] the IR spectra show one strong peak around 423 – 426 cm^{-1}, which is not present in the aged 2:1 Mg-Al LDH-Cl with Co(II), and at a different wavenumber from that in the fresh 2:1 Mg-Al LDH-Cl treated with Co(II). The XRD patterns show an improvement in crystallinity for the aged sample, and the DR-UV-Vis-NIR spectra are similar to the fresh 2:1 Mg-Al LDH-Cl treated with Co(II). This was expected since both aged and fresh 2:1 Co-Al LDH-Cl were red in color.

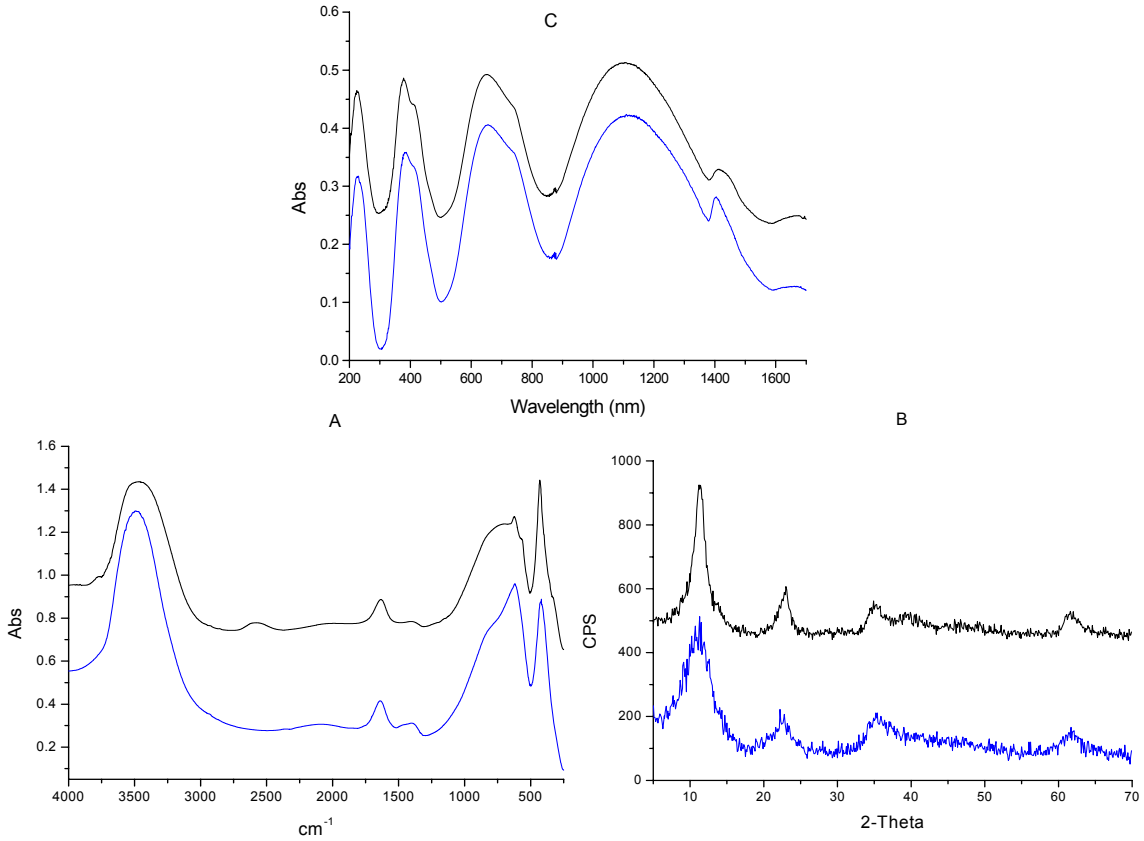

Figure 4.9: A) FT-IR spectra (blue-fresh, black-aged), B) XRD patterns (blue-fresh, black-aged) and C) DR-UV-Vis-NIR spectra (blue-fresh, black-aged) of 2:1 Ni-Al LDH-Cl.

For the 2:1 Ni-Al LDH-Cl samples,[23,24] the IR spectra show one strong peak around 419 – 430cm^{-1}, which is not present in the aged 2:1 Mg-Al LDH-Cl with Ni(II), and at a different wavenumber for the fresh 2:1 Mg-Al LDH-Cl with Ni(II). The XRD patterns do not show much increase in crystallinity on aging in either of these two sets of materials. The DR-UV-Vis-NIR spectra are similar to the aged and fresh Mg-Al LDH-Cl after treatment with Ni(II).

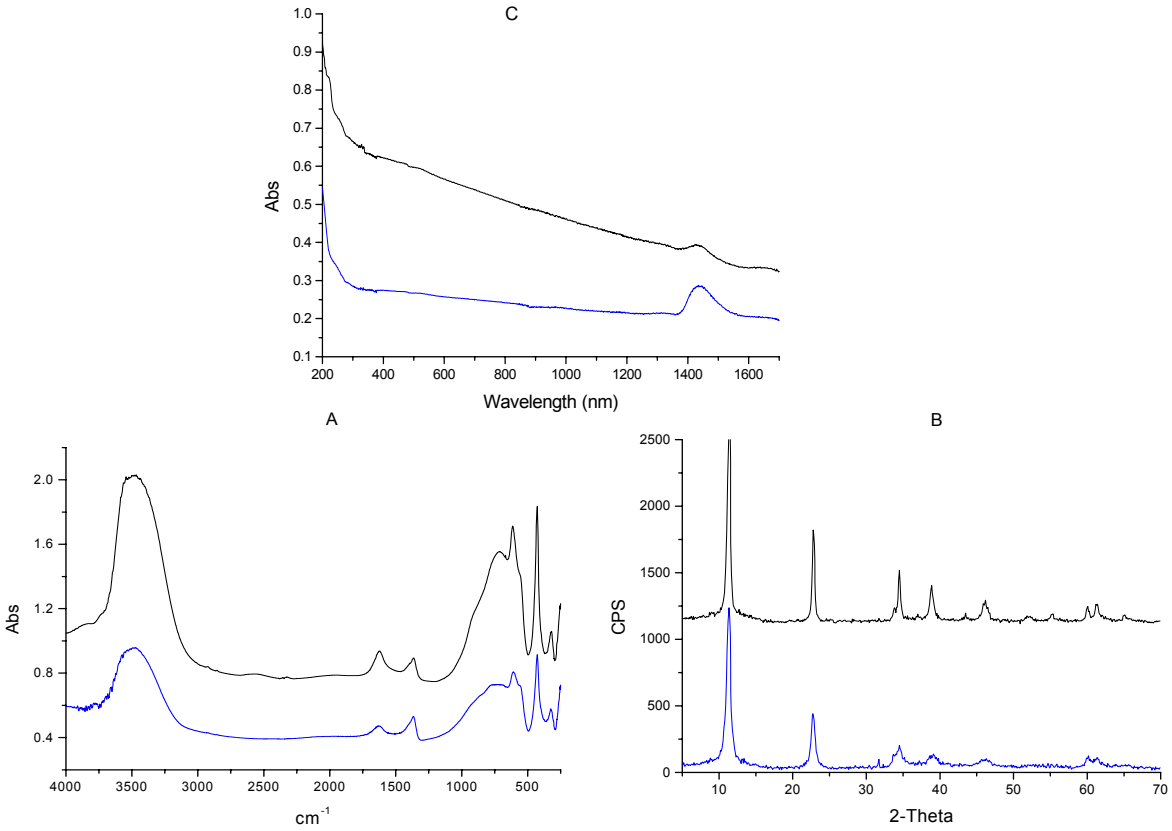

Figure 4.10: A) FT-IR spectra (blue-fresh, black-aged), B) XRD patterns (blue-fresh, black-aged) and C) Transmission-UV-Vis-NIR spectra (blue-fresh, black-aged) of 2:1 Zn-Al LDH-Cl.

For the 2:1 Zn-Al LDH-Cl samples,[25,26] the IR spectra show one strong peak around 427 cm^{-1}, which is not present in the aged 2:1 Mg-Al LDH-Cl with Zn(II), and at a different wavenumber for the fresh 2:1 Mg-Al LDH-Cl with Zn(II). The XRD patterns show an improvement in crystallinity, for the aged LDH sample. The DR-UV-Vis-NIR spectra are similar to the aged and fresh 2:1 Mg-Al LDH-Cl with Zn(II).

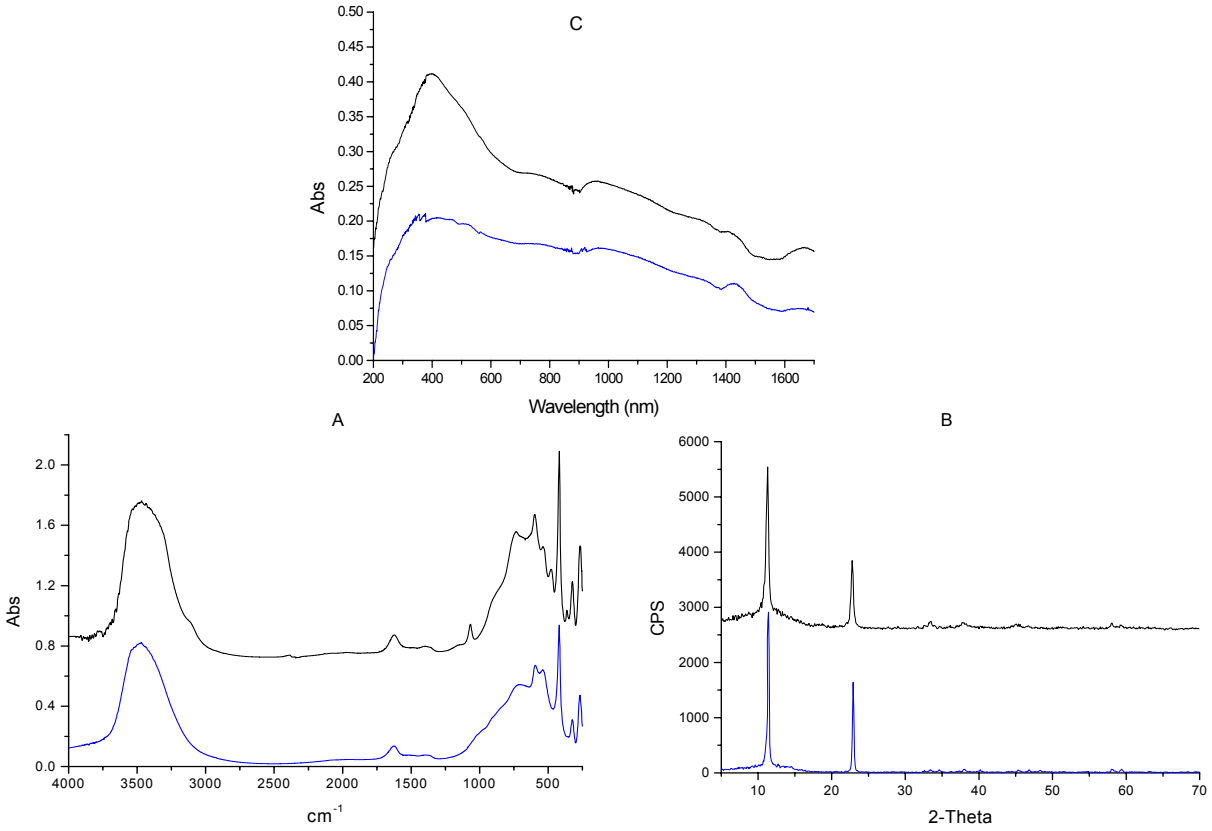

Figure 4.11: A) FT-IR spectra (blue-fresh, black-aged), B) XRD patterns (blue-fresh, black-aged) and C) DR- UV-Vis-NIR spectra (blue-fresh, black-aged) of 2:1 Mn-Al LDH-Cl.

For the 2:1 Mn-Al LDH-Cl samples,[27] the IR spectra show several strong peaks below 500 cm^{-1}. These peaks are not present in the aged 2:1 Mg-Al LDH-Cl with Mn(II), and quite different for the fresh 2:1 Mg-Al LDH-Cl with Mn(II). The XRD patterns show no significant differences between these samples and the fresh 2:1 Mg-Al LDH-Cl with Mn(II), but the 110 and 113 reflections are below 60º (2θ), for the aged 2:1 Mn-Al LDH- There are also no significant differences in the DR-UV-Vis-NIR spectra between the two sets of materials.

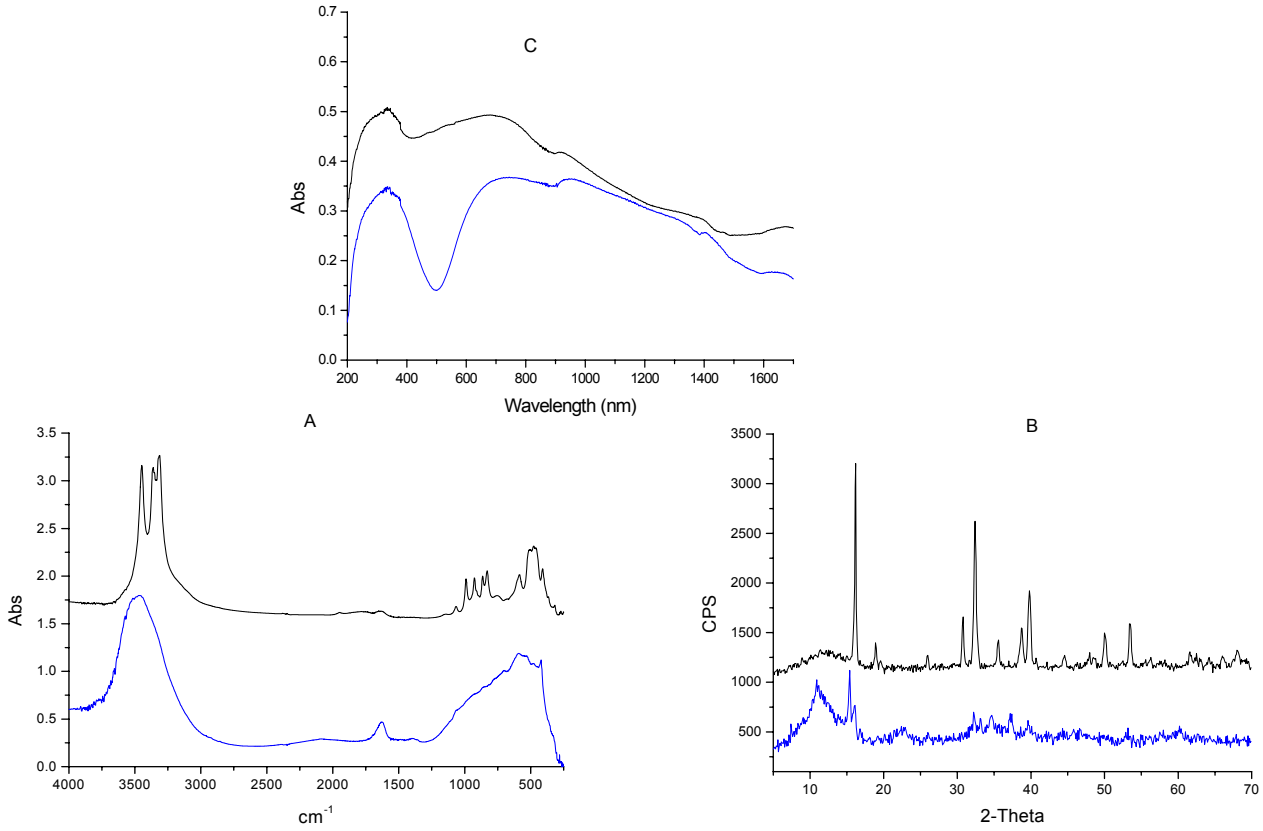

Figure 4.12: A) FT-IR spectra (blue-fresh, black-aged), B) XRD patterns (blue-fresh, black-aged) and C) DR- UV-Vis-NIR spectra (blue-fresh, black-aged) of 2:1 Cu-Al LDH-Cl.

For the 2:1 Cu-Al LDH-Cl samples,[28-30] the IR spectra also show several peaks below 500 cm^{-1}, but not as strong as the 2:1 Mn-Al LDH-Cl samples. These peaks are not present in the aged 2:1 Mg-Al LDH -Cl with Cu(II), and quite different for the fresh 2:1 Mg-Al LDH-Cl with Cu(II). In fact these two sets of IR spectra are not similar. The XRD patterns show material that is not LDH, as was also found for the 2:1 Mg-Al LDH-Cl with Cu(II) samples. The DR-UV-Vis-NIR spectra look similar to the aged and fresh 2:1 Mg-Al LDH-Cl with Cu(II).

Since the XRD patterns could not provide any information that would be useful in differentiating between the sets of materials, they will not be discussed any further. For almost all of the materials studied, the transmission or DR-UV-Vis-NIR spectra were also too similar to make any distinctions (except for the aged 2:1 Mg-Al LDH-Cl with Co(II)), so they will also not be discussed any further. The FT-IR spectra do show significant differences, so we can elaborate on them a bit further.

Table 4.6 lists all the pertinent peaks that would differentiate between the various metals based on their respective IR assignments. Different metals in the LDH lattice will produce different wavenumber values due to differences in their mass and force constants (k).

For a simple two-atom system, the observed frequency obeys the equation below. For an extended system such as ours, the situation is much more complicated. We can note, however, how both force constant and atomic mass affect frequency.

$$\tilde{\nu} = \frac{1}{2\pi c}\sqrt{k/\mu} \qquad \mu = \frac{m_1 m_2}{m_1 + m_2}$$

Table 4.6: List of specific IR peaks among the Mg-M(II)-Al LDH, $M(II)_2$-Al LDH, and Mg_2Al LDH samples.

LDH Material	Pertinent Peaks (cm^{-1})
Fresh Mg_2Al LDH-Cl	449,396
Aged Mg_2Al LDH-Cl	447,391
Fresh 2:1 Mg-Al LDH-Cl/Ni(II)	423
Aged 2:1 Mg-Al LDH-Cl/Ni(II)	447,391
Fresh 2:1 Mg-Al LDH-Cl/Co(II)	431
Aged 2:1 Mg-Al LDH-Cl/Co(II)	446,391
Fresh 2:1 Mg-Al LDH-Cl/Zn(II)	434,343
Aged 2:1 Mg-Al LDH-Cl/Zn(II)	447,391
Fresh 2:1 Mg-Al LDH-Cl/Cu(II)	451,409
Aged 2:1 Mg-Al LDH-Cl/Cu(II)	447,391
Fresh 2:1 Mg-Al LDH-Cl/Mn(II)	419
Aged 2:1 Mg-Al LDH-Cl/Mn(II)	447,391
Fresh Ni_2Al LDH-Cl	419
Aged Ni_2Al LDH-Cl	430
Fresh Co_2Al LDH-Cl	426
Aged Co_2Al LDH-Cl	423
Fresh Zn_2Al LDH-Cl	427,326
Aged Zn_2Al LDH-Cl	427,319
Fresh Cu_2Al LDH-Cl	417
Aged Cu_2Al LDH-Cl	410, 478
Fresh Mn_2Al LDH-Cl	419,324,267
Aged Mn_2Al LDH-Cl	478,419,363,323

For example, the pertinent peaks for a fresh Mg_2Al LDH-Cl are at 449 cm^{-1} and 396 cm^{-1}. For a fresh Ni_2Al LDH-Cl, one peak is at 419 cm^{-1}. For a fresh Mg-Ni-Al LDH-Cl, one peak is at 423 cm^{-1}. These differences are due to two metals versus three metals in the LDH lattice. It is worth stating that peaks for $M(II)_2Al(OH)_6Cl$ do not match those for $M(II)MgAl(OH)_6Cl$, and do not on the whole show much change or extra structure on aging; perhaps $M(II)_2Al(OH)_6Cl$ develop structure much more quickly (or more slowly) than the Mg_2Al analogs.

Table 4.7: Bragg reflection angles and interlayer spacings (uncorrected) for the 003 and 110 reflections in each of the 2:1 M(II)-Al LDH-Cl samples. The 110 reflections could not be resolved for the 2:1 Ni-Al LDH samples.

LDH Material	003 Reflection Angle (2θ)	Interlayer Spacing (Å)	110 Reflection Angle (2θ)	110 d-spacing (Å)
Fresh 2:1 Ni-Al LDH-Cl	11.12	7.95	61.10	1.52
Aged 2:1 Ni-Al LDH-Cl	11.21	7.89	62.59	1.51
Fresh 2:1 Co-Al LDH-Cl	11.30	7.83	60.49	1.53
Aged 2:1 Co-Al LDH-Cl	11.39	7.77	60.11	1.54
Fresh 2:1 Cu-Al LDH-Cl	11.49	7.70	60.00	1.54
Aged 2:1 Cu-Al LDH-Cl	11.32	7.81	61.67	1.50
Fresh 2:1 Zn-Al LDH-Cl	11.38	7.77	60.18	1.54
Aged 2:1 Zn-Al LDH-Cl	11.39	7.76	60.10	1.54
Fresh 2:1 Mn-Al LDH-Cl	11.31	7.82	58.09	1.59
Aged 2:1 Mn-Al LDH-Cl	11.46	7.71	58.20	1.58

From Table 4.7, we can note that the interlayer spacings are not significantly different from each other and from the values in Table 4.4.

The 110 reflections in Table 4.7, compared to their Mg-M(II)-Al LDH analogs, are the most important values for discussion. The size of the metal directly affects the 110 d-spacing, and the lattice parameter, a ($a = 2*d_{110}$). The fresh and aged 2:1 Mn-Al LDH-Cl samples have 110 d-spacings similar to the fresh 2:1 Mg-Al LDH-Cl/Mn(II), but not similar to the aged 2:1 Mg-Al LDH-Cl/Mn(II). The fresh and aged 2:1 Zn-Al LDH-Cl samples have 110 d-spacings close to, but somewhat larger than the fresh 2:1 Mg-Al LDH-Cl/Zn(II) sample, but are both larger than the aged 2:1 Mg-Al LDH-Cl/Zn(II) sample. The fresh and aged 2:1 Cu-Al LDH-Cl samples are significantly different to both fresh and aged Mg-Al LDH-Cl/Cu(II) samples, which will not be discussed further. The fresh and aged 2:1 Co-Al LDH-Cl samples are significantly different to their fresh and aged Mg-Al LDH-Cl/Co(II) samples. The 110 d-spacing for the fresh 2:1 Co-Al LDH-Cl sample is close to both of the aged and fresh Mg-Al LDH-Cl/Co(II) samples, but

the aged 2:1 Co-Al LDH-Cl sample is larger than both of the aged and fresh Mg-Al LDH-Cl/Co(II) samples. The fresh and aged 2:1 Ni-Al LDH-Cl samples are close to the fresh Mg-Al LDH-Cl/Ni(II) sample, but are both smaller than the aged Mg-Al LDH-Cl/Ni(II) sample (although the 110 reflections could not be adequately resolved).

The aged and fresh 2:1 M(II)-Al LDH-Cl samples have their divalent metals in the LDH lattice (except for the copper case). For most of the fresh Mg-Al LDH-Cl/M(II) samples, their 110 d-spacings are generally close to the values for the 2:1 M(II)-Al LDH samples, but the aged Mg-Al LDH-Cl/M(II) samples have 110 d-spacings close to the 2:1 Mg-Al LDH samples. This is complementary evidence for partial magnesium replacement.

4.6 Conclusions/Future Directions

We have shown that LDH can undergo facile cation exchange with a variety of divalent metal cations. Depending on the starting material, the successful uptake of free divalent cations can occur by replacement of the LDH magnesiums or by surface/edge adsorption.

The key to these two possibilities occurring is based on the post-synthesis treatment of a freshly prepared 2:1 Mg-Al LDH-Cl. By allowing the pre-formed LDH to undergo one-day aging, before mixing with the divalent cations, only a small amount of divalent cations were adsorbed, with no notable change in the magnesium content. By subjecting the pre-formed LDH, without any aging, to mixing with the divalent cations, approximately one-half of the LDH magnesiums were replaced.

Six different divalent metal cations were tested with fresh and aged 2:1 Mg-Al LDH-Cl. The Mg(II) cations were used to see if any increase in magnesium content , or if an increase in particle crystallinity would result. We did not notice any change in magnesium content, in both samples, but we did see an increase in crystallinity, for the fresh sample, based on the IR spectra and XRD patterns.

The Mn(II) cations were used, knowing that the ease of oxidation of Mn(II), in the presence of oxygen and high pH, would occur and the manganese may not likely survive in the divalent state. This seems to have been observed with the color changing from a light pink to dark brown within seconds of addition of $MnCl_2$ to the aged 2:1 Mg-Al LDH-Cl sample. We were surprised to see the faint pink color persist in the fresh 21 Mg-Al LDH-Cl sample for the five-day mixing stage. Once the washing stage occurred, the faint pink color quickly turned brown, signifying oxidation of Mn(II). This is significant because the fresh LDH was able to protect the incorporated manganese from further oxidation, as long as the solution was kept in an inert environment. There remains a conflict between the metals analysis and the aged LDH sample, in that a 1:1 Mg:Al ratio should not produce 447 cm^{-1} and 390 cm^{-1} peaks.

The Cu(II) cations were used in anticipation of complications based on Jahn-Teller distortions of copper. The numerous IR peaks present in the fresh LDH sample, coupled with the basic copper chloride peaks in the respective XRD pattern hint at the possible pre-incorporation of copper into the LDH lattice. Due to the distortions that copper has in a six-coordinate environment, the pre-incorporated Cu(II) likely compromised the structural integrity of the LDH lattice sheets, thus breaking-up the sheets, forming two or more different materials.

The other divalent metal cations, Ni(II), Zn(II) and Co(II) were predicted to undergo no complications with the LDH materials. The Ni(II) and Zn(II) cations showed stoichiometric replacement for the fresh LDH samples and surface adsorption for the aged LDH samples. No problems were observed with these two divalent cations. The case of Co(II) was a pleasant surprise. The were no complications with these materials, but the result of a blue, aged LDH sample and a red, fresh LDH sample, having a T_d Co(II) or a O_h Co(II), respectively was not anticipated.

This project will undoubtedly be the starting point for numerous future experiments with LDH as a cation-incorporating material. We only dealt with a LDH having a Mg:Al ratio of 2:1. There is no doubt that Mg-Al LDH having a 3:1 Mg:Al ratio can also undergo similar results. We also designed our experiment for a stoichoimetric replacement of one-half of the LDH magnesiums. Experiments designed to undergo full magnesium replacement or even less than one-half replacement would be worth doing.

On a larger note, LDH starting with divalent metals other than magnesium look promising. Experiments starting with a 2:1 Ni-Al LDH-Cl, 2:1 Co-Al LDH-Cl or a 2:1 Zn-Al LDH-Cl and the same six divalent metal cations would clearly be worth investigating. There are many other divalent metals combinations that could be studied. Once compiled, a cationic preference range can be produced that would accompany the groundbreaking anionic preference range by Miyata.

The results also show the importance of freshly precipitated LDH versus aged LDH. Since there was such a noticeable difference between these two, freshly prepared LDH deserves to be studied much more than it has in the past, or is currently.

The potential applications for these materials (Mg-M(II)-Al and M(II)-Al LDH) would obviously be as catalysts/catalyst precursors.[31-37]

Since this project dealt with the LDH magnesiums, the possibility of similar results occurring with the LDH aluminums would be equally important to investigate. This is the subject for part II of the title “LAYERED DOUBLE HYDROXIDES AS CATION-EXCHANGING MATERIALS”.

4.7 References

(1) Velu, S.; Swamy, S. *J. Mater. Sci. Lett.* **1996**, *15*, 1674.

(2) Iglesias, A. H.; Ferreira, O. P.; Gouveia, D. X.; Souza Filho, A. G.; de Paiva, J.A.C.; Mendes Filho, J.; Alves, O.L. *J. Solid State Chem.* **2005**, *178*, 142.

(3) Velu, S.; Shah, N.; Jyothi, T.M.; Sivasanker, S. *Micro. Meso. Mater.* **1999**, *33*, 61.

(4) Crivello, M.; Perez, C.; Herrero, E.; Ghione, G.; Casuscelli, S.; Rodriguez-Castellon, E. *Catal. Today* **2005**, *107*, 215.

(5) Kooli, F.; Kosuge, K.; Tsunashima, A. *J. Solid State Chem.* **1995**, *118*, 285.

(6) Zeng, H.C.; Xu, Z.P.; Qian, M. *Chem. Mater.* **1998**, *10*, 2277.

(7) Fernandez, J.M.; Barriga, C.; Ulibarri, M.A.; Labajos, F.M.; Rives, V. *J. Mater. Chem.* **1994**, *4*, 1117.

(8) Morpugo, S.; Lo Jacono, M.; Porta, P. *J. Solid State Chem.* **1996**, *122*, 324.

(9) Kameda, T.; Saito, S.; Umetsu, Y. *Separation and Purification Technology* **2005**, *47*, 20.

(10) Perez, M.R.; Pavlovic, I.; Barriga, C.; Cornejo, J.; Hermosin, M.C.; Ulibarri, M.A. *Appl. Clay Sci.* **2006**, *32*, 245.

(11) Tsyganok, A.; Sayari, A. *J. Solid State Chem.* **2006**, *179*, 1829.

(12) Komarneni, S.; Kozai, N.; Roy, R. *J. Mater. Chem.* **1998**, *8*, 1329.

(13) Lazaridis, N.K. *Water, Air, and Soil Pollut.* **2003**, *146*, 127.

(14) Labajos, F.M.; Rives, V. *Spectrosc. Lett.* **1991**, *24*, 499.

(15) Labajos, F.M.; Rives, V. *Inorg. Chem.* **1996**, *35*, 5313.

(16) Frost, R.L.; Ding, Z.; Kloprogge, J.T. *Can. J. Anal. Sci. and Spectrosc.* **2000**, *45*, 96.

(17) Morpurgo, S.; Jacono, M. L.; Porta, P. *J. Mater. Chem.* **1994**, *4*, 197.

(18) Leroux, F.; Moujahid, E.M.; Taviot-Gueho, C.; Besse, J.P. *Solid State Sci.* **2001**, *3*, 81.

(19) Krivoruchko, O.P.; Anufrienko, V.F.; Paukshtis, E.A.; Larina, T.V.; Burgina, E.B.; Yashnik, S.A.; Ismagilov, Z.R.; Parmon, V.N. *Dokl. Phys. Chem.* **2004**, *398*, 226.

(20) Crivello, M.; Perez, C.; Herrero, E.; Ghione, G.; Casuscelli, S.; Rodriguez-Castellon, E. *Catal. Today* **2005**, *107*, 215.

(21) Barriga, C.; Fernandez, J.M.; Ulibarri, M.A.; Labajos, F.M.; Rives, V. J*. Solid State Chem.* **124**, 205, 213

(22) Kannan, S.; Velu, S.; Ramkumar, V.; Swamy, C.S. *J. Mater. Sci.* **1995**, *30*, 1462.

(23) d'Espinose de la Caillerie, J.B.; Kermarec, M.; Clause, O.*J. Am. Chem. Soc.* **1995**, *117*, 11471.

(24) Rajamathi, M.; Kamath, P. V. *Bull. Mater. Sci.* **2000**, *23*, 335.

(25) Ishikawa, T.; Matsumoto, K.; Kandori, K.; Nakayama, T. *J. Solid State Chem.* **2006**, *179*, 1110.

(26) Feng, Y.; Li, D.; Wang, Y.; Evans, D. G.; Duan, X. *Polym. Degrad. Stab.* **2006**, *91*, 789.

(27) Obalová, L.; Jirátová, K.; Kovanda, F.; Pacultová, K.; Lacný, Z.; Mikulová, Z. *Appl. Catal. B: Environmental* **2005**, *60*, 289.

(28) Park, I.Y.; Kuroda, K.; Kato, C. *Solid State Ionics* **1990**, *42*, 197.

(29) Lwin, Y.; Yarmo, M.A.; Yaakob, Z.; Mohamad, A.B.; Ramli, W.; Daud, W. *Mater. Res. Bull.* **2001**, *36*, 193.

(30) Velu, S.; Swarmy, C.S. *Appl. Catal. A: General* **1996**, *145*, 141.

(31) Sychev, M.; Prihod'ko, R.; Erdmann, K.; Mangel, A.; van Santen, R.A. *Appl. Clay Sci.* **2001**, *18*, 103.

(32) Zhu, K.; Liu, C.; Ye, X.; Wu, Y. *Appl. Catal. A: General* **1998**, *168*, 365.

(33) Dumitriu, E.; Hulea, V.; Cherlaru, C.; Catrinescu, C.; Tichit, D.; Durand, R. *Appl. Catal. A: General* **1999**, *178*, 145.

(34) Shishido, T.; Sukenobu, M.; Morioka, H.; Kondo, M.; Wang, Y.; Takaki, K.; Takehira, K. *Appl. Catal. A: General* **2002**, *223*, 35.

(35) Alzamora, L.E.; Ross, J.R.H.; Kruissink, E.C.; van Reijin, L.L. *J. Chem. Soc.*, *Faraday Trans.* **1981**, *1*, 77, 665.

(36) Watanabe, Y.; Yamamoto, K.; Tatsumi, T. *J. Mol. Catal;. A: Chemical* **1991**, *145*, 281.

(37) Dandl, H.; Emig, G. *Appl. Catal. A: General* **1998**, *168*, 261.

CHAPTER 5

LAYERED DOUBLE HYDROXIDES AS CATION-EXCHANGING MATERIALS

II. TRIVALENT CATION EXCHANGE WITH Mg-Al LDH

5.1 LDH as Cation-Exchanging Materials

Due to the success of layered double hydroxides (LDHs) in the incorporation of some of the divalent cations from Chapter 4, it seems plausible that the next step would be to investigate the possibility of either exchanging some of the LDH aluminums with selected trivalent metal cations, or having another case of surface adsorption.

The results from Chapter 4 are profound in one simple way: They have taught us that clay-like materials, namely the synthetic kind, have not been fully explored. From Chapter 1, LDH materials have many different polytypes, based entirely on their layer-stacking sequences. Since we have been able to show that the $3R_1$ polytype is capable of selective cation replacement, the others may show a similar behavior.

The results from Chapter 4 should spark an interest in the potential application of LDH, both academically and possibly industrially, as a type of natural and synthetic clay-like material that can interact with metal cations.

5.2 Purpose of Experiment

This project is the second part of a two-part project dealing with LDH as cation-exchanging materials. For this part, we will attempt to exchange one-half of the LDH aluminums with the following trivalent metals: Fe(III), Cr(III), Ga(III) and Al(III). All of these metals are in the form of chloride salts.

The purpose of working with more aluminum is similar to the first project with magnesium. From Chapter 4, the fresh LDH was aged by the presence of magnesiums, so we set out to see if an aluminum solution will do the same.

5.3 Experimental Procedure

The parent 2:1 Mg-Al LDH-Cl was prepared using the exact same approach as done in Chapter 4. Eight 2.0 g batches of 2:1 Mg-Al LDH-Cl (same general formula) were prepared by the precipitation of solutions containing 0.2 M $MgCl_2$ and 0.1 M $AlCl_3$ with 50% NaOH. Four of these LDH materials were subjected to a one-day aging step and the other four were kept as fresh.

Once all eight LDH materials were ready for the trivalent metals, they were all placed in 250 mL roundbottomed flasks, with 50 mL of deionized water (Millipore MilliQ Academic, 18.2 $M\Omega\ cm^{-1}$). A steady blanket of high purity nitrogen gas was passed over the LDH suspensions and maintained throughout the five-day mixing period. The MCl_3 solutions were prepared by dissolving the stoichiometric amounts of each salt in 50 mL of deionized water.

As calculated by the one-half molar amount of LDH aluminums, the amounts of each trivalent metal chloride salt: 1.12 g $FeCl_3 \bullet 6H_2O$, 1.11 g $CrCl_3 \bullet 6H_2O$ (actually the trans-dichloro isomer; $[CrCl_2(H_2O)_4]Cl \bullet 2H_2O$), 1.00 g $AlCl_3 \bullet 6H_2O$ and 0.732 g $GaCl_3$ (anhydrous) were dissolved in deionized water and their respective pH values were documented.

We had to work with care for the $GaCl_3$ solution. The only way that we were able to purchase this salt was for the anhydrous version. Anhydrous $GaCl_3$, like anhydrous $AlCl_3$, is very reactive with water.[1] Keeping this in mind, and the possibility that the hydration of $GaCl_3$ could liberate HCl, we placed the 0.732 g of anhydrous $GaCl_3$ in a centrifuge tube, with the 50 mL of deionized water. Once the salt was added, the tube was quickly sealed and vigorously shook, until quickly and completely dissolved. If some small amount of HCl were lost, it would not pose a problem, because we only needed the gallium.

These metal salt solutions were then introduced to the LDH suspensions. After five minutes and five days, their respective pH values were also documented. We did not expect to have any oxidation problems with these metals, as was expected with the LDH sample containing Mn(II), so the time taken obtaining stable pH measurements was not a factor in the stability of any of the metals in the LDH suspensions.

After the five-day mixing period, the eight solutions were removed from mixing and thoroughly separated/washed. As with the LDH-M(II) samples, the aged LDH-M(III) samples were difficult to separate during centrifugation. After the solids were washed, they were then placed in vacuum desiccators, for drying, by a mixture of molecular sieves/drierite.

As a comparison, 2.0 g batches of fresh and aged 2:1 Mg-Cr LDH-Cl and 2:1 Mg-Fe LDH-Cl were prepared, along with 1.0 g batches of 2:1 Mg-Ga LDH-Cl. Each of these three LDH materials was prepared by dissolving the following salts in 50 mL deionized water: 2.964 g $MgCl_2 \bullet 6H_2O$, 1.944 g $FeCl_3 \bullet 6H_2O$; 2.924 g $MgCl_2 \bullet 6H_2O$, 1.942 g $CrCl_3 \bullet 6H_2O$ ($[CrCl_2(H_2O)_4]Cl \bullet 2H_2O$); 0.966 g $GaCl_3 \bullet 6H_2O$, 1.383 g

$MgCl_2 \bullet 6H_2O$. We could not prepare 2.0 g batches of 2:1 Mg-Ga LDH-Cl, due to the limited availability of $GaCl_3 \bullet 6H_2O$.

To each of these solutions (stirring under a nitrogen gas blanket), 2.3 mL (Mg_2-Cr and Mg_2-Fe) or 1.1 mL (Mg_2-Ga) 50% NaOH was added. The suspensions were allowed to mix for one hour, and then 25 mL were removed. These five samples (designated fresh LDH) were then washed/centrifuged, and placed in a vacuum desiccator for drying. The other 25 mL were then placed in a hot oil bath (100 °C) for overnight reflux (also under a nitrogen gas blanket). These five LDH materials were then washed/centrifuged, and placed in a separate vacuum desiccator for drying.

The same set of characterizations tools used for the LDH-M(II) samples; FT-IR, XRD, AAS and transmission or DR-UV-Vis-NIR were used for these eight samples.

5.4 Results

The first observation, learned from the LDH-M(II) samples, is color. The LDH samples with iron had a brown color, with the fresh LDH being much darker. The LDH samples with gallium and aluminum show no color (or color changes), as expected, but another anomalous color change occurred with the LDH samples with chromium. The fresh LDH-Cr(III) sample had a violet color, but the aged LDH-Cr(III) has a dark green color. We could anticipate this color difference due to incorporation versus adsorption, or from the formation of $Cr(OH)_3$, at the expense of the Mg_2Al LDH. The violet color was expected, in both cases, because of the well-known purple color of the Zn_2Cr LDH materials, in which the chromiums were incorporated into the LDH layers.[2]

The pH measurements for the metal salts solutions and the LDH suspensions after five minutes and five days mixing are shown in Table 5.1.

Table 5.1: The pH values of the LDH-M(III) materials. Columns below both Fresh and Aged LDH-Cl: Left column (five minutes mixing) and right column (five days mixing).

Metal Salt	Solution	Fresh LDH-Cl			Aged LDH-Cl	
$FeCl_3$	1.73	7.38	7.68		2.32	6.84
$CrCl_3$	3.00	5.38	7.48		3.86	6.92
$GaCl_3$	2.26	4.01	7.69		2.56	3.64
$AlCl_3$	2.85	5.14	7.68		3.81	3.55

At first glance we can see a similar pattern as for the LDH-M(II) materials. The fresh LDH samples show high pH values after five days mixing. This was not expected because replacement of the LDH aluminums should produce a solution with a much lower pH. The five-minute fresh LDH samples also show higher than expected pH values. A similar observation is seen for some of the aged LDH samples. The five-minute samples show pH values that are low, which indicates either no aluminum replacement (the trivalent cations are still in solution) or some aluminum is in solution, by replacement. The five-day samples are mixed. The higher pH values are similar to the five-day fresh LDH samples and the low pH values are as low as could be expected.

If this table is indicative of the way that the divalent metals interacted with LDH, we may be seeing magnesium in solution, due to the simple action of acid on LDH, whether or not aluminum is exchanged.

5.4.1 Mg-Al LDH-Cr(III)

Figure 5.1 shows the IR spectra, XRD patterns and DR UV-Vis-NIR spectra for the LDH samples treated with Cr(III).

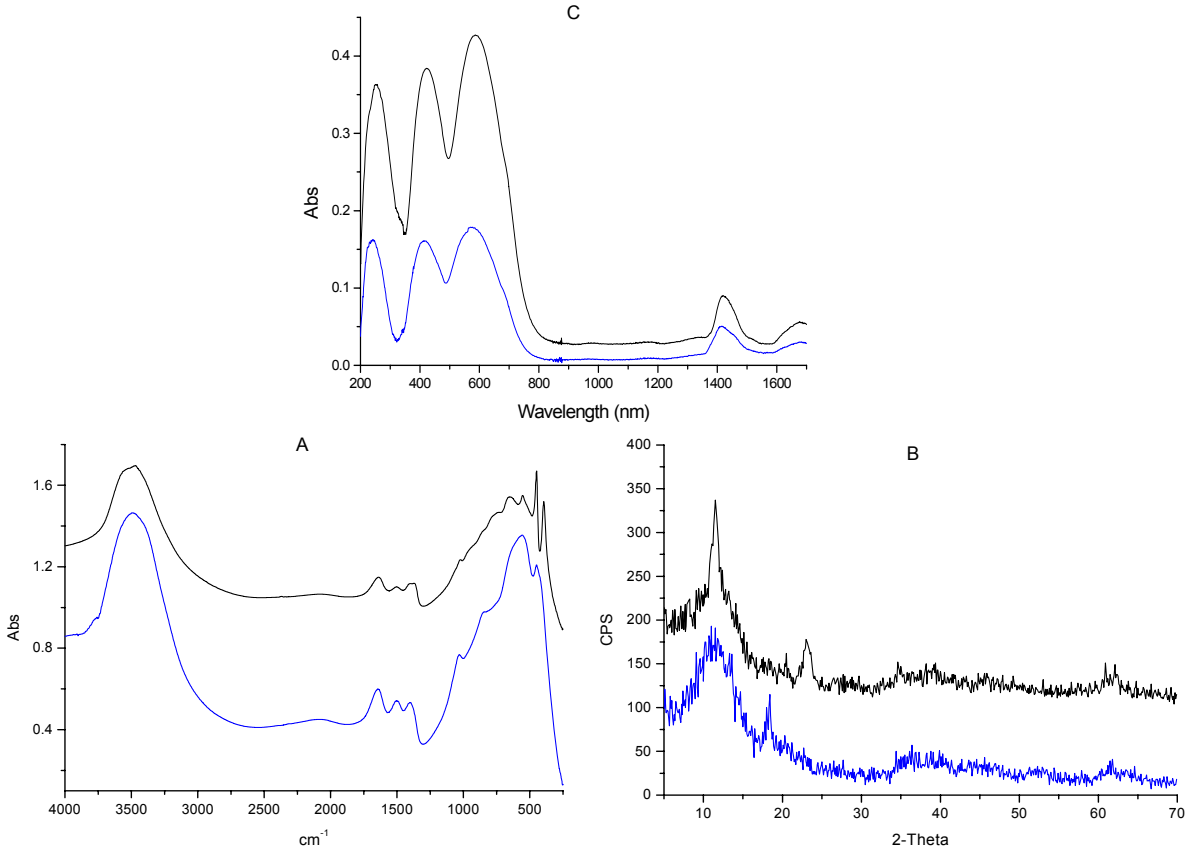

Figure 5.1: A) FT-IR spectra (blue-fresh, black-aged), B) XRD patterns (blue-fresh, black-aged) and C) DR- UV-Vis-NIR spectra (blue-fresh, black-aged) of 2:1 Mg-Al LDH-Cl with Cr(III).

The IR spectrum of the aged LDH sample resembles that of an aged 2:1 Mg-Al LDH-Cl, with the possible exception of the two peaks below 500 cm^{-1}. These peaks, at 448 cm^{-1} and 395 cm^{-1} are considerably different to an aged LDH, in that the 395 cm^{-1} peak is much less intense (not equal or close to equal as 448 cm^{-1} peak).

The IR spectrum of the fresh LDH sample shows a 448 cm^{-1} peak and a broad 558 cm^{-1} peak. This spectrum does not appear to correspond to an LDH containing magnesium and aluminum.

Both XRD patterns show poorly crystalline materials with differing d-spacings. The fresh LDH-Cr(III) sample has a peak with a d-spacing of 8.26 Å at 10.70º (2θ), along with a peak having a d-spacing of 7.54 Å at 11.72º (2θ), and the aged LDH-Cr(III) sample has a d-spacing of 7.52 Å at 11.76º (2θ).

The DR UV-Vis-NIR spectra show no differences in the shapes of the observable bands, but there is a slight but possibly significant difference in the positions. Since one sample is violet and the other is green, we hoped that the visible region would reflect such subtle color differences. In both cases, the DR-UV-Vis-NIR spectra support a trivalent state for both chromiums[3-5], with observable bands characteristic of high spin d^3 Cr(III) ions. The fact that the two bands are higher in frequency, in the visible region, for the fresh material is the difference between the purple and green colors (Table 5.2).

The same NIR bands described in Chapter 4 will also apply to the materials in this chapter.

Table 5.2: DR-UV-Vis-NIR peaks and transitions for the LDH-Cr(III) samples. Purple sample on left and green sample on right.

Wavelength (nm)	Transition
415	$^4A_{2g}(F) \rightarrow {}^4T_{1g}(F)$
571	$^4A_{2g}(F) \rightarrow {}^4T_{2g}(F)$
1438	NIR

Wavelength (nm)	Transition
446	$^4A_{2g}(F) \rightarrow {}^4T_{1g}(F)$
584	$^4A_{2g}(F) \rightarrow {}^4T_{2g}(F)$
1438	NIR

The case for chromium can be tricky because the initial chloride salt comes in several different isomers (hydration isomers).[6] The color of the fresh LDH sample is evidence for incorporation of chromium in the LDH lattice, as shown by comparison with

many M(II)-Cr(III) LDH materials that have been prepared over the years (most notably Zn_2Cr LDH). The fact that the aged LDH sample has maintained its dark green color could be attributed to the complex retaining its structural integrity during the mixing, and what we can tentatively describe as adsorption.

5.4.2 Mg-Al LDH-Fe(III)

Figure 5.2 shows the IR spectra, XRD patterns and DR-Vis-NIR spectra for the LDH samples containing iron.

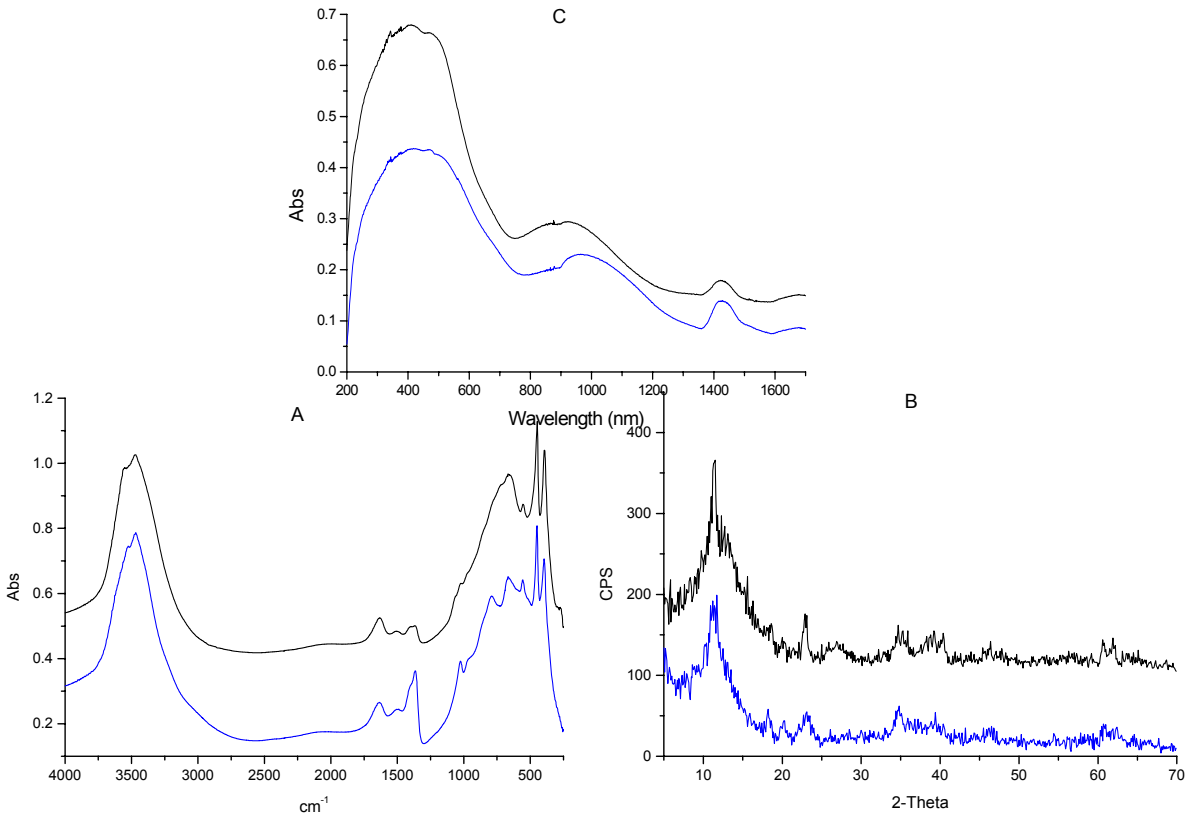

Figure 5.2: A) FT-IR spectra (blue-fresh, black-aged), B) XRD patterns (blue-fresh, black-aged) and C) DR- UV-Vis-NIR spectra (blue-fresh, black-aged) of 2:1 Mg-Al LDH-Cl with Fe(III).

Both IR spectra show peaks below 500 cm^{-1}. The fresh LDH sample has peaks at 449 cm^{-1} and 395 cm^{-1}, whereas the aged LDH sample has peaks at 447 cm^{-1} and 391 cm^{-1}. The two spectra resemble the fresh and aged LDH-Mg(II) samples. There are two possible scenarios for this case: The first is that no iron is in the LDH lattice (fresh LDH sample) and the second is that iron is in the LDH lattice, but somehow produces the same two peaks as in an aged Mg_2Al LDH. This last case is unlikely because the Fe-O(H) force constant should be different than the Al-O(H) force constant. This would result in different lattice peak frequencies.

The XRD patterns show poorly crystalline materials. As in the chromium case, the fresh LDH sample has a d-spacing of 9.93 Å at 8.90º (2θ), along with a peak having a d-spacing of 7.69 Å at 11.50º (2θ), whereas the aged LDH sample has a d-spacing of 7.87 Å at 11.23º (2θ).

The DR-UV-Vis-NIR spectra are similar in both cases. We would expect any d-d transitions for a high spin d^5 Fe(III) ion to be very weak, being both spin- and parity-forbidden, and it would be unlikely that any reduction of Fe(III), to Fe(II) would occur. The broad peaks around 1000nm have been attributed to octahedral distortions and those around 400nm are due to charge transfer ($OH^- \rightarrow Fe^{3+}$).[7]

5.4.3 Mg-Al LDH-Ga(III)

Figure 5.3 shows the IR spectra, XRD patterns and transmission UV-Vis-NIR spectra for the LDH samples containing gallium.

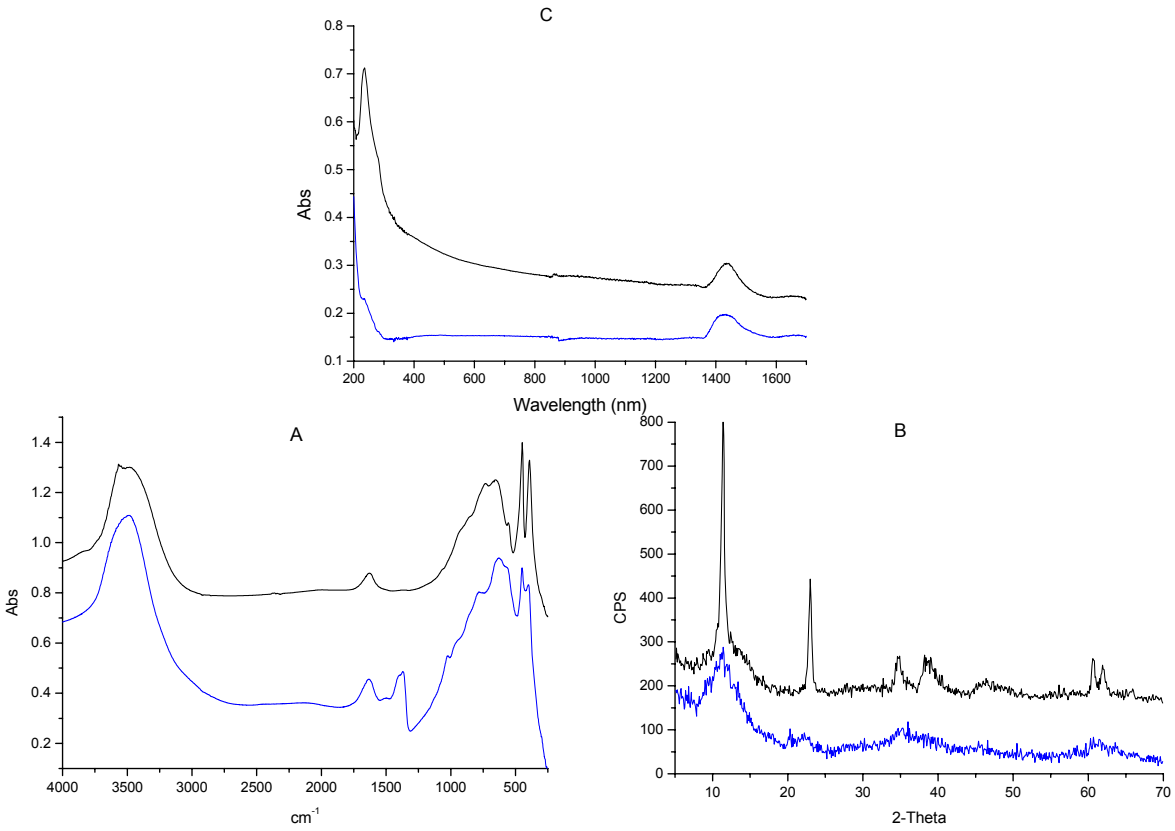

Figure 5.3: A) FT-IR spectra (blue-fresh, black-aged), B) XRD patterns (blue-fresh, black-aged) and C) Transmission-UV-Vis-NIR spectra (blue-fresh, black-aged) of 2:1 Mg-Al LDH-Cl with Ga(III).

The case of gallium resembles the observations with the LDH-Cr(III) samples. The aged LDH sample shows two peaks at 447 cm^{-1} and 391 cm^{-1}. The fresh LDH sample shows a 448 cm^{-1} peak and a very small 398 cm^{-1} peak. We can begin hypothesizing that these M(III) cations are affecting the normally strong 393 cm^{-1}peak more than they are affecting the normally strong 447 cm^{-1} peak.

The XRD patterns are obviously different for the two samples. The aged LDH sample is identical to an aged 2:1 Mg-Al LDH-Cl, with a d-spacing of 7.75 Å at 11.41º (2θ). The fresh LDH sample shows poor crystallinity with a d-spacing of 8.03 Å at 11.01º (2θ).

The transmission UV-Vis-NIR spectra are typical for metals having either a d^0 or d^{10} electron configuration due to the lack of any noticeable d-d transition bands, in the visible region (see the 2:1 Mg:Al LDH-Cl with Zn(II) samples in Chapter 4).

5.4.4 Mg-Al LDH-Al(III)

Figure 5.4 shows the IR spectra, and XRD patterns for the LDH samples containing aluminum.

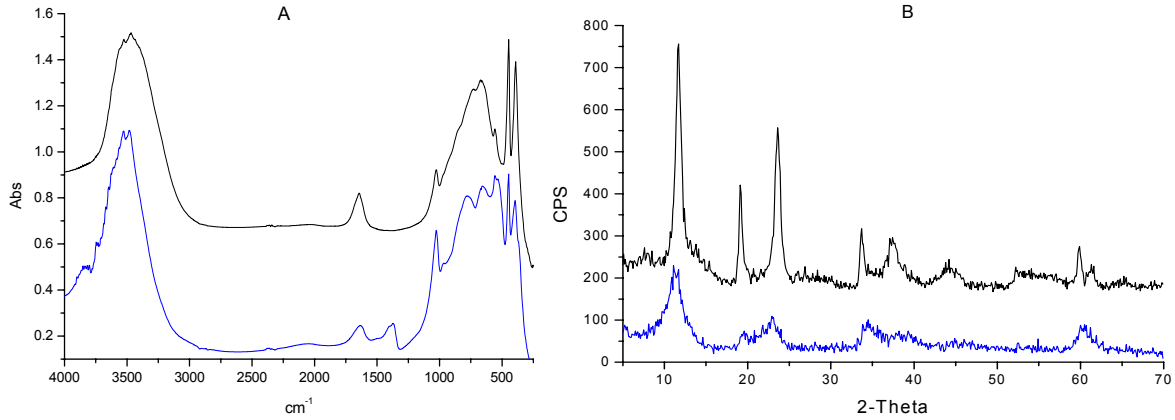

Figure 5.4: A) FT-IR spectra (blue-fresh, black-aged), and B) XRD patterns (blue-fresh, black-aged) of 2:1 Mg-Al LDH-Cl with Al(III).

We did not record the UV-Vis-NIR spectra for these samples, because only aluminum and magnesium were present.

The IR spectra show an aged LDH sample with peaks at 447 cm^{-1} and 391 cm^{-1}, typical for an aged 2:1 Mg-Al LDH-Cl. The fresh LDH sample shows a 448 cm^{-1} peak and a weak 395 cm^{-1} peak.

The XRD patterns are nearly identical, with the aged LDH sample having a d-spacing of 7.69 Å at 11.50º (2θ), and the fresh LDH sample having a d-spacing of 7.83 Å at 11.30º (2θ). Both samples show gibbsite formation at 18º and 20º (2θ).

Table 5.3 shows the reflections and interlayer spacings for each of the eight materials.

Table 5.3: Bragg reflection angles and interlayer spacings (uncorrected) for the 003 and 110 reflections in each of the 2:1 Mg-Al LDH-M(III) samples.

LDH Material	003 Reflection Angle (2θ)	Interlayer Spacing (Å)	110 Reflection Angle (2θ)	110 d-spacing (Å)
Fresh 2:1 Mg-Al LDH-Cl/Cr(III)	11.72	7.54	61.01	1.52
Aged 2:1 Mg-Al LDH-Cl/Cr(III)	11.76	7.52	60.98	1.52
Fresh 2:1 Mg-Al LDH-Cl/Fe(III)	11.50	7.69	60.71	1.52
Aged 2:1 Mg-Al LDH-Cl/Fe(III)	11.23	7.87	60.78	1.52
Fresh 2:1 Mg-Al LDH-Cl/Ga(III)	11.01	8.03	60.69	1.53
Aged 2:1 Mg-Al LDH-Cl/Ga(III)	11.41	7.75	60.71	1.52
Fresh 2:1 Mg-Al LDH-Cl/Al(III)	11.30	7.83	60.70	1.53
Aged 2:1 Mg-Al LDH-Cl/Al(III)	11.50	7.69	60.79	1.52

The metals analysis is shown in Table 5.4. The gallium analysis was not performed. From Table 2 we can see that, instead of partial aluminum replacement, magnesium loss has occurred. We attribute this to the more acidic trivalent cations disrupting the LDH lattice, expelling the LDH magnesiums and aluminums.

Table 5.4: Metals analysis for the LDH-M(III) samples. Gallium analysis was not performed.

LDH Material	Mg : Al	Mg : M(III)	Al : M(III)
Fresh 2:1 Mg-Al LDH-Cl/Cr(III)	0.92	1.40	1.50
Aged 2:1 Mg-Al LDH-Cl/Cr(III)	1.12	1.50	1.30
Fresh 2:1 Mg-Al LDH-Cl/Fe(III)	1.05	0.13	0.13
Aged 2:1 Mg-Al LDH-Cl/Fe(III)	0.64	0.07	0.11
Fresh 2:1 Mg-Al LDH-Cl/Ga(III)	0.43	---	---
Aged 2:1 Mg-Al LDH-Cl/Ga(III)	1.50	---	---
Fresh 2:1 Mg-Al LDH-Cl/Al(III)	0.05	---	---
Aged 2:1 Mg-Al LDH-Cl/Al(III)	1.36	---	---

The high pH values, obtained after the five-day mixing period, are a result of incorporation of the trivalent metals. If any of the trivalent ions were in solution, the pH would be much lower.

5.5 Comparison of Mg-Al-M(III) LDH-Cl with 2:1 Mg-M(III) LDH-Cl

In the above sections, the first conclusion that cationic uptake has occurred was based on the positions of the IR peaks below 1000 cm^{-1}. Comparing each spectrum with an aged 2:1 Mg-Al LDH-Cl was easy to do because of the noticeable peaks around 447 cm^{-1} and 393 cm^{-1}. In order to supply evidence concerning aluminum replacement, fresh and aged 2:1 LDH-Cl samples containing: Mg-Cr, Mg-Fe and Mg-Ga were prepared. Each of these materials will produce characteristic IR peaks, within the 1000 – 250 cm^{-1} range, that can be directly compared to the fresh and aged Mg-Al-M(III) LDH materials.

Along with the IR spectra, XRD patterns and either transmission or DR-UV-Vis-NIR spectra were also obtained for the six 2:1 Mg-M(III) LDH-Cl samples. These IR spectra, XRD patterns and DR-UV-Vis-NIR spectra are shown in Figures 5.5-5.7.

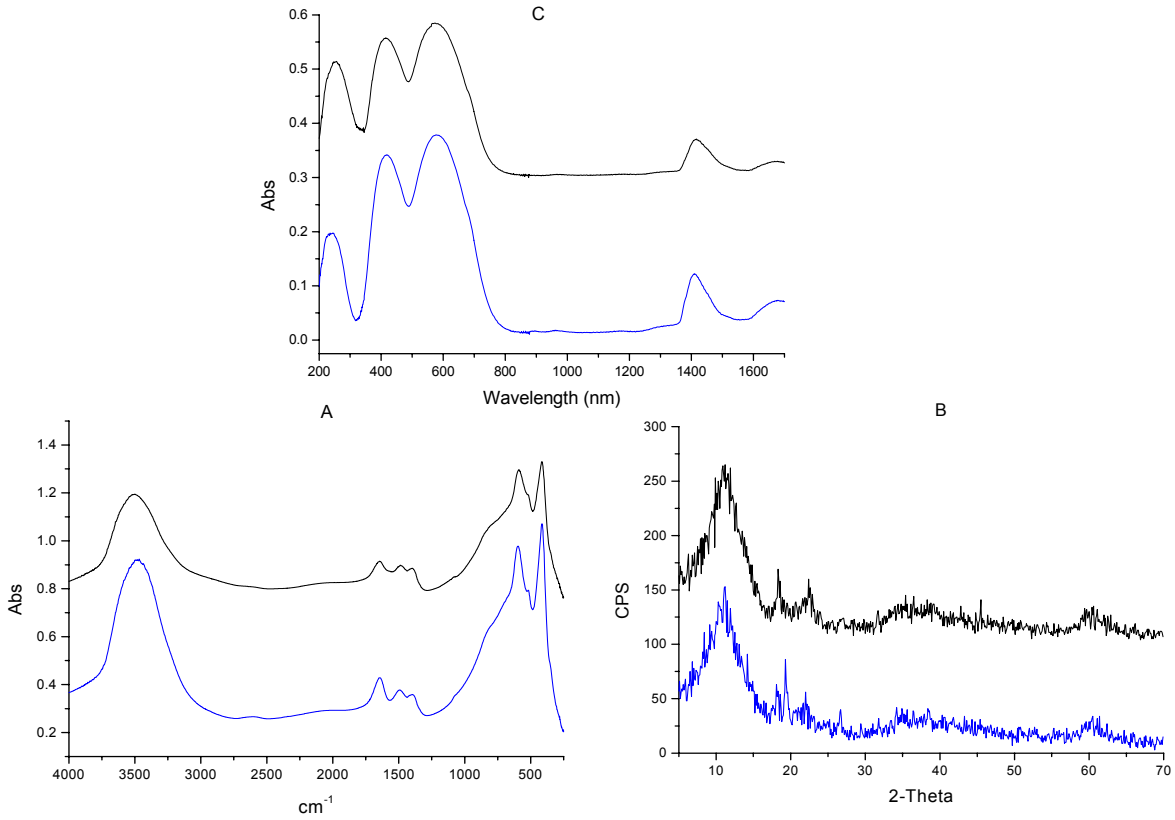

Figure 5.5: A) FT-IR spectra (blue-fresh, black-aged), B) XRD patterns (blue-fresh, black-aged) and C) DR- UV-Vis-NIR spectra (blue-fresh, black-aged) of 2:1 Mg-Cr LDH-Cl.

For the aged and fresh 2:1 Mg-Cr LDH-Cl samples,[8,9] which are known compounds, the IR spectra show one strong peak around 415 cm^{-1}. This peak is not present in the aged or fresh 2:1 Mg-Al LDH-Cl with Cr(III) samples. The XRD patterns are too similar for any significant differences between the two sets of materials. The DR-UV-Vis-NIR spectra are indistinguishable. Both aged and fresh 2:1 Mg-Cr LDH-Cl had the same violet color to them, as did the fresh 2:1 Mg-Al LDH-Cl treated with Cr(III).

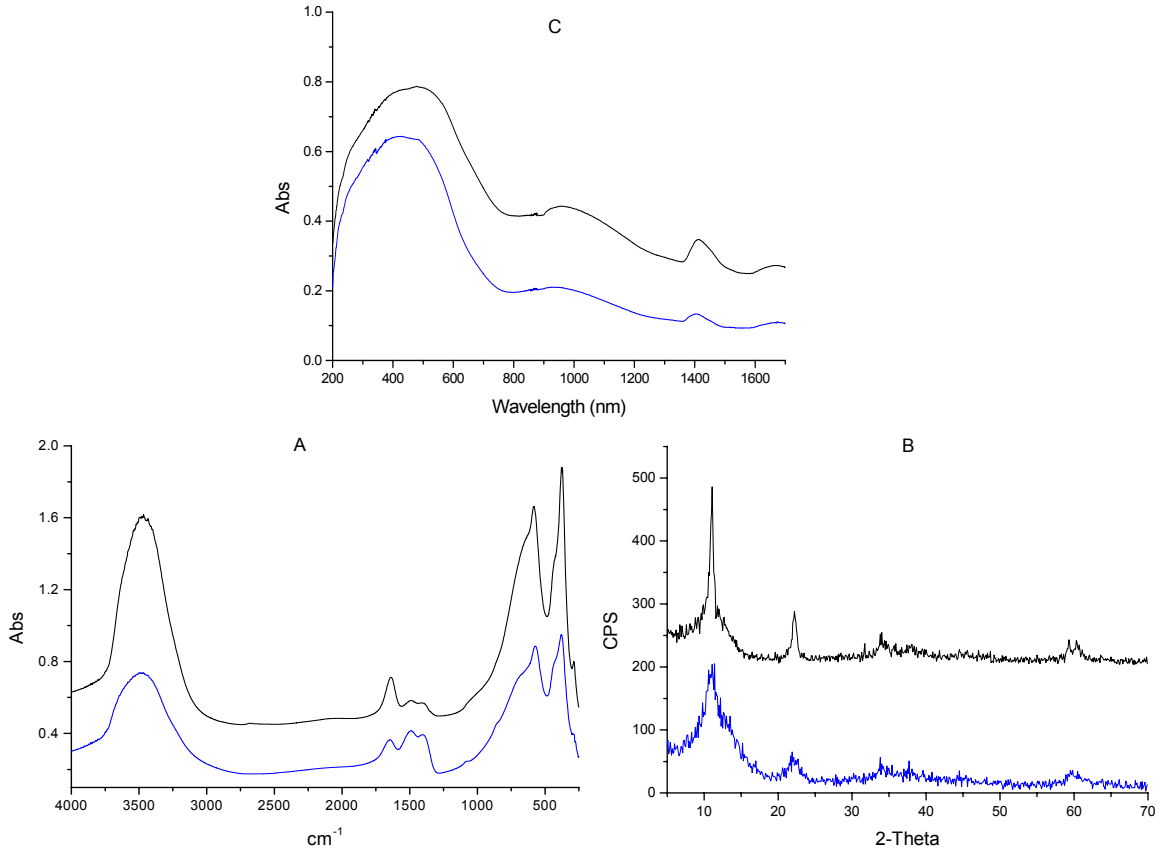

Figure 5.6: A) FT-IR spectra (blue-fresh, black-aged), B) XRD patterns (blue-fresh, black-aged) and C) DR-UV-Vis-NIR spectra (blue-fresh, black-aged) of 2:1 Mg-Fe LDH-Cl.

For the aged and fresh 2:1 Mg-Fe LDH-Cl samples,[10,11] the IR spectra show one strong peak around 375 – 379 cm^{-1}. This peak is not present in the aged or fresh 2:1 Mg-Al LDH-Cl with Fe(III) samples, in fact both aged and fresh 2:1 Mg-Al LDH-Cl with Fe(III) samples showed two peaks. The XRD patterns show sharper peaks for the aged materials, and the DR-UV-Vis-NIR spectra do not show any significant differences between the two sets of materials.

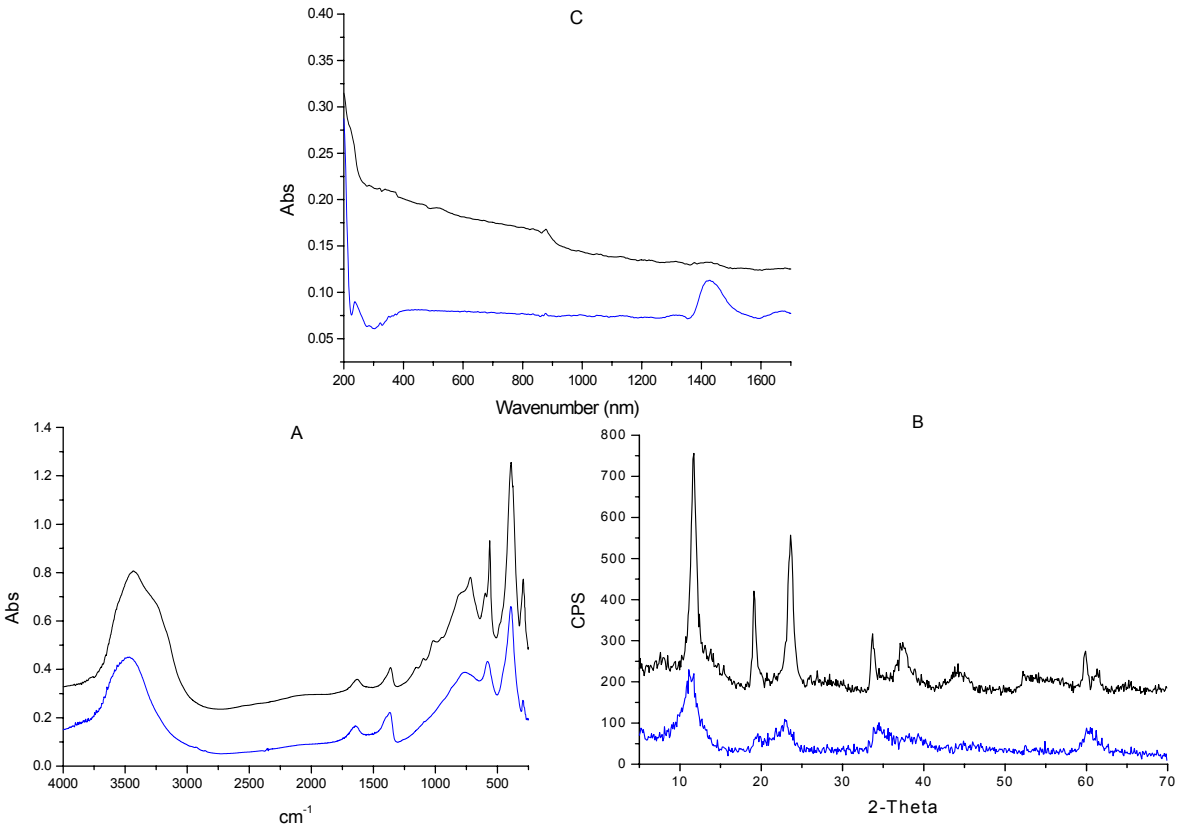

Figure 5.7: A) FT-IR spectra (blue-fresh, black-aged), B) XRD patterns (blue-fresh, black-aged) and C) Transmission-UV-Vis-NIR spectra (blue-fresh, black-aged) of 2:1 Mg-Ga LDH-Cl.

For the aged and fresh 2:1 Mg-Ga LDH-Cl samples,[12,13] the IR spectra show two strong peaks around 292 cm^{-1} and 390 cm^{-1}. The XRD patterns show sharper peaks for the aged materials, and the transmission UV-Vis-NIR spectra do not show any significant differences (except in the 200 – 300 nm range).

Since the major differences between the 2:1 Mg-M(III) LDH-Cl and 2:1 Mg-Al LDH-Cl with M(III) samples will once again be observed through FT-IR spectroscopy, these differences will be discussed.

By tabulating the notable IR peaks between the 2:1 Mg-MIII LDH-Cl and the Mg-Al-MIII LDH-Cl materials, we can clearly see differences, as was the case for the divalent metals project. Table 3 lists the notable peaks between these materials. What we are specifically looking for are differences among a LDH containing magnesium and aluminum, LDH containing magnesium, aluminum and a trivalent metal and LDH containing trivalent metals and aluminum.

Table 5.5: Comparison of specific IR peaks between the Mg-Al-M(III) LDH and Mg_2-M(III) LDH samples.

LDH Material	Pertinent Peaks (cm^{-1})
Fresh 2:1 Mg-Al LDH-Cl/Cr(III)	558, 448
Aged 2:1 Mg-Al LDH-Cl/Cr(III)	558, 448
Fresh 2:1 Mg-Al LDH-Cl/Fe(III)	449, 395
Aged 2:1 Mg-Al LDH-Cl/Fe(III)	447, 391
Fresh 2:1 Mg-Al LDH-Cl/Ga(III)	448, 398
Aged 2:1 Mg-Al LDH-Cl/Ga(III)	447, 391
Fresh 2:1 Mg-Al LDH-Cl/Al(III)	448, 395
Aged 2:1 Mg-Al LDH-Cl/Al(III)	447, 391
Fresh Mg_2-Cr LDH-Cl	415
Aged Mg_2-Cr LDH-Cl	415
Fresh Mg_2-Fe LDH-Cl	379
Aged Mg_2-Fe LDH-Cl	375
Fresh Mg_2-Ga LDH-Cl	391, 292
Aged Mg_2-Ga LDH-Cl	390, 292

Based on the data from Table 5.5, major differences are observed between the aged and fresh Mg-Al LDH-Cl-M(III) and the aged and fresh Mg_2-M(III) LDH-Cl samples. Among the aged and fresh Mg_2-M(III) LDH-Cl materials, no significant differences are observed between the aged and fresh Mg_2-M(III) LDH-Cl samples. Therefore, as with the partly exchanged $(M(II),Mg)_2Al$ systems, the differences are due to three different LDH lattice metals versus two different LDH lattice metals.

Table 5.6: Bragg reflection angles and interlayer spacings (uncorrected) for the 003 and 110 reflections in each of the 2:1 Mg-M(III) LDH-Cl samples.

LDH Material	003 Reflection Angle (2θ)	Interlayer Spacing (Å)	110 Reflection Angle (2θ)	110 d-spacing (Å)
Fresh 2:1 Mg-Cr LDH-Cl	11.30	7.82	60.24	1.54
Aged 2:1 Mg-Cr LDH-Cl	11.10	7.96	59.88	1.54
Fresh 2:1 Mg-Fe LDH-Cl	10.10	8.04	59.41	1.55
Aged 2:1 Mg-Fe LDH-Cl	11.09	7.97	60.12	1.54
Fresh 2:1 Mg-Ga LDH-Cl	11.21	7.89	60.58	1.53
Aged 2:1 Mg-Ga LDH-Cl	11.79	7.50	59.89	1.54

Upon comparing Table 5.6 with Table 5.3, we do not see any notable differences in the interlayer spacings. The 110 d-spacings are larger for the fresh and aged 2:1 Mg-Cr LDH-Cl samples with respect to the fresh and aged 2:1 Mg-Al LDH-Cl/Cr(III) samples. We see the same for the 2:1 Mg-Fe LDH-Cl samples and the 2:1 Mg-Ga LDH-Cl samples (the fresh 2:1 Mg-Ga LDH-Cl sample is close to the fresh and aged 2:1 Mg-Al LDH-Cl/Ga(III) samples).

As seen and discussed with the Mg-M(II)-Al LDH-Cl samples, we attribute these observations to the difference between two metals in the LDH lattice and three metals in the LDH lattice, but in this case it is not due to partial aluminum replacement. These differences should also be due to the differences in the ionic radii of the trivalent metals.

5.6 Conclusions/Future Directions

The main goal of this project was to see if we could extend the success of cation exchange, from the LDH lattice divalent metals, to the LDH lattice trivalent metals. Unfortunately the trivalent metals did not replace the aluminum metals, but instead

destroyed the LDH lattice framework, as was observed in the magnesium to aluminum content.

The first explanation for this observation has to be due to the very low pH values that the trivalent metal chloride salts had. These pH values may have been too acidic for the LDH to survive.

Another explanation may be due to these trivalent metals forming materials other than LDH. From Chapter 1, it is our belief that the mechanism of LDH formation most likely passes through an initial $M(III)(OH)_3$ stage. For M(III) cations, such as iron and chromium, these hydroxides may also be in the form of basic hydroxides (i.e. ferrihydrite).[14] This formation would be a difficult template for further hydroxide additions that are necessary for LDH lattice construction.

Although this project did not produce the surprising results from Chapter 4, we were slightly surprised by the color differences between the aged and fresh 2:1 Mg-Al LDH-Cl with Cr(III) samples.

Although trivalent cation exchange did not seem to occur with a Mg:Al based LDH, perhaps it can occur with other trivalent metals in the pre-formed LDH lattice. It may be worth studying the effects of chromium, iron or gallium exchange with aluminum, or chromium, gallium and aluminum exchange with iron, etc.

There is also the possibility of studying the potential trivalent cation exchange with LDH having other divalent metals, such as 2:1 LDH-Cl containing Ni-Al, Co-Al and Zn-Al. We can also study 2:1 LDH-Cl containing Ni-Cr, Ni-Ga, Co-Cr, Co-Fe, Zn-Cr, Zn-Fe, etc. The list of possibilities is vast.

Since we did not have any aluminum replacement success with the 2:1 Mg-Al LDH-Cl materials, we may or may not have success with higher divalent-to-trivalent metals ratios, such as 3:1 M(II)-M(III) LDH-Cl. Regardless of any initial predictions, these materials would be worth studying.

As with the materials from Chapter 4, these materials may also hold some catalytic potential.[15-21]

5.6 References

(1) Burgess, J.; Kijowski, J. *J. Inorg. Nucl. Chem.* **1981**, *43*, 2649.

(2) de Roy, A.; Besse, J.P.; Bondot, P. *Mat. Res. Bull.* **1985**, *20*,1091.

(3) del Arco, M.; Gutierrez, S.; Rives, V. *Inorg. Chem.* **2003**, *42*, 4232.

(4) Evans, J.; Pillinger, M.; Zhang, J. *J. Chem. Soc., Dalton Trans.* **1996**, 2963.

(5) Gutmann, N.; Muller, B. *J. Solid State Chem.* **1996**, *122*, 214.

(6) Miessler, G.L.; Tarr, D.A. Inorganic Chemistry, 3rd ed: Pearson Prentice Hall, Upper Saddle Rive, N.J., 2004.

(7) Bhattacharjee, S.; Anderson, J.A. *J. Mol. Catal. A: Chemical* **2006**, *249*, 103.

(8) Prakash, A.S.; Vishnu Kamath, P.; Hegde, M.S. *Mater. Res. Bull.* **2000**, *35*, 2189.

(9) Kooli, F.; Rives, V.; Ulibarri, M.A. *Inorg. Chem.* **1995**, *34*, 5122.

(10) Ferreira, O. P.; Alves, O. L.; Gouveia, D. X.; Souza Filho, A.G.; de Paiva, J. A. C.; Filho, J. M. *J. Solid State Chem.* **2004**, *177*, 3058.

(11) Meng, W.; Li, F.; Evans, D. G.; Duan, X. *Mater. Res. Bull.* **2004**, *39*,1185.

(12) Lopez-Salinas, E.; Garcia-Sanchez, M.; Montoya, J.A.; Acosta, D.R.; Abasolo, J.A.; Schifter, I. *Langmuir* **1997**, *13*, 4748.

(13) Aramendia, M.A.; Aviles, Y.; Benitez, J.A.; Borau, V.; Jimenez, C.; Marinas, J.M.; Ruiz, J.R.; Urbano, F.J. *Microporous Mesoporous Mater.* **1999**, *29*, 319.

(14) Bishop, J. L.; Pieters, C. M.; Burns, R. G.; Edwards, J. O.; Mancinelli, R. L.; Froschl, H. *Icarus* **1995**, *117*, 101.

(15) Mulukutla, R.S.; Detellier, C. J*. Mater. Sci. Lett.* **1996**, *15*, 797.

(16) Velu, S.; Swamy, C.S. *Appl. Catal. A: General* **1997**, *162*, 81.

(17) Choudhary, V. R.; Jana, S.K.; Mandale, A.B. *Catal. Lett.* **2001**, *74*, 95.

(18) Salinas, E. L.; Sanchez, M. G.; Serrano, M.E.L.; Bolanoz, J.N. *J. Phys. Chem. B* **1997**, *101*, 5112.

(19) Prinetto, F.; Tichit, D.; Teissier, R.; Coq, B. *Catal. Today* **2000**, *55*, 103.

(20) Kunbar, P.S.; Valente, J.S.; Figueras, F. *Tetrahedron Lett.* **1998**, *39*, 2573.

(21) Mimura, N.; Takahara, I.; Saito, M.; Sasaki, Y.; Murata, K. *Catal. Lett.* **2002**, *78*, 125.

CHAPTER 6

ORIENTATION EFFECTS OF THE IR ACTIVE MODES IN LDH*

6.1 FT-IR Spectroscopy and LDH

In Chapter 1, Fourier-transform infrared (FT-IR) spectroscopy was described as one of the main characterization tools used in the study of layered double hydroxides (LDH). FT-IR spectroscopy is mainly used to verify and/or identify the types of anions incorporated in LDH.

In Chapter 2, the IR spectra in the transition-metallocyanide region showed orientation effects, when small amounts of dilute 2:1 Mg-Al LDH-CO_3/ferrocyanide and 2:1 Mg-Al LDH-CO_3/ruthenocyanide suspensions were placed on BaF_2 support discs. The explanation given was based on the suppression of the IR active modes along the z-axis, while those in the x,y plane remained allowed.

Since this type of FT-IR procedure proved insightful for the metallocyanide complexes, it could be applied to LDH, in general. From the model in Chapter 1 (Figure 1.1), the LDH lattice shows the M-OH lattice framework along all three Cartesian axes. These metal hydroxide bonds would stretch and bend in all directions, so by theory, placing small amounts of an LDH suspension on a pre-formed support could show suppression and/or polarization of some of these IR active metal hydroxide lattice modes, provided all of the LDH particles would be lying flat on the support surface. If too much sample is placed on such supports, the particles may end up stacked on other particles, such that any orientation effects would be compromised.

* This chapter is adapted from an article accepted for publication by the Journal of Physical Chemistry C, by M.C. Richardson and P.S. Braterman.

6.2 Purpose of Experiment

While this project is wholly an FT-IR project, we will set out to demonstrate that infrared spectroscopy can give insight, not obtainable by other means, into the structural details of the LDH metal-hydroxide lattice. We aim to show that useful information is obtainable in the region between 400 cm^{-1} and 250 cm^{-1}, now accessible using commercial infrared spectrometers with cesium iodide optics/background. We also intend to report on ways of extending our technique of oriented infrared spectroscopy, previously limited to the range above 800 cm^{-1} (Chapter 2, BaF_2 support), to the full wavelength region, and demonstrate its use as an aid in the vibrational assignments of the metal-hydroxide lattice regions. As sample materials, we used LDH with Mg:Al ratios of 2:1 and 3:1, both freshly prepared and aged (by reflux). As anions, we used chloride (because of its absence of internal vibrations), and ferrocyanide (because its internal vibrations, and the effect of orientation on these when incorporated into LDH, are well understood, as discussed in Chapter 2).

In the case of order versus disorder, PXRD and EXAFS[1] has been used to obtain information about the nearest and next nearest neighbors of the metal ions in the LDH lattice sheets, with implications about the possibility of short-range order. Simple orderly stacking of layers one above the other gives rise to a range of possible polytypes, distinguishable from each other by x-ray diffraction, as discussed in Chapter 1. In a few cases, x-ray diffraction also reveals orderly arrangements of cations, and sometimes of anions, giving rise to what is described as superlattice spacings.[2] It is also possible for such superlattice spacings to arise in synthetic material from orderly arrangements of the interlayer anions,[3] but it is not possible to say whether such order

is also present in the cation distribution. Unfortunately, Mg(II) and Al(III), which give rise to the most common LDH, both natural and synthetic, are indistinguishable by x-ray techniques.

6.3 Experimental Procedure

6.3.1 Parent LDH Preparation

The parent LDH-Cl materials were prepared, under a steady stream of nitrogen gas in order to prevent adventitious CO_2 uptake, by the standard technique of addition of the stoichiometric amounts of 50% NaOH (Alfa Aesar) (6 mol OH^- for every Al^{3+} for 2:1 LDH and 8 mol OH^- for every Al^{3+} for 3:1 LDH) to a solution 0.1 M in $AlCl_3$ and either 0.2 M or 0.3 M in $MgCl_2$ (both salts supplied by Aldrich).

Neither of the above LDH materials was prepared using an excess amount of $MgCl_2$. The exact stoichiometric amounts were used, in contrast to the excess magnesium-buffer scenario.

The fresh LDH was collected after 1 hr stirring, while the aged materials were washed once by centrifuge and gently refluxed in water for 24 hours. Both fresh and aged materials were thoroughly washed/centrifuged using Millipore Milli-Q Academic water (18.2 $M\Omega\ cm^{-1}$). Materials for exchange with ferrocyanide were used as prepared; materials for spectroscopic examination were dried in a vacuum desiccator over a mixture of drierite and molecular sieves.

6.3.2 LDH-Ferrocyanide Preparation

For the LDH-ferrocyanide samples, 1.0 g fresh or aged LDH chloride (as calculated from the conditions of preparation) was suspended in 25 mL water and the calculated amount of potassium ferrocyanide (i.e., ¼$[Fe(CN)_6]^{4-}$: 1$[Al^{3+}]$) was dissolved in 25 mL water. Use of excess ferrocyanide led to the formation of the cubic material that our research group has described previously.[4] The materials were stirred under a nitrogen gas blanket for one hour, thoroughly washed by centrifuge, and dried in a vacuum desiccator over a mixture of drierite and molecular sieves.

Infrared spectra were obtained using a Perkin-Elmer Spectrum One spectrometer, with internal CsI beam-splitter and automatic water and CO_2 absorption correction. Supporting and reference materials were of infrared grade and supplied through: KBr by Alfa Aesar, CsI by Wilmad, CdTe discs by New Era Enterprises and the polyethylene ST-IR cards by Thermo Electron Corp. All spectra were averaged over 40 scans, at a resolution of 4 cm^{-1}, and normalized in absorbance mode to an ordinate maximum of 1.0 for consistency of interpretation.

6.3.3 FT-IR Samples using KBr and CsI

The conventional IR spectra were obtained using KBr (FT-IR grade, Fluka) and CsI (FT-IR grade, Wilmad), against discs consisting of either KBr or CsI alone (0.2000 g KBr or 0.2500 g CsI, respectively) as reference. The samples were prepared by weighing out approximately 1% sample (with respect to the background amounts), then adding either KBr or CsI in order to come as close to the original background weights as possible, since we have found that differences as small as 0.5 mg between the sample

disc weight and background disc weight are enough to observe, what appears to be background peaks, in the sample spectrum. The spectra were scanned and collected from 4000 cm^{-1} to 400 cm^{-1}, for KBr and from 4000 cm^{-1} to 250 cm^{-1}, for CsI.

6.3.4 FT-IR Samples using CdTe and Polyethylene

Oriented IR spectra were obtained using CdTe (polished discs, 13mm x 2mm, New Era Enterprises) and polyethylene (ST-IR cards, Thermo Electron Corporation) both as pre-formed supports, chosen for their insolubility in water and transparency over a useful range of wavelengths. For each CdTe sample, approximately three to five drops of a dilute LDH suspension was placed on top of each disc and allowed to dry, at room temperature, in a vacuum desiccator. If the infrared spectrum was too weak, more material was added. The polyethylene samples were prepared in a similar fashion, but more of the LDH suspension (seven to ten drops) was required.

Infrared absorbances will appear in the pellet samples regardless of polarization, while, to the extent that the material is deposited as horizontal platelets on the support, only in-plane polarized absorption bands will appear in the oriented spectra. This orientation effect is well-established for the ferrocyanide materials (Chapter 2), so it can be used as a comparison for these materials. Also of note, by adding more of the LDH suspension onto the CdTe and polyethylene supports, we run the risk of having too much sample, which would hinder our goal of causing the LDH particles to lie down flat on the support surface.

6.4 Results and Discussion

6.4.1 Evaluation of the Background Sources

The polyethylene ST-IR cards performed well around 2000 cm^{-1} and below 600 cm^{-1}. In the 3000 – 4000 cm^{-1} region, and also in comparison with air, they gave rise to a weak modulation (wavy lines between peaks), which we attribute to imperfectly compensated interference effects, strongest near an absorption band (Figure 6.1). As a result, we confined our use of polyethylene to the regions around 2,000 cm^{-1} and below 600 cm^{-1}.

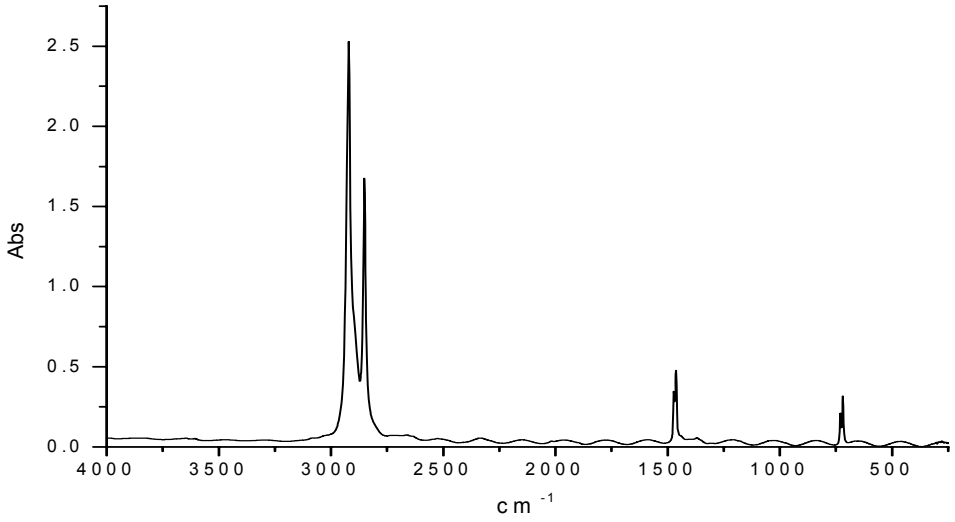

Figure 6.1: FT-IR spectrum of polyethylene film against polyethylene film reference.

For most work, potassium bromide remains to be the preferred choice, but cannot be used below 400 cm^{-1}. Cesium iodide can easily be used below 400 cm^{-1}, but major distortions in observed spectra in the neighborhood of strong, sharp peaks are observed (Figure 6.2).

Regardless of this major pitfall and its higher cost, greater tendency to adsorb water, and greater chemical reactivity under the conditions of localized pressure and temperature that take place during pellet formation, CsI has initially proven itself to be a viable background source for IR studies of LDH.

Cadmium telluride discs were suitable substrates down to 400 cm^{-1}, but like KBr, they cannot go down below 400 cm^{-1}. The pre-formed CdTe discs are expensive, toxic, and easily damaged. We initially attempted to prepare our own cadmium telluride discs, from the powder in an ordinary pellet press, but were not successful.

Although each of these background materials has their own individual strengths and weaknesses, they can be extremely useful and informative when used to complement each other.

6.4.2 Group Theoretical Analysis and Its Limitations

Published treatments[5,6] of the hydroxide layer vibrations of LDH containing Mg:Al ratios of 2:1 and 3:1 assume an idealized orderly arrangement, with the factor group D_{3d}, signifying a trigonal antiprismatic structure (Figure 1.6, Chapter 1). The factor group analysis proceeds in much the same way as the familiar point group analysis of individual molecules, except that translationally equivalent atoms are treated as formally identical. Those motions that correspond to an overall translation or rotation of the unit cell are discarded, and the number of allowed modes is compared with the observed spectra. This procedure can be regarded as an extension of the work done by Mitra,[7] for magnesium hydroxide, and the modifications that follow are closely related to those

that Braterman and Cygan have offered, for magnesium hydroxide,[8] on the basis of more extensive vibrational mode analysis and molecular dynamics simulations.

The use of the factor group method implies an orderly arrangement, forming a superlattice, of the two different kinds of metal cations, although this need not be sufficiently extensive to give rise to superlattice spacings in the XRD pattern. Such order is bound to arise locally in LDH materials of type $M^{(II)}_2M^{(III)}(OH)_6$, if $M^{(III)} – M^{(III)}$ nearest metal neighbor approaches are to be avoided (compare Lowensteins rule),[9] but the same is not true for LDH materials of type $M^{(II)}_3M^{(III)}(OH)_8$. As shall be discussed and shown below, there is good evidence from our spectra for local symmetry in the aged 2:1 Mg-Al LDH samples, but not in freshly prepared 2:1 Mg-Al LDH samples. In all cases of the 3:1 Mg-Al LDH samples, the degree of local symmetry seems similar to that in the freshly prepared 2:1 LDH samples.

The factor group treatment finds only those vibrations in which all unit cells are moving in phase; what is sometimes referred to as the k = 0 member of the Brillouin zone associated with each mode. This scenario neglects all motions in which groups in neighboring unit cells are moving more or less out of phase with each other, giving rise to motions of higher frequency than the k = 0 member.[6] In magnesium hydroxide, these modes are inactive in infrared and Raman spectroscopy, but active in neutron scattering (there are no selection rules for neutron scattering). In LDH, there is the added complication that the interlayer anions and water molecules form a dynamic system of no particular symmetry (regardless of how complex or simple the interlayer anion is), hydrogen bonded to each other and to the lattice hydroxides.[10,11] This has the effect of localizing the hydroxide modes, and of undermining the k = 0 selection rule and

its corollary, the predicted absence from the spectrum of modes corresponding to the translation or rotation of the entire chosen unit cell.[12]

For completeness, we give the results of formal factor group analysis, classified by the group or atom motions principally involved, in Tables 6.1 and 6.2. Of course, different modes of the same symmetry will mix, especially if they involve the same kind of motion. It is worth noting that several formally symmetry-allowed modes involving the hydroxide groups are expected to be weakly observed. This is because these groups reside on sites of less than 3-fold symmetry, so that some combinations of z-direction motions are formally allowed to have components in the x,y plane, and vice versa.

6.4.3 FT-IR Spectra

In all cases, as expected, the H_2O bending mode (1620 cm^{-1} to 1640 cm^{-1})[13] did not show any major orientation effects. This peak remains consistent in all samples, and will not be further discussed.

6.4.3.1 The CN Stretching Region of LDH-Ferrocyanides

We must first consider the aged materials $Mg_2Al(OH)_6.1/4\ Fe(CN)_6.xH_2O$, as a test of our methodology. Earlier work using barium fluoride as support had established that the T_{1u} infrared active mode is split into two components; a slightly sharper band at 2034 cm^{-1}, absent in the oriented spectrum, and a broader band at 2045 cm^{-1} that is still present on orientation (compare Chapter 2). We interpreted this finding as consistent with D_{3d} site symmetry for the ferrocyanide, which will split T_{1u} (O_h) into A_{2u} (z-oriented) and E_u (x,y-oriented) components.

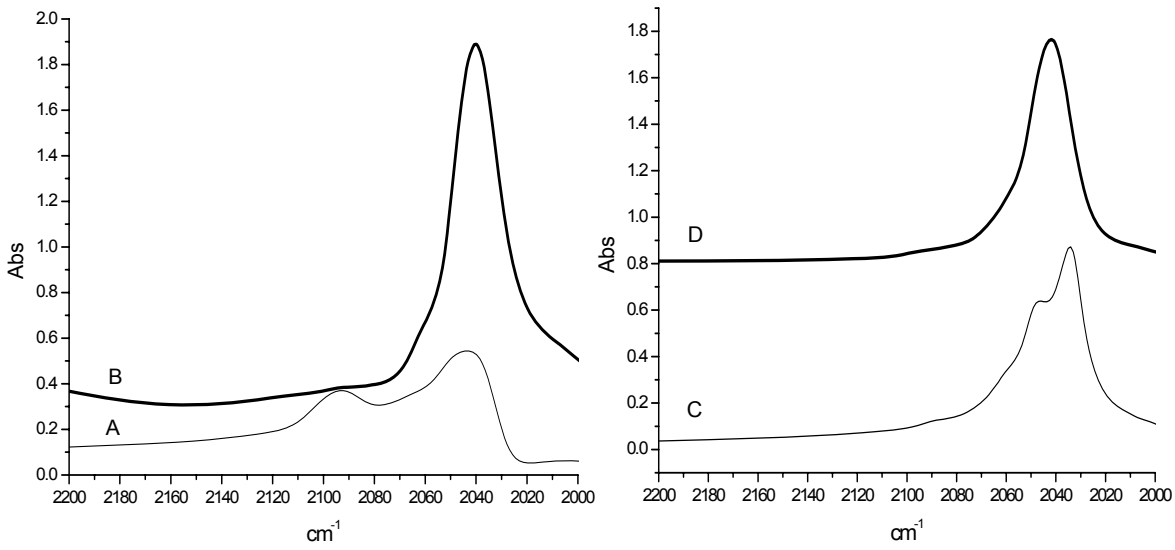

Figure 6.2: Infrared spectra of aged 2:1 Mg-Al LDH-ferrocyanide (2200 –2000 cm^{-1}) from aged chloride precursor: (A) CsI; (B) polyethylene, oriented; (C) KBr; (D) CdTe, oriented. Note the difference between spectrum A and spectrum C, and the correspondence between B and D.

Figure 6.2 compares the spectra obtained with CdTe support, polyethylene support, KBr disc and CsI disc in this region. The suppression of the 2034 cm^{-1} band in the supported materials shows that orientation has indeed taken place, and establishes the suitability of both these supports. The spectrum in CsI shows a new broad peak around 2094 cm^{-1}, clearly indicative of reaction of some kind, together with an apparent shift of the authentic ferrocyanide feature to slightly higher frequency, and a minimum at its low wavenumber edge. We regard these effects as optical artefacts, perhaps connected with the high refractive index of CsI, and/or some kind of mechano-chemical effect with the CsI material and the LDH material.

Figure 6.3 shows the spectrum in this region of fresh 2:1 LDH chloride, exchanged with ferrocyanide. In this case, the separate components are not resolved, and, somewhat remarkably, the ordering of A_{2u} and E_u components appears to be reversed.

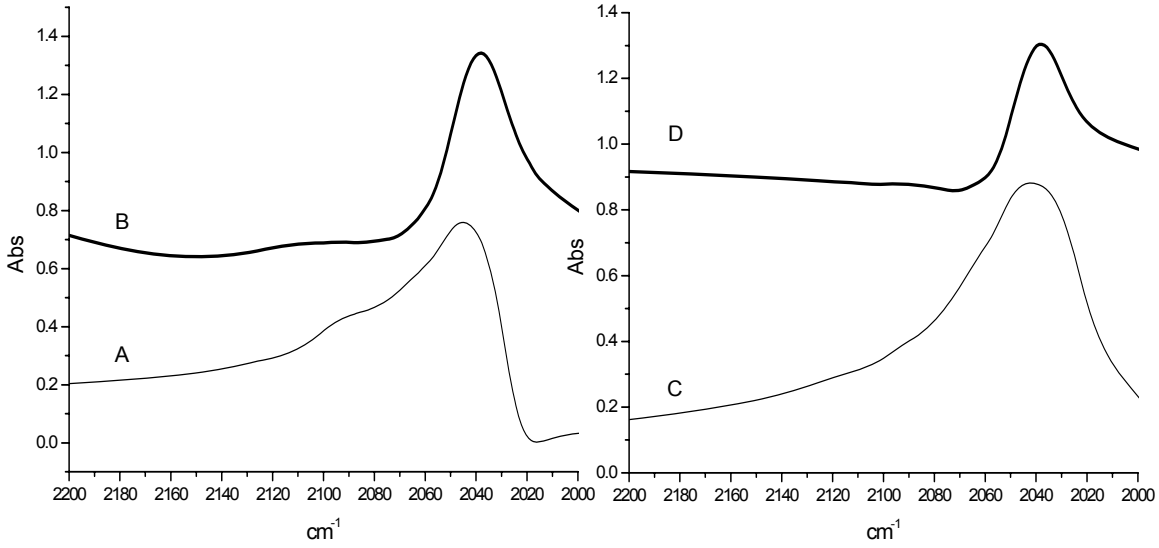

Figure 6.3: Infrared spectra of fresh 2:1 Mg-Al LDH-ferrocyanide (2200 – 2000 cm^{-1}) from fresh chloride precursor: (A) CsI; (B) polyethylene, oriented; (C) KBr; (D) CdTe, oriented.

We can take note of the fact that the ferrocyanide stretching modes are directionally dependent, no doubt due to the hydrogen bonding between the cyano ligands and the lattice hydroxides, and that there is a noticeable difference between the fresh and aged materials.

The seeming reversal of the A_{2u} and E_u components are best seen from the spectra labeled C and the spectra labeled D in Figures 6.2 and 6.3.

6.4.3.2 OH bend – MOH lattice region, 1100 – 250 cm^{-1}

There are major differences between fresh and aged 2:1 Mg-Al LDH-Cl in this region, and significant orientation effects.

The most obvious difference between these two materials is within the 1100 cm^{-1} to 250 cm^{-1} range (Figures 6.4 and 6.5). The aged material in CsI shows a sharp peak at 447 cm^{-1}, which is weak or on occasion absent in the fresh material, together with a sharp peak at 390 cm^{-1}; the 447 cm^{-1} peak is also present in the KBr pellet spectrum, as expected. The fresh material in CsI or on polyethylene shows a broad peak with a maximum around 395 cm^{-1}. In addition, all of the spectra show broad features extending from low frequencies to 1000 cm^{-1} or beyond, with defined peaks at around 560 cm^{-1} and 1025 cm^{-1} (KBr and CdTe only, in the aged materials). The non-oriented specimens (KBr and CsI only) show a broad absorption around 600 cm^{-1} or 700 cm^{-1}, absent in the oriented specimens.

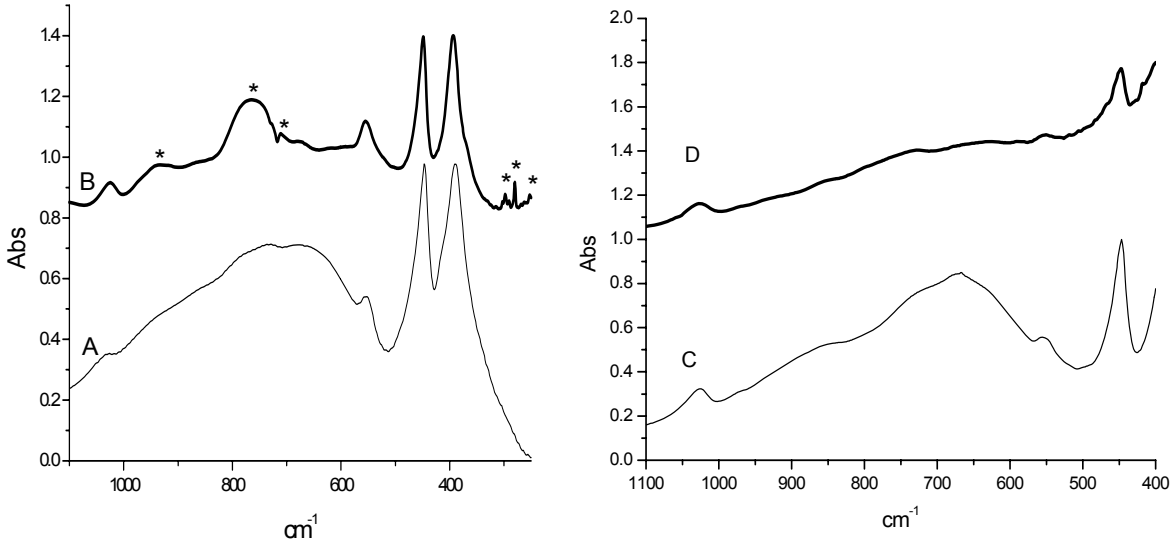

Figure 6.4: Infrared spectra of aged 2:1 Mg-Al LDH-Cl (1100 – 400/250 cm^{-1}): (A) CsI; (B) polyethylene, oriented; (C) KBr; (D) CdTe, oriented. Possible artefacts from polyethylene are labeled with *.

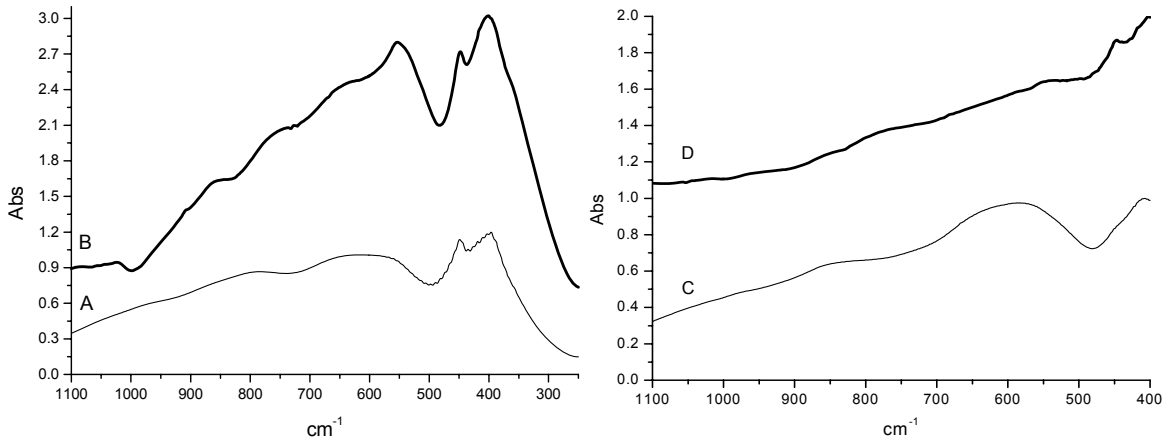

Figure 6.5: Infrared spectra of fresh 2:1 Mg-Al LDH-Cl (1100 – 400/250 cm^{-1}): (A) CsI; (B) polyethylene, oriented; (C) KBr; (D) CdTe, oriented.

The 447 cm^{-1} band is diagnostic of lattice ordering, which is required if the system is to avoid having tervalent cations as each other's nearest neighbors. This supports the suggestion that a disorderly pre-formed material matures by a solution-reprecipitation process (Ostwald Ripening), since it is not clear how Mg and Al could change places within an intact metal-hydroxide lattice. However, even this initially formed material must show sufficient crystallinity for orientation effects to be significant. Although OH rotation (MOH bending) and OH x,y-translation (mainly MO bending/stretching) modes are allowed to mix, we would suggest that the broad, orientation-independent absorption corresponds mainly to the former, and that this is confirmed by the existence of inelastic neutron scattering modes found in this region and regarded as diagnostic of motions that correspond to large displacements of hydrogen atoms. They are closely related to similar modes in $Mg(OH)_2$[8,14] except that (as confirmed by molecular dynamics models[12]) hydrogen bonding to interlayer water causes loss of microscopic symmetry and allows spectroscopic activity. The minor

differences between nominally similar spectra may be caused by small changes in water content.

Absorptions due to the A_{2u} modes are selectively suppressed by orientation, and three such modes are formally predicted by the group-theoretical treatment (Table 1); however, only one of these derives from a motion that will in reality convey z-oriented intensity. We therefore assign the z-oriented absorption around 700 cm^{-1} to this mode, the OH z-direction translation with its associated M-O stretching and MOM bending.

Table 6.1. Formal analysis of the motions of the $Mg_2Al(OH)_6$ unit, factor group D_{3d}. The superscripts: [a] R, Raman-allowed; pol, polarized; depol, depolarized; z, z-axis (c-direction) polarized; (x,y) x,y-axis (a, b-plane) polarized; f, formally (group-theoretically) allowed , but expected to be vanishingly weak (see text); [b] Also contributes significantly to unit cell translation or rotation (total $A_{2u} + E_u + A_{2g} + E_g$), spectroscopically inactive)

Group or Atom	**Type of Motion**	**Effect on Bonding**	**Irreducible Representations Spanned and Predicted Activity[a]**
OH	Stretch	O-H Stretch	A_{1g} (R,pol) + A_{2u} (IR;z) + E_g (R,depol) + E_u (IR;x,y;f)
OH	z-axis motion	M-O-M Stretch/Bend	A_{1g} (R,pol) + A_{2u} (IR;z)[b] + E_g (R,depol)[b] + E_u (IR;x,y;f)
OH	x,y-axis motion	M-O-M Stretch/Bend	A_{1g} (R,pol) + A_{1u} + A_{2g}[b] + A_{2u} (IR;z,f) + $2E_g$ (R,depol) + $2E_u$ (IR;x,y)[b]
OH	Rotation	M-O-H Bend	A_{1g} (R,pol) + A_{1u} + A_{2g} + A_{2u} (IR;z,f) + $2E_g$ (R,depol) + $2E_u$ (IR;x,y)
Al	z-axis motion	M-O-M Stretch/Bend	A_{2u} (IR;z)[b]
Al	x,y-axis motion	M-O-M Stretch/Bend	E_u (IR;x,y)[b]
Mg	z-axis motion	M-O-M Stretch/Bend	A_{1g} (R,pol) + A_{2u} (IR;z)[b]
Mg	x,y-axis motion	M-O-M Stretch/Bend	E_g (R,depol) + E_u (IR;x,y)[b]

There remain the sharp peaks at 447 and 393 cm^{-1} in the aged materials, and at 390 cm^{-1} in the fresh LDH. We assign these to the two allowed E_u modes derived from OH x,y translational (M-O-M bend stretching) motions. The existence of two such modes within the same unit cell is a result of coupling between groups of the same type, (OH groups with one Al and two Mg neighbors). We then attribute the fact that the peak is broader, and unsplit, in fresh LDH, to the absence of a superlattice, which will in this case imply the existence of OH groups in slightly different environments.

In the region below 1000 cm^{-1}, the ferrocyanides show the same the behavior as their parent chlorides, with the expected addition in both support and pellet spectra of the known[14] M-C-N bending mode at 590 cm^{-1} (literature value 583 cm^{-1} in water), and a band at 560 cm^{-1} of unknown origin, perhaps related to the effect of the M-C-N bend on the near continuum of x,y-polarized motions. The MC stretching mode expected at 416 cm^{-1} is not detectable against the strong layer absorption in this region, but the suppression of the above mentioned 700 cm^{-1} (OH z-motion) peak in the oriented spectra is particularly clear.

In contrast to the 2:1 materials, the fresh and aged 3:1 materials (Figures 6.6 and 6.7) show little difference in any frequency range. A single broad peak, close to 400 cm^{-1}, replaces all the features around 450 – 380 cm^{-1} that were in the 2:1 materials. This could be the result of overlap between the absorption bands of the two distinct types of OH present (Mg_3-OH vs. Mg_2Al-OH), in a well-ordered structure, which seems to us unlikely, especially in fresh LDH. On the contrary, we note that in the 3:1 material, it is possible to avoid nearest metal neighbor Al-Al approaches without

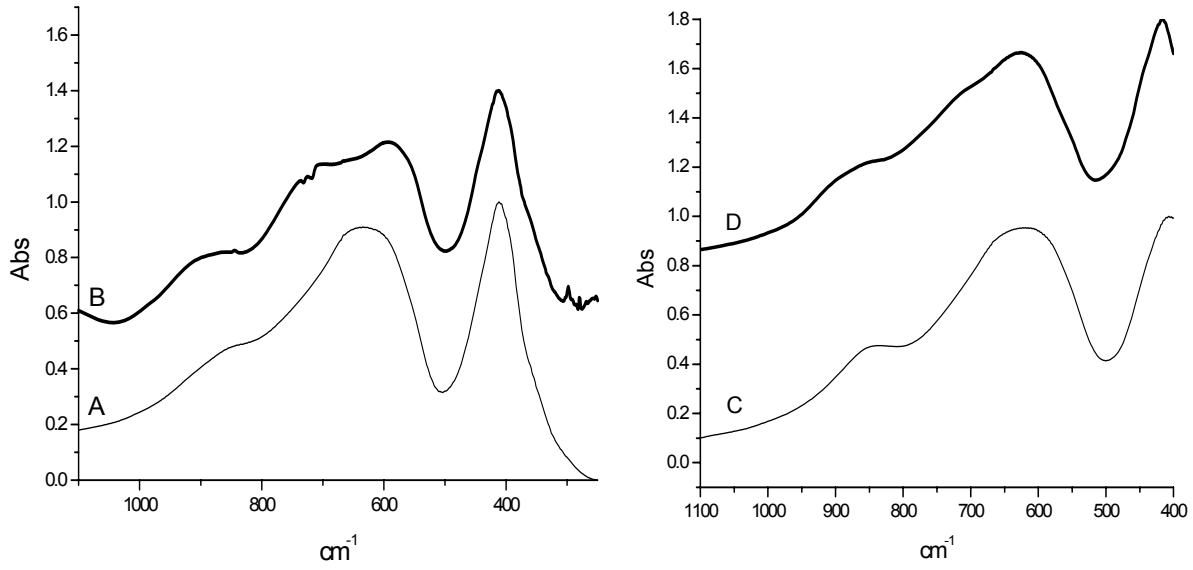

Figure 6.6: Infrared spectra of aged 3:1 Mg-Al LDH-Cl (1100 – 400/250 cm^{-1}): (A) CsI; (B) polyethylene, oriented; (C) KBr; (D) CdTe, oriented.

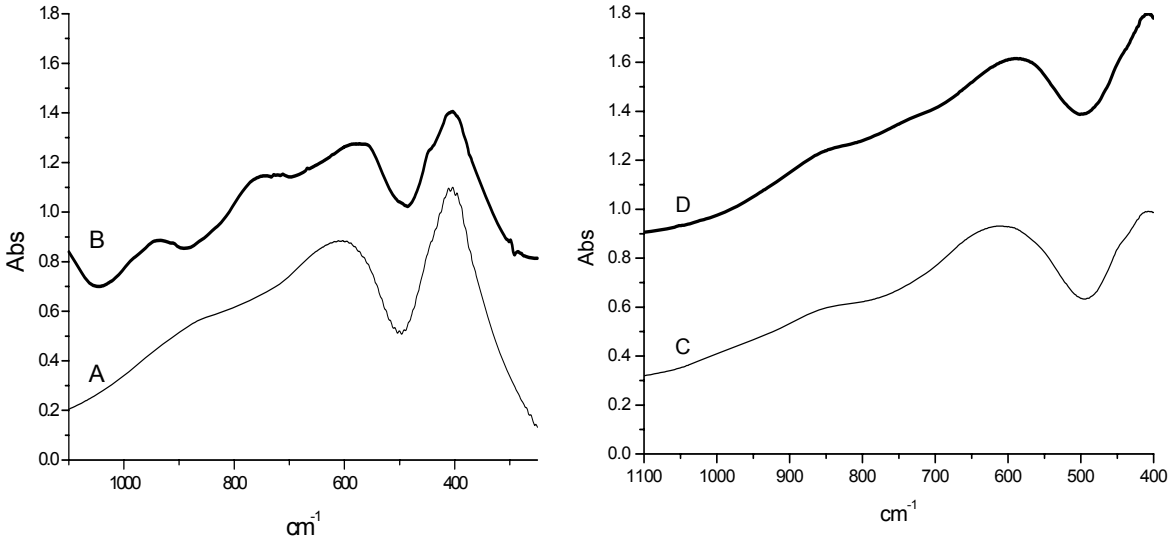

Figure 6.7: Infrared spectra of fresh 3:1 Mg-Al LDH-Cl (1100 – 400/250 cm^{-1}): (A) CsI; (B) polyethylene, oriented; (C) KBr; (D) CdTe, oriented.

imposing any regularity of structure, and infer that both aged and fresh 3:1 materials lack superlattice ordering. Slightly more structure is apparent in the oriented than in the non-oriented spectra, a fact that we very tentatively attribute to suppression of the OH z-axis motion in the former. Table 6.2 presents the group theoretical treatment for the 3:1 Mg-Al LDH.

Table 6.2. Formal analysis of the motions of the $Mg_3Al(OH)_8$ unit, factor group D_{3d}. The superscripts: [a] R, Raman-allowed; pol, polarized; depol, depolarized; z, z-axis (c-direction) polarized; (x,y) x,y-axis (a, b-plane) polarized; f, formally (group-theoretically) allowed, but expected to be vanishingly weak (see text); [b] OH(1) bridges two Mg and one Al. OH(2) bridges three Mg. OH(1) and OH(2) modes of the same symmetry will be strongly mixed, especially when derived from the same type of motion; [c] Also contributes significantly to unit cell translation or rotation (total $A_{2u} + E_u + A_{2g} + E_g$), spectroscopically inactive.

Group or Atom	**Type of Motion**	**Effect on Bonding**	**Irreducible Representations Spanned and Predicted Activity[a]**
OH(1)[b]	Stretch	O-H Stretch	
OH(2)[b]	Stretch	O-H Stretch	$A_{2g} + A_{2u}$(IR;z)
OH(1)	z-axis motion	M-O-M Stretch/Bend	
OH(2)	z-axis motion	M-O-M Stretch/Bend	$A_{2g} + A_{2u}$(IR;z)[c]
OH(1)	x,y-axis motion	M-O-M Stretch/Bend	
OH(2)	x,y-axis motion	M-O-M Stretch/Bend	E_u (IR;x,y)[c] + E_g(R,depol)
OH(1)	Rotation	M-O-H Bend	
OH(2)	Rotation	M-O-H Bend	E_u (IR;x,y) + E_g(R,depol)
Al	z-axis motion	M-O-M Stretch/Bend	A_{2u} (IR;z)[c]
Al	x,y-axis motion	M-O-M Stretch/Bend	E_u (IR;x,y)[c]
Mg	z-axis motion	M-O-M Stretch/Bend	A_{2u} (IR;z)[c] + E_u IR;x,y,f)
Mg	x,y-axis motion	M-O-M Stretch/Bend	$A_{1u} + A_{2u}$ (IR;z,f) + 2_{Eu} (IR;x,y)[c]

6.4.3.3 OH Stretching Region, 3000 – 4000 cm^{-1}

For the 2:1 materials, all the spectra show strong, broad, absorption in the range 3600 – 3200 cm^{-1}, (Figures 6.8 and 6.9), with subtle but consistent differences between the oriented and the pellet spectra. The pellet spectra have their intensity at somewhat higher frequency, and in the aged chloride material, there is evidence for a resolvable band around 3500 cm^{-1}, especially in the oriented specimens. We therefore relate the 3500 cm^{-1} band and the low-end intensity to the antisymmetric and symmetric OH stretching modes of interlayer water, which in liquid water occur at 3490 and 3280 cm^{-1}.

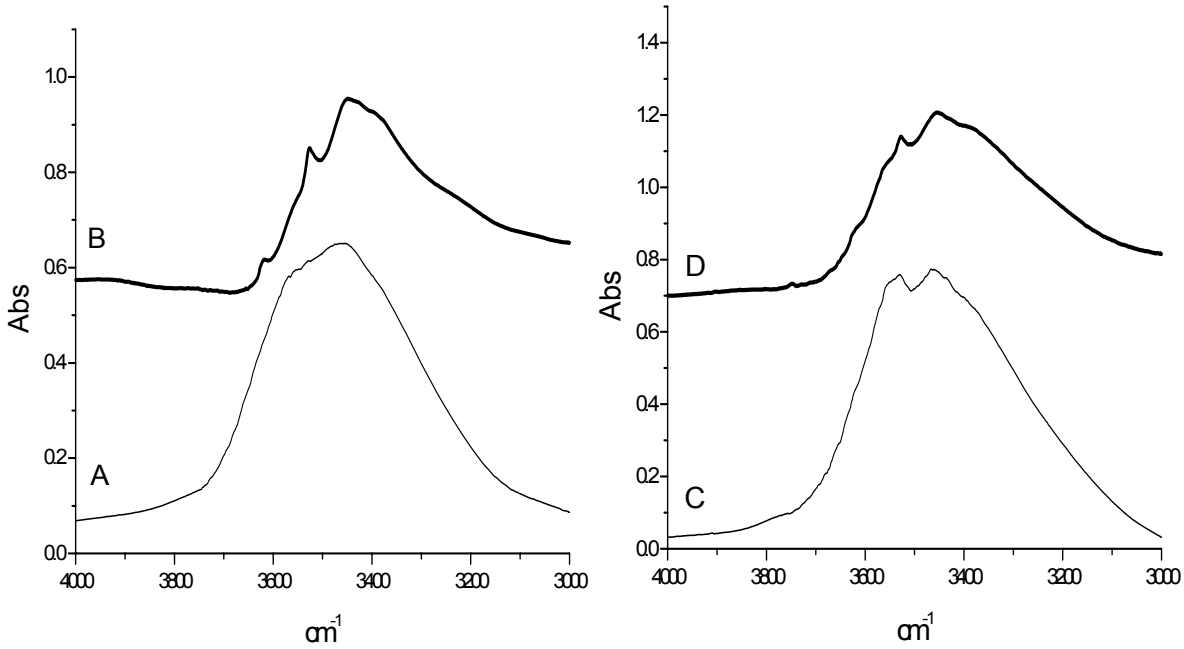

Figure 6.8: Infrared spectra of aged 2:1 Mg-Al LDH-Cl (4000 – 3000 cm^{-1}): (A) CsI; (B) polyethylene, oriented; (C) KBr; (D) CdTe, oriented.

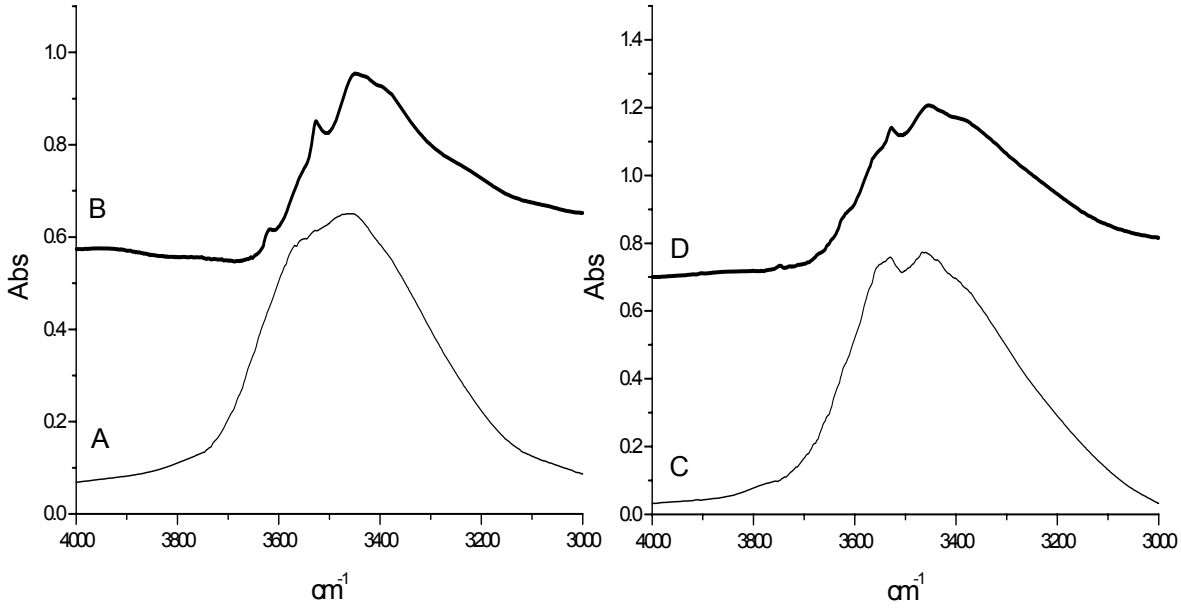

Figure 6.9: Infrared spectra of fresh 2:1 Mg-Al LDH-C (4000 – 3000 cm^{-1})l: (A) CsI; (B) polyethylene, oriented; (C) KBr; (D) CdTe, oriented.

These vibrations are expected to be largely confined to the x,y plane[10], leading us to locate the OH stretch (which is, of course, predominantly z-polarized) towards the higher frequency end of the feature, perhaps with intensity concentrated around 3450 cm^{-1}, although it will presumably be broadened by local fluctuations in hydrogen bonding.[11] We also note an overall reduction in the width of the absorption on ageing, suggesting that the cation ordering also, indirectly, affects the interlayer water.

For the 2:1 ferrocyanides (Figures 6.10 and 6.11), the differences between fresh and aged materials, and between oriented and pellet spectra, are qualitatively similar to those found for the chloride, and we invoke similar explanations. We draw attention to the small sharp resolved in-plane absorption at 3600 cm^{-1}. We ascribe this to interstitial water in an environment with very little hydrogen bonding; a situation more readily achieved with ferrocyanide (or with nickelocyanide, Figure 3.1, Chapter 3) than with chloride. This frequency is too low for brucite or gibbsite contamination, and in any case the in-plane orientation excludes assignment to layer hydroxide. Note also that ageing leads, at it did with 2:1 chloride, to a general reduction in the width of the OH stretching absorption.

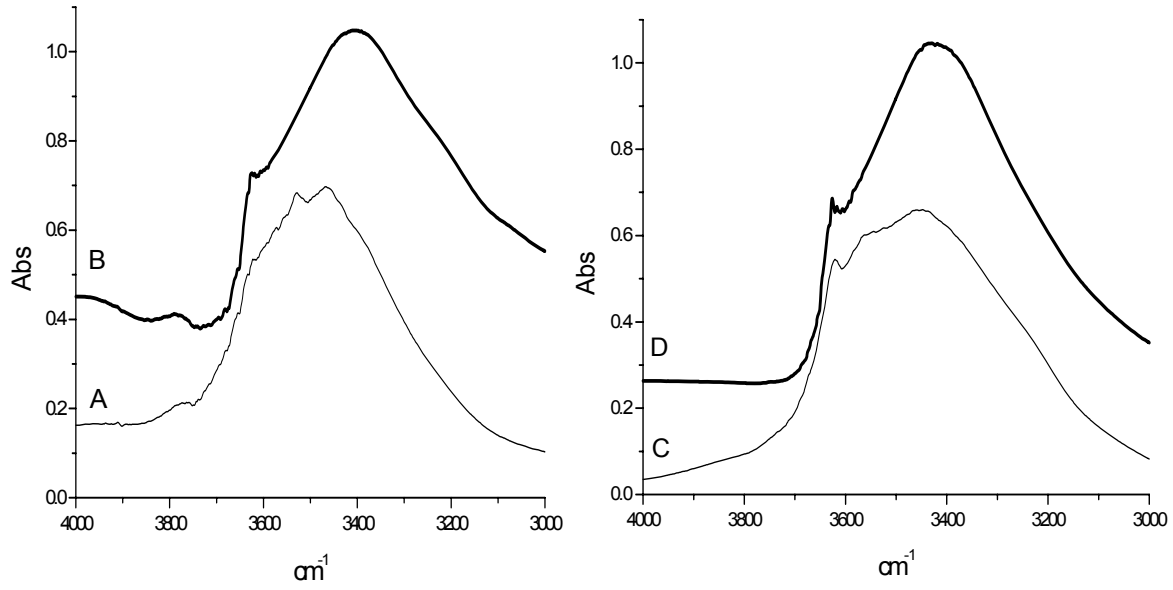

Figure 6.10: Infrared spectra of aged 2:1 Mg-Al LDH-ferrocyanide (4000 – 3000 cm^{-1}): (A) CsI; (B) polyethylene, oriented; (C) KBr; (D) CdTe, oriented.

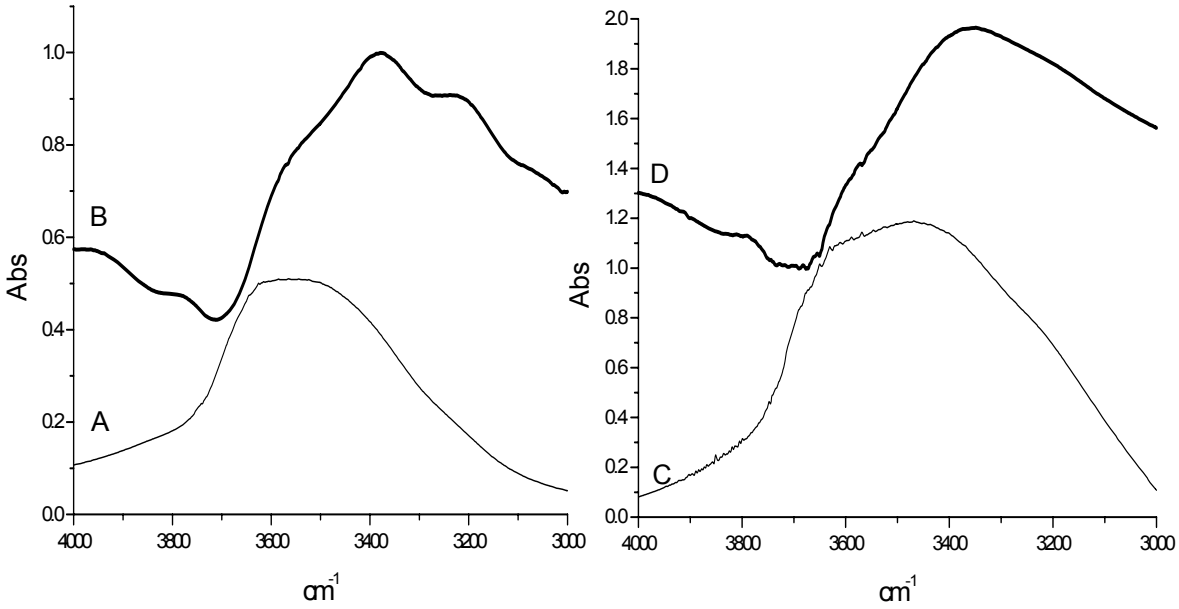

Figure 6.11: Infrared spectra of fresh 2:1 Mg-Al LDH-ferrocyanide (4000 – 3000 cm^{-1}): (A) CsI; (B) polyethylene, oriented; (C) KBr; (D) CdTe, oriented.

In the 3:1 materials as well (Figures 6.12 – 6.15), the oriented spectra in this region carry more intensity at lower frequencies. We offer the same explanation as we did in the 2:1 case in that the layer OH stretch is towards the higher frequency end of the range spanned by water OH. Again, we find less structure, and less difference between fresh and aged materials, than in the case of 2:1 LDH. This is consistent with our suggestion that the development of spectroscopically significant structure on ageing is limited to the 2:1 materials.

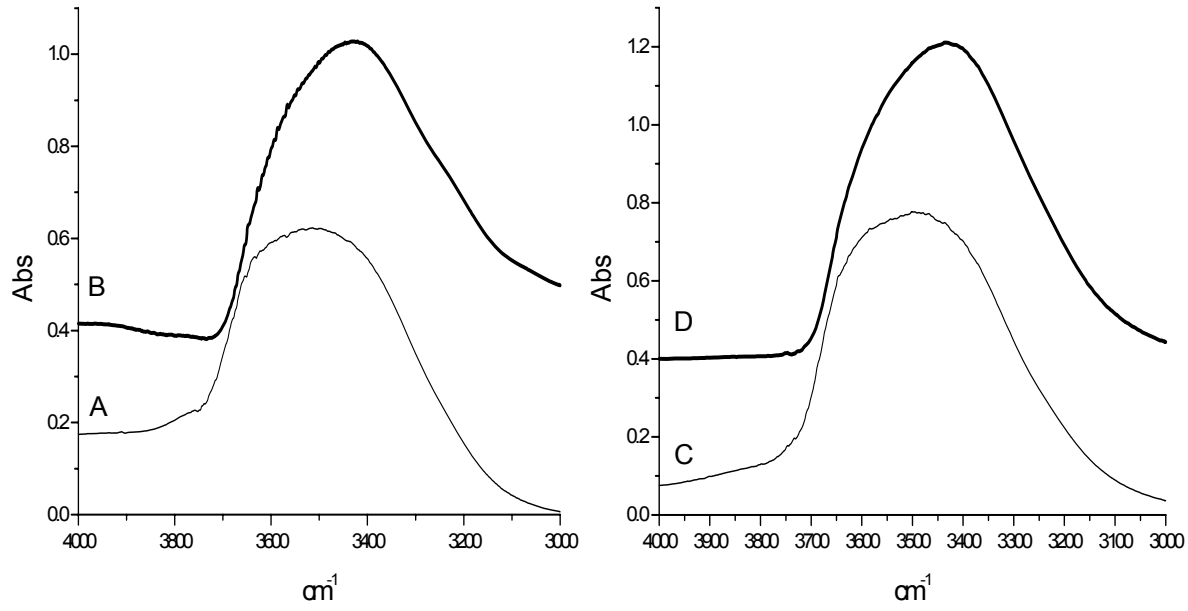

Figure 6.12: Infrared spectra of aged 3:1 Mg-Al LDH-Cl (4000 – 3000 cm^{-1}): (A) CsI; (B) polyethylene, oriented; (C) KBr; (D) CdTe, oriented.

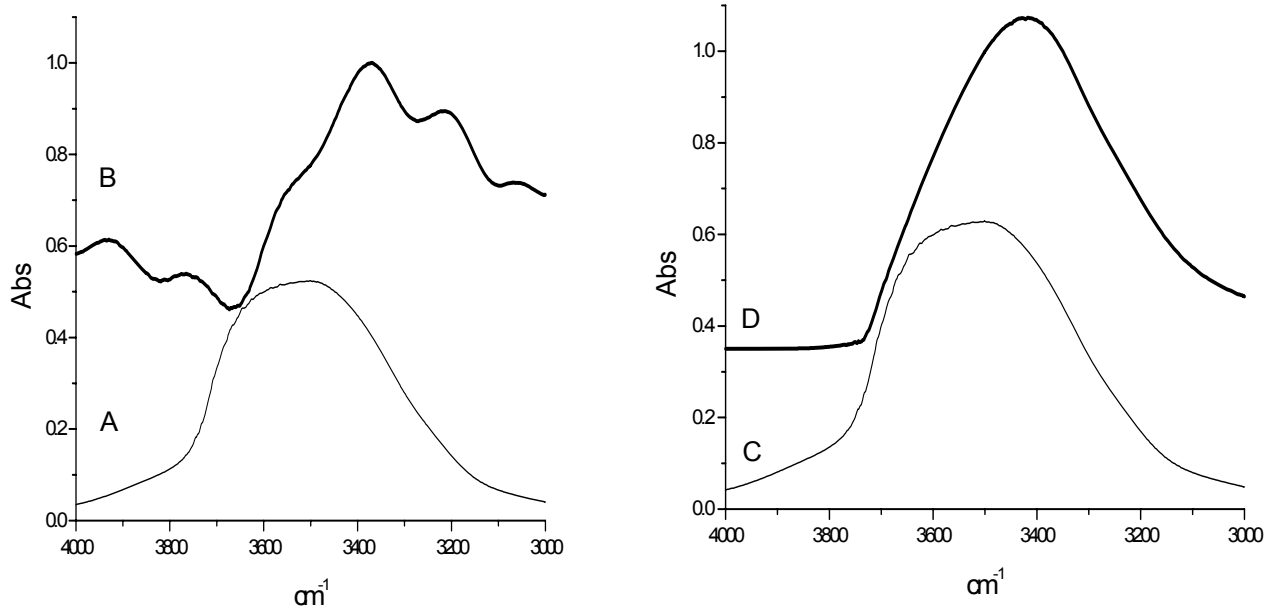

Figure 6.13: Infrared spectra of fresh 3:1 Mg-Al LDH-Cl (4000 – 3000 cm^{-1}): (A) CsI; (B) polyethylene, oriented; (C) KBr; (D) CdTe, oriented.

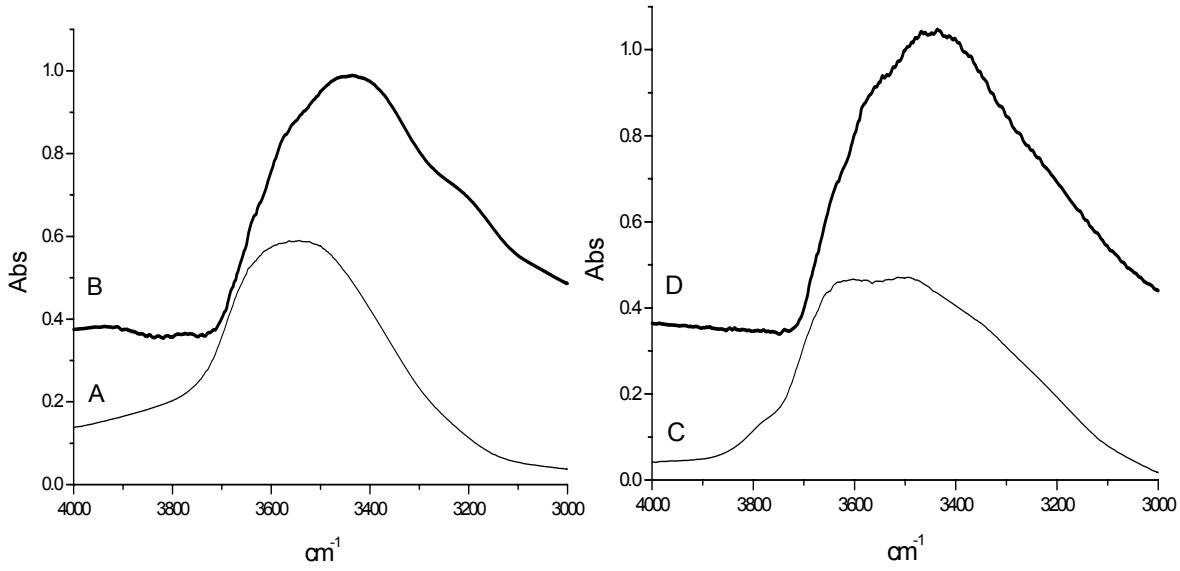

Figure 6.14: Infrared spectra of aged 3:1 Mg-Al LDH-ferrocyanide (4000 – 3000 cm^{-1}): (A) CsI; (B) polyethylene, oriented; (C) KBr; (D) CdTe, oriented.

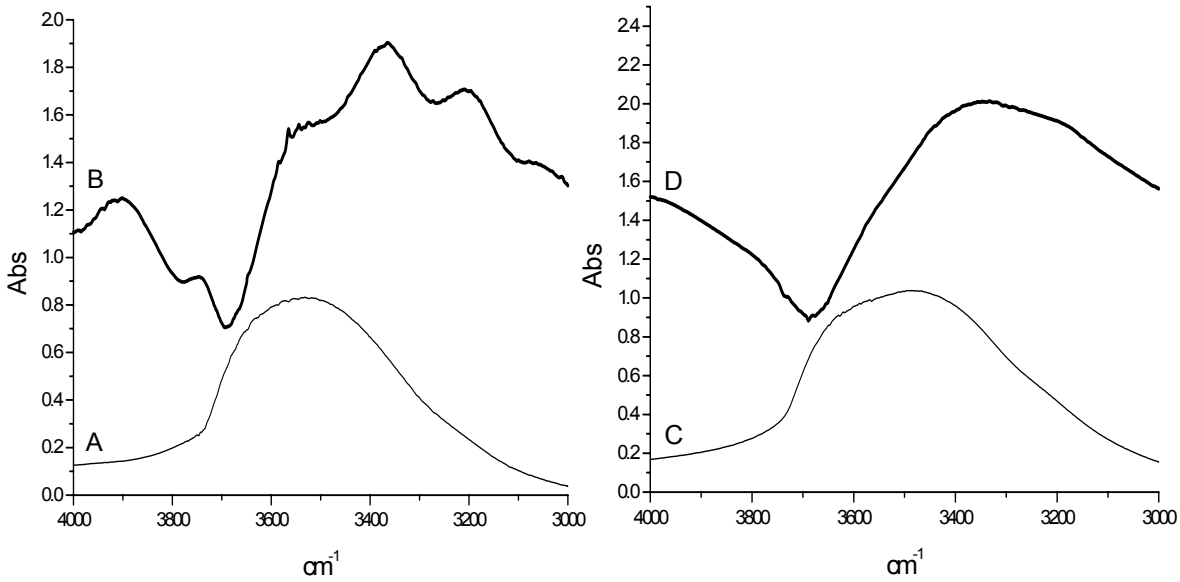

Figure 6.15: Infrared spectra of fresh 3:1 Mg-Al LDH-ferrocyanide (4000 – 3000 cm^{-1}): (A) CsI; (B) polyethylene, oriented; (C) KBr; (D) CdTe, oriented.

6.4.4 Metals Analysis for all LDH Samples

In order to ensure that the materials that we were studying were what we claimed they were, we performed AAS for the Mg, Al and Fe elements, on all eight LDH samples. Table 6.3 shows the metals analysis by AAS.

Table 6.3: Metals Analysis for the eight LDH samples.

LDH Sample	% Mg	% Al	% Fe	Mg : Al	Al : Fe	Mg : Fe
Fresh 2:1 Mg-Al LDH-Cl	15.85	9.95	---	1.8	---	---
Aged 2:1 Mg-Al LDH-Cl	15.34	8.52	---	2.0	---	---
Fresh 3:1 Mg-Al LDH-Cl	23.50	6.21	---	2.7	---	---
Aged 3:1 Mg-Al LDH-Cl	23.82	6.18	---	2.8	---	---
Fresh 2:1 Mg-Al LDH-ferro	15.41	8.32	4.02	2.1	4.3	8.8
Aged 2:1 Mg-Al LDH-ferro	14.63	8.29	4.39	2.0	3.9	7.7
Fresh 3:1 Mg-Al LDH-ferro	23.06	6.55	3.63	3.1	3.1	9.5
Aged 3:1 Mg-Al LDH-ferro	23.29	6.37	3.11	3.2	3.5	11.2

For the 2:1 Mg-Al LDH samples, the Mg:Al ratios are all close to the ideal 2:1 ratio. These samples also show close to the ideal 4:1 Al:Fe ratio, dictated by the ¼$[Fe(CN)_6]^{4-}$: Al^{3+} molar amounts in the general LDH formula.

For the 3:1 Mg-Al LDH samples, the Mg:Al ratios were also close enough to the ideal 3:1 ratio, but the Al:Fe ratios were lower than expected.

6.5 Conclusions/Future Directions

We have shown that the use of pellet and oriented specimens, using different background sources, gives novel information about band assignments and about the degree of order in LDH materials containing Mg:Al ratios of 2:1 and 3:1. It is possible to distinguish between OH (x,y motions) around 400 cm^{-1}, OH rotations (MOH bending modes) across the region below 1000 cm^{-1}, and the OH (z-oriented motion) around 700

cm^{-1}. In addition, it is apparent that aged $Mg_2Al(OH)_6Cl.xH_2O$ shows a degree of ordering[16-18] absent in the fresh material, which we attribute to the achievement of a local superlattice structure, as required for this ratio by an $Al^{(III)}$-$Al^{(III)}$ neighbor avoidance rule.

Both fresh and aged $Mg_3Al(OH)_8Cl.xH_2O$ show spectra very similar to those of fresh $Mg_2Al(OH)_6Cl.xH_2O$, and we infer that in this case the materials achieve $Al^{(III)}$-$Al^{(III)}$ neighbor avoidance without developing regular repeat structure. In the OH stretching region, intensity is in all cases concentrated towards lower frequency in the oriented spectra, indicating that the lattice hydroxide absorption is concentrated more towards higher frequencies. In $Mg_2Al(OH)_6Cl.xH_2O$ and its ferrocyanide derivatives, ageing leads to a reduction in band width in the OH stretching region, indicating that the cation order in the aged material also influences the interlayer water.

It was stated earlier that XRD has been used in the past to determine atomic positioning, but due to the similarities in X-ray scattering, for magnesium and aluminum, this characterization tool has not been very useful. Now with the oriented IR results, FT-IR spectroscopy has shown itself to be worth far more than anion identification.

What we have shown for LDH, containing magnesium and aluminum, should be worth exploring for other divalent-trivalent metal LDH materials. The concept of a superlattice formation should not, in theory, be dependent on the types of the common metals used for LDH lattice construction. Other commonly prepared LDH materials, having both 2:1 and 3:1 metals ratios, such as: Zn_2Al, Zn_3Al, Ni_2Al, Ni_3Al, Co_2Al, Co_3Al, Zn_2Cr, Zn_3Cr, Ni_2Cr, Ni_3Cr, Co_2Cr, Co_3Cr, etc. could produce similar results, although

only an aged Mg_2Al, at this time, has been shown to exhibit two strong bands below 500 cm^{-1}.

These LDH materials were studied at room temperature, all of them being dried by a vacuum desiccator. As described in the thermogravimetric section of Chapter 1, loosely bound water begins to be driven off around 100 ºC. These LDH materials may be worth studying after heating near this temperature, in order to observe any differences in the hydroxide stretching region (3000 – 4000 cm^{-1}). This may be more valuable for the LDH containing ferrocyanide and nickelocyanide, due to their high frequency bands around 3600 cm^{-1}. Due to the hygroscopic nature of dry LDH, the materials will have to be placed on the polyethylene and CdTe supports from non-aqueous suspensions.

Infrared Spectroscopy has been a valuable characterization tool for the study of LDH. Since the mid 1960s,[19,20] IR spectroscopy has become increasingly popular as a technique for the identification and elucidation of the composition and structure of the numerous variations of these mixed-metal hydroxide compounds. Our results show that the use of cesium iodide, and the collection of oriented spectra, significantly extends the range of information obtainable from IR, including in favorable cases giving information about medium-range order that could not be obtained in any other way.

6.6 References

(1) H Roussel, H., Briois, V.,Elkaim, E., de Roy, A., Besse, J.P., Jolivet, J.P. *Chem. Mater.* **2001***, 13*, 329.

(2) Solin, S.A.; Hines, D.R.; Seidler, G.T.; Treacy, M.M.J. *J. Phys. Chem. Solids* **1996**, *57*,1043.

(3) Vucelic, M.; Moggridge, G.D.; Jones, W. *J. Phys. Chem.* **1995**, 99, 8328.

(4) Boclair, J. W.; Braterman, P. S.; Brister, B. D.; Wang, Z.; and Yarberry, F. *J. Solid State Chem.* **2001**, *161*, 249.

(5) MJ Hernandez-Moreno, MA Ulibarri, JL Rendon, CJ Serna. *Phys. Chem. Miner.* **1985,** *12*, 34.

(6) Kagunya, W.; Baddour-Hadjean, R.; Kooli, F.; Jones, W. *Chem. Phys.* **1998**, *236*, 225.

(7) Mitra, S.S. *Solid State Phys.* **1962**, *13*, 1.

(8) Braterman, P.S.; Cygan, R.T. *Am. Miner.* **2006**, *91*, 1188.

(9) Lowenstein, W. *Am. Miner*. **1954**, *39*, 92.

(10) Wang, J.; Kalinichev, A.G.; Amonette, J.E.; Kirkpatrick, R.J. *Am. Miner.* **2003**, *88*, 398.

(11) Kirkpatrick, R.J.; Yu, P.; Hou, X.; Kim, Y. *Am. Miner.* **1999**, *84*, 1186.

(12) D. Eisenberg and W. Kauzmann, *The structure and properties of water* (Oxford University Press, London, 1969); 3490, 3280.

(13) The Application of Vibrational Spectroscopy to Clay Minerals and Layered Double Hydroxides, J. Theo Kloprogge, Ed., CMS Workshop Lectures, Vol. 13, 2005.

(14) Chakoumakos, B.C.; Loong, C.-K.; Schultz, A.J. *J. Phys. Chem. B* **1997**, *101*, 9458.

(15) Jones, L.H. *Inorg. Chem.* **1963**, *2*, 777.

(16) Vucelic, M.; Jones, W.; Moggridge, G.D.; *Clays Clay Miner.* **1997**, *45*, 803.

(17) Yao, K.; Taniguchi, M.; Nakata, M.; Takahashi, M.; Yamagishi, A. *Langmuir* **1998**, *14*, 2410.

(18) Cai, H.; Hiller, A.C.; Franklin, K.R.; Nunn, C.C.; Ward, M.D. *Science* **1999**, *266*, 1 551.

(19) Mumpton, F.A.J.H.W.; Thompson, C.S. *Am. Miner.* **1965**, *50*, 1893.

(20) Ross, G.J.; Kodama, H. *Am. Miner.* **1967**, *52*, 1036.